1-1-2002

Vegetation effects on airborne particles and soil gradation near mesquite dunes

Ann Marleau Pitchford
University of Nevada, Las Vegas

VEGETATION EFFECTS ON AIRBORNE PARTICLES AND SOIL GRADATION NEAR MESQUITE DUNES

by

Ann Marleau Pitchford

Bachelor of Science
Physics
University of Nevada, Reno
1975

Master of Science
Physics
University of Nevada, Las Vegas
1978

A dissertation submitted in partial fulfillment
of the requirements for the

Doctor of Philosophy Degree
Department of Civil and Environmental Engineering
Howard R. Hughes College of Engineering

Graduate College
University of Nevada, Las Vegas
December 2002

UMI Number: 3084150

UMI Microform 3084150

ProQuest Information and Learning Company
300 North Zeeb Road
P.O. Box 1346
Ann Arbor, MI 48106-1346

UNLV

Dissertation Approval
The Graduate College
University of Nevada, Las Vegas

July 29, 2002

The Dissertation prepared by

Ann Marleau Pitchford

Entitled

Vegetation Effects on Airborne Particles and Soil Gradation near Mesquite Dunes

is approved in partial fulfillment of the requirements for the degree of

Doctor of Philosophy

Moses Karakouzian
Examination Committee Chair

Dean of the Graduate College

Gerald R. Fredrick / William Culbert
Examination Committee Member

David E. James
Examination Committee Member

Vernon Hodge
Graduate College Faculty Representative

1017-52

ABSTRACT

Vegetation Effects on Airborne Particles and Soil Gradation Near Mesquite Dunes

by

Ann Marleau Pitchford

Dr. Moses Karakouzian, P.E., Examination Committee Chair
Professor of Civil Engineering
University of Nevada, Las Vegas

This study investigated the effect of vegetation on gradation of surficial soils and airborne concentrations of particulate matter at a site in the mesquite sand dunes within the Jornada Experimental Range, a research ranch near Las Cruces, New Mexico. Particles less than 10 microns in diameter were of particular interest. This study site was chosen because it had been in used in previous studies, and meteorological instruments and dust collectors were already installed. Aerodynamic size distributions for soil and airborne particulate matter samples collected at different positions near and on the dunes were determined using a laboratory settling tube apparatus. In addition, 6 continuous aerosol monitors were operated at locations upwind, downwind and on top of a sand dune during two dust storms.

Locations of vegetation determined using aerial photographs with 1-m resolution compared well with manually-determined vegetation locations with

0.5-m resolution. Soil sample analysis showed significant differences in the particle size distributions for the samples collected from the streets, dune tops, and dune sides. Fine sand comprised a much larger component of the dune top samples (60%) compared to the street samples (48%), and soil particles less than 16 microns in diameter comprised 0.1% of the dune top samples compared to 0.0% for dune sides. Dust collector samples showed that amounts collected increased with the length of bare area, or "street," in front of the sampler along the predominant wind direction. A threshold velocity for fine particle emissions was identified at approximately 65 to 80 cm s^{-1}. A flux model was based on continuous measurements along a mesquite dune centerline and wind data from nearby sensors for 10-minute periods when wind flow aligned with the dune. Wind data were borrowed from a collocated study, and thus were not positioned directly in line with the dune. Two combinations of wind sensors were chosen to estimate flow in front of, on top of, and behind the dune. Comparing the outcomes based on the DustTrak™ data and the two combinations of sensors revealed that the selection of the wind speed information was critical to the overall model results.

TABLE OF CONTENTS

ABSTRACT iii

LIST OF FIGURES vii

LIST OF TABLES x

ACKNOWLEDGMENTS xii

CHAPTER 1 INTRODUCTION 1

CHAPTER 2 BACKGROUND 5
Jornada Experimental Range Study Area 5
Climatology, Geology, Soils, and Vegetation 8
Principles of Wind Erosion 10
Methods for Particle Sizing 18
Methods for Sampling Airborne Dust 21

CHAPTER 3 METHODOLOGY 29
Summary of Tasks 29
Facilities and Equipment 31
Quality Assurance 31

CHAPTER 4 FIELD SAMPLING 33
Description of Sampling Sites 33
Instruments and Measurements 42
Dust and Soil Measurements 49
Data Preparation 56

CHAPTER 5 LABORATORY ANALYSES OF SOIL AND AIRBORNE PARTICLE SAMPLES 57
Apparatus 58
Theory and Data Analysis 63
Data Quality 66

CHAPTER 6 RESULTS FOR VEGETATION AND SOIL DATA 74
Determining Locations of Vegetation 75
Influence of Vegetation on Soil Particle-Size Distributions 86

CHAPTER 7 DUST STORMS: RESULTS FOR AIRBORNE PARTICLE DATA 92
Meteorological Data 95
Dust Collector Results 98
Continuous Meteorological and Aerosol Monitor Results 109

CHAPTER 8 FLUX MODELING 123
Description of the Box Models 123
Input Data Description 125
Model Calculations 128
Results 129
Propagation of Errors 131

CHAPTER 9 SUMMARY, CONCLUSIONS, AND RECOMMENDATIONS FOR FUTURE WORK 134
Summary 134
Conclusions 135
Recommendations for Future Work 137

BIBLIOGRAPHY 140

APPENDICES 147
Copyright Permission Letters 147
VSAT Program 150
Plots of Dust Collector Data for Both Periods Combined 162
Minute-by-Minute DustTrak™ Data 165

VITA 168

LIST OF FIGURES

Figure 2-1 Location of Jornada Experimental Range in southern New Mexico 6
Figure 2-2 Layout of Jornada Experimental Range facilities. 7
Figure 2-3 Modes of particle movement depend on particle size (after Shao, 2000, with kind permission of Kluwer Academic Publishers; and Pye, 1987 with kind permission of Academic Press and Elsevier Science.) 13
Figure 2-4 a) Typical conditions at MNORT site meteorological tower showing that winds increase logarithmically with height; friction velocity is calculated based on this change in wind speed. Horizontal dashed lines show approximate range in mesquite dune heights 16
b) Same typical conditions at MNORT site meteorological tower with wind speeds measured at different heights z plotted versus $ln\ z$, resulting in a straight line with a slope of U_* / κ, and an intercept of $(U^* / \kappa)\ ln\ [-d/z_o]$. 17
Figure 2-5 Relationship between flow conditions and particle motion (after Shao, 2000, with kind permission of Kluwer Academic Publishers) 19
Figure 2-6 The BSNE dust samplers were configured with catchers at 5 heights 24
Figure 2-7 Generalized light-scattering detection system of the type used in the DustTrak™ and GRIMM™ monitors 26
Figure 2-8 The cylindrical Sensit™ detects particle motion near the ground surface. 28
Figure 3-1 The relationships and sequence of the tasks in the study 30
Figure 4-1 Three of the main study sites, MNORT, MRABB, and MWELL, are collocated with LTER net primary productivity sites for mesquite while the fourth, Scrape site, is a unique vegetation-free area . 34
Figure 4-2 Much of the JER plain is dominated by mesquite (Prosopis glandulosa var. glandulosa) while creosote bush (Larrea tridentata) is common in the upland areas 36
Figure 4-3 The mesquite dunes give the landscape a distinctive stippled appearance and cover extensive areas within the JER 37
Figure 4-4 The main sites are contained within three different soil groups: Scrape Site–Berino-Bucklebar (BJ) Association; MWELL–Onite-Pajarito (OP) Association; and MNORT and MRABB–Onite-Pintura (OR) Complex. 39

Figure 4-5 The MNORT site instrumentation included 14 sand collectors; a meteorological tower and 5 masts; a Sensit™; and aerosol monitors at three locations along the centerline of one mesquite sand dune 45
Figure 4-6 The MRABB site instrumentation included 9 sand collectors; a meteorological tower and 5 masts; and a Sensit™ 46
Figure 4-7 The MWELL site instrumentation included 15 sand collectors . . 47
Figure 4-8 The Scrape site instrumentation included 3 sand collectors aligned along the dominant wind direction 48
Figure 4-9 At MNORT, the ladders were aligned along the longer dune axis, at locations upwind, in the middle, and downwind of the dune 50
Figure 4-10 Each 1.8-meter-high ladder supported 2 DustTrak™ samplers. The ladders were secured by using duct tape and 0.6 m steel stakes pounded into the ground. The samplers were secured to the ladder with rubber cords 51
Figure 4-11 Because of the height of the dune, the DustTrak™ samplers were located at three different heights. Although the samplers appear to be aligned vertically in this figure, for each ladder, the lower sampler inlet was approximately 1 m further northwest than the upper sampler inlet. (See Figure 4-10) 52
Figure 4-12 With its 15-m height and multiple wind speed measurements, the meteorological tower was designed for determining friction velocities 54
Figure 4-13 The meteorological masts were intended for understanding the microscale winds within the streets of the dune field 55
Figure 5-1 The Vertical Settling Aerosol Tube was located in a temperature-controlled closet. The glass fall column was not sealed although the top of the column was enclosed in a small box to prevent dust and turbulence from affecting the tests 59
Figure 5-2 (a) Values of cumulative weight and time are recorded on a data acquisition system at 0.2 s intervals (not all data are shown). (b) Travel times for particles ranging in size from 10 to 500 μm are computed for spherical particles of the same density of the soil being characterized, and Stokes diameters are determined by matching the computed with the actual arrival times 62
Figure 5-3 Particle size distributions for the 10 μm and the 1 to 40 μm standard samples demonstrate clumping while the 30 μm sample does not 71
Figure 6-1 Vegetation at MNORT site, mapped manually (courtesy of LTER Wind Erosion Study) 76
Figure 6-2 Vegetation at MRABB site, mapped manually (courtesy of LTER Wind Erosion Study) 77
Figure 6-3 Vegetation at MWELL site, mapped manually (courtesy of LTER Wind Erosion Study) 78

Figure 6-4 Comparison of manually mapped data and the digital orthophoto image for the same area at the MNORT site 79
Figure 6-5 Comparison of manually mapped data and the digital orthophoto image for the same area at the MRABB site 80
Figure 7-1 The LTER weather station at the Jornada Ranch Headquarters provides continuous, hourly averaged wind speed and direction data; this excerpt is for the intensive field study session. 96
Figure 7-2 Sand collector data for MNORT site for Period A (top) and Period B (bottom) plotted versus height. The decline in mass with height was present at all the sites. 100
Figure 7-3 Comparison of flux means and quartiles for each of the main sites for Periods A and B. 103
Figure 7-4 Measured and linear model prediction for flux at the four main sites for Period A. 107
Figure 7-5 Measured flux values and linear model prediction for flux at the four main sites for Period B. 108
Figure 7-6 Data for the windy periods of April 18 and 19, 2000 with DustTrak™ data and the corresponding friction velocities, U. (U Star). 115
Figure 7-7 The individual DustTrak™ data for April 18, 2000 for each location at the dune site versus time, arranged on the page to suggest the spatial relationships of the instruments. 116
Figure 7-8 The individual DustTrak™ data for April 19, 2000 for each location at the dune site versus time, arranged on the page to suggest the spatial relationships of the instruments. 117
Figure 7-9 Determination of threshold friction velocity based on Sensit™ data for sand movement for the four storms of the intensive session. The threshold friction velocity is approximately 70 cm s^{-1}. 120
Figure 7-10 Determination of threshold friction velocity based on DustTrak™ data for the upwind bottom instrument for all four storms of the intensive session. The threshold friction velocity is approximately 80 cm s^{-1} for PM_{10}. 121
Figure 8-1 The 2-box model encompasses the dune in the lower box and has a second box directly above it. 124
Figure 8-2 The 1-box model combines the two boxes from the 2-box model 126
Figure 8-3 The 4-box model has additional faces at the center of the dune. 127
Figure 8-4 Standard deviation of DustTrak™ measurements compared to group mean concentration. 133

LIST OF TABLES

Table 2-1 Examples of modes of movement, particle sizes, and terminal velocities, computed using methods described in Chapter 5. (*assumes spherical particles with a density of 2.6 g/cm^{-3} at 25 °C, 36% relative humidity and 680.4 mm Hg). 12

Table 2-2 Diameter types, symbols, and definitions used in this study 20

Table 2-3 Performance characteristics for the airborne particle samplers and monitors used in this study 22

Table 4-1 Soil relationships for the main sites (summarized from Bulloch and Neher, 1980) 40

Table 4-2 Descriptive information for map units (extracted from Bulloch and Neher, 1980) 41

Table 4-3 Measurements conducted at the main sites during Spring 2000 intensive; na means not available 44

Table 5-1 Particle sizes and approximate travel times versus temperature in the VSAT for 36% relative humidity, 680.4 mm Hg, and particle densities of 2600 kg m^{-3}. The typical temperature during the analyses was 25 °C; the other temperatures are provided for comparison 61

Table 5-2 Particle sizes, Reynolds numbers, and terminal velocities determined for 25 °C, 36% relative humidity, 680.4 mm Hg, and particle density of 2600 kg m^{-3} 66

Table 5-3 Names for different mineral particle sizes less than 2 mm in various diameters; and corresponding d_a computed using Equations 2-4 and 2-5; est. means estimated ([1]Chen, personal communication, 1998; [2]Pye and Tsoar, 1990; [3]Bulloch and Neher, 1980) 67

Table 5-4 (a) Differences, mean difference, and standard deviation of differences in cumulative size distributions for duplicate samples analyzed by the VSAT. (b) Differences, mean difference, and standard deviation of differences for mean sample size in Phi and millimeter units, standard deviation of mean sample size in millimeters, skewness, and kurtosis for duplicate samples analyzed by the VSAT 68

Table 5-5 Comparison of differences from duplicate samples analyzed by the VSAT when data are classified into size categories 69

Table 5-6 Materials used for accuracy comparisons (obtained from Duke Scientific Corporation) 70

Table 6-1 Vegetation types and amounts for main sites (based on manual enumeration data from LTER Wind Erosion Study and analysis of the DOQQs). DOQQ reflectances are measured on a scale of 0 to 255; the red spectral band was used. 83
Table 6-2 One-sided non-parametric tests were applied for each site to check whether means for distances to nearest vegetation in any direction were significantly less than distances upwind to nearest vegetation. Additional t-tests were applied among the sites to check whether the means for the upwind distances were different from site to site. Highlights show probabilities that are significantly different at the 95% confidence level. Note that there is no vegetation within the Scrape site. 85
Table 6-3 Means and standard deviations for soils collected from MNORT streets, dunes, and dune sides 89
Table 6-4 One-sided t-tests were applied to check whether a mean for a given particle size and setting was less than means for the same size range in other settings. Highlights show results that are significant at the 95% confidence level 91
Table 7-1 Dates for integrated BSNE sampling during the intensive session 97
Table 7-2 Basic statistics for the sand collectors at the four main study sites 98
Table 7-3 One-sided, non-parametric t-test approximations for mean flux at each site were applied to check whether a selected site mean was less than each of the others. Highlights show probabilities that indicate one mean is significantly less than the other at the 95% confidence level 102
Table 7-4 Coefficients for flux model. The variable "veg" refers to the distance to the nearest upwind vegetation from the sand collector 105
Table 7-5 DustTrak™ correction equations based on side-by-side measurements 106
Table 7-6 Dates and times for continuous DustTrak™ sampling at MNORT during the intensive session. The gap in the data on April 18th occurred when batteries were changed between two 6-hour periods 110
Table 7-7 Potential role of middle- and long-range transport at MNORT site. H = high, M = medium, and L = low relative concentrations for the individual storm. [1]10-minute average at 9:00 PM; [2] 7-minute average at 5:42 PM; [3] 6-minute average at 6:29 PM 113

Table 7-8. Potential role of middle- and long-range transport to the MNORT site, evaluated by using the two upwind DustTrak™ sensors (Upwind Top and Upwind Bottom, "Bot") and the Middle Top (highest) sensor and comparing the values measured. These values are coded as H = high, M = medium, and L = low based on relative concentrations for the individual storm. [1]10-minute average at 9:00 PM; [2] 7-minute average at 5:42 PM; [3] 6-minute average at 6:29 PM. 119

Table 8-1. Statistical results for flux differences and propagated errors for both options for wind data. Positive values are indicative of erosion from the dune, while negative values are indicative of deposition. The propagated errors were based on standard deviations for wind speed and the DustTrak™ data; Option1 used a constant standard deviation for the DustTrak™ data while Option 2 estimated the standard deviation as 10% of the DustTrak™ concentration; both options used a constant standard deviation for the wind speed 130

ACKNOWLEDGMENTS

This research would not have been technically possible without the special involvement of two people, my research advisor, Dr. Moses Karakouzian, and my mentor for the field research, Dr. Dale Gillette. Dr. Karakouzian introduced me to the field of geotechnical engineering, and encouraged me in my pursuit of this advanced degree. I have learned a tremendous amount from him. Dr. Gillette provided access to his study sites and data at the Jornada Experimental Range, and shared his field expertise and extensive understanding of wind blown dust in the development and implementation of this research project.

I would like to thank the University of Nevada, Las Vegas professors Dr. William Culbreth, Dr. Gerald Frederick, Dr. David James, Dr. Samaan Ladkany, and Dr. Vernon Hodge for serving on my examination committee. Their insights and help with the manuscript are truly appreciated. This study would not have been possible without the assistance of many individuals. I would like to thank Dr. Dan Upchurch, Lab Director and Research Leader, U.S. Department of Agriculture (USDA), Agricultural Research Service, Lubbock, and the current and retired staff of the USDA Big Spring Station including Dr. Scott Van Pelt, Mr. Charles Yates, and Mr. William Fryrear, for allowing access to their soil laboratory, and National Research Council Associate, Dr. Weinan Chen, for training me in the use of the laboratory instrumentation. I would like to thank the

staff of the Desert Research Institute including Dr. John Bowen, Dr. Judy Chow, Dr. Vicken Etymezian, Dr. Mark Green, Dr. Hampden Kuhns, and Dr. John Watson for encouraging me to pursue this topic and loaning me equipment for the field study. I would like to thank Dr. Jeffrey Kirkpatrick and the U.S. Army, Aberdeen Proving Grounds, for supporting a portion of the field and laboratory work. I would like to thank the staff of the U.S. Department of Agriculture Jornada Experimental Range in New Mexico, for the loan of equipment when I worked at the field sites, and the staff at the Jornada Long Term Ecological Research (LTER) project for their support, especially Ms. Barbara Nolen, for providing LTER data. Funding for these data was provided by the U.S. National Science Foundation (Grant DEB-92-40261). I would like to thank my colleagues at the U.S. Environmental Protection Agency, Mr. Donald Ebert, Dr. Maliha Nash, and Ms. Anne Neale, who helped me learn to use ArcView and SAS.

Finally, I want to thank my husband and daughter, Marc and Clair Pitchford for their patience, understanding, and encouragement during my time as a graduate student.

CHAPTER 1

INTRODUCTION

Wind erosion has been observed and studied by geomorphologists and agricultural engineers for many years, but the focus has been on soil loss, visibility impacts, and damage to crops and property rather than on the airborne particulate matter concentrations associated with these effects. Recent regulations by the EPA have focused attention on particulate matter of aerodynamic diameter 10 microns (μm) and smaller in size (PM_{10}) because of their health consequences. The regulations address both manmade and natural sources of dust. Fugitive dust is a term that describes particulate matter suspended in the air either by mechanical disturbance of surficial material or by wind blowing across mechanically disturbed surface areas. In the United States, a recent emissions inventory showed wind erosion accounting for approximately 20% of the 25 million tons per year of fugitive dust emissions nationwide (U.S. Environmental Protection Agency, 1998).

This dissertation presents the results of a study that investigated the effects of vegetation on soil particle-size distributions and airborne particle concentrations and characteristics with an emphasis on PM_{10}. Although the basics of wind erosion, and interactions of sand dune dynamics and vegetation

are understood, the relationship of PM_{10} concentrations to these processes is only now being investigated. The questions being addressed by this study for a mesquite dune setting include:

- how does soil size distribution vary in bare and vegetated soils?
- how does mass vary in airborne samples collected at various distances from vegetation?
- what is the threshold friction velocity for PM_{10}, and
- how do PM_{10} concentrations vary upwind and downwind of a mesquite dune?

The location of vegetation is important to several aspects of the study, therefore a different type question must also be asked:

- how do locations of vegetation determined manually compare to locations determined using digital photos?

These questions will be the focus of this dissertation.

The purpose of this study is to answer questions about a natural source of fugitive dust, the mesquite sand dunes of southern New Mexico. To investigate these processes in detail, a study was conducted during April, 2000 during several dust storms at several locations within a mesquite dune research area. The vegetation in the study area was located and identified both manually and using digital orthophoto images. Soil samples collected at the base of vegetation on the sand dunes and in the bare areas between sand dunes were compared over a series of size classes, including PM_{10}. Airborne particles were addressed in several ways. Samples were collected at 5 standard heights from samplers

located within several mesquite dune settings and at a bare soil site. Selected samples were analyzed for PM_{10} content. Concurrent measurements of meteorological and ambient PM_{10} data during two dust storms were used to identify the threshold friction velocity for PM_{10} emissions within the mesquite dune study area. These measurements were then utilized in a flux model to better understand the effects of the mesquite dune on PM_{10} concentrations.

This dissertation consists of nine chapters. Chapter 2, Background, discusses selection of the study area, the characteristics of the research site, the principles of wind erosion, methods for particle sizing, and the methods for sampling airborne dust.

Chapter 3, Methodology, describes how this study was conducted. To accomplish the goals of the study, the research was divided into five tasks. The purpose of each of these tasks is discussed. Facilities, equipment, and quality assurance are also discussed.

Chapter 4, Field Sampling, describes the sampling sites, the types of instruments and measurements used at each site and the time period each method was used, and data preparation.

Chapter 5, Laboratory Analyses of Soil and Airborne Particle Samples, discusses the laboratory measurements that were used to determine particle size distributions for the soil and airborne particle samples collected at the study sites. Apparatus, theory and data analysis, and data quality are discussed.

Chapter 6, Results for Vegetation and Soil Data, discusses the performance of the manual and digital orthophoto methods for determining locations of

vegetation and compares soil particle-size distributions for locations with and without vegetation.

Chapter 7, Results for Airborne Particle Data, discusses the results of the data analyses for the sand collectors, portable dust monitor, and continuous wind and aerosol monitors.

Chapter 8, Flux Models, provides an analysis of the PM_{10} concentrations upwind and downwind of a mesquite sand dune.

Chapter 9, Summary, Conclusions, and Recommendations, summarizes and provides perspective on the results; and gives recommendations for further research.

CHAPTER 2

BACKGROUND

This Background Chapter summarizes general information on the study area and information in the technical literature that is important to this research. The topics discussed include the Jornada Experimental Range study area, principles of wind erosion, and methods for particle sizing and airborne particle sampling.

Jornada Experimental Range Study Area

Situated in a flat sand plain called "Jornada del Muerto (Journey of Death)" by early settlers, the Jornada Experimental Range (JER) is north of Las Cruces, in southern New Mexico (Figure 2-1), between the San Andres mountains on the east and the Dona Ana mountains to the southwest. The JER is managed by the U.S. Department of Agriculture (USDA). In 1912, the area was designated as a research ranch operated by the predecessors to the USDA and New Mexico State University. A long history of land practices and management scenarios and other information is available for this area, some dating back to the 1850s. It now consists of 426 square kilometers containing pastures, two large exclosures, and the ranch headquarters (Figure 2-2).

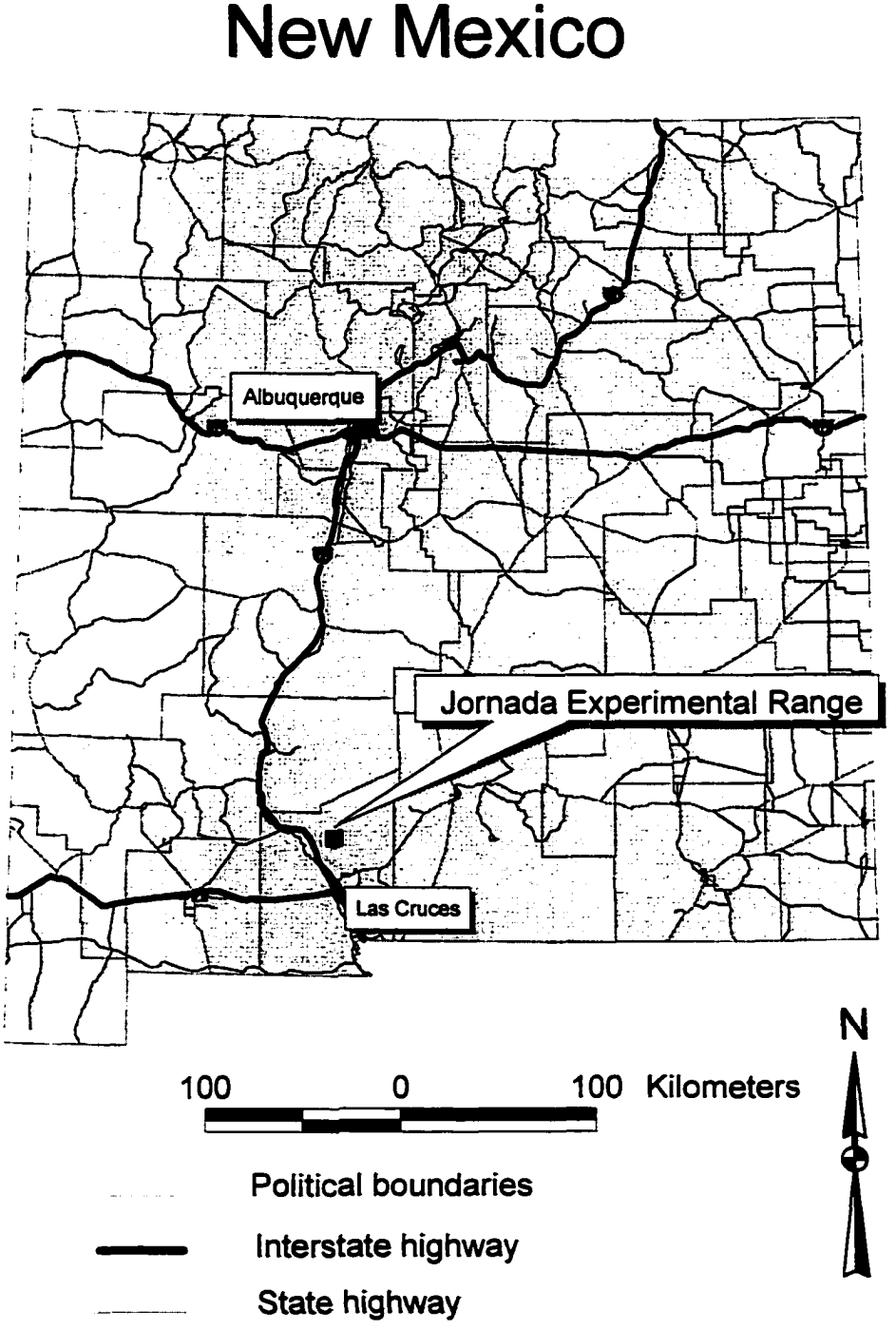

Figure 2-1 Location of Jornada Experimental Range in southern New Mexico.

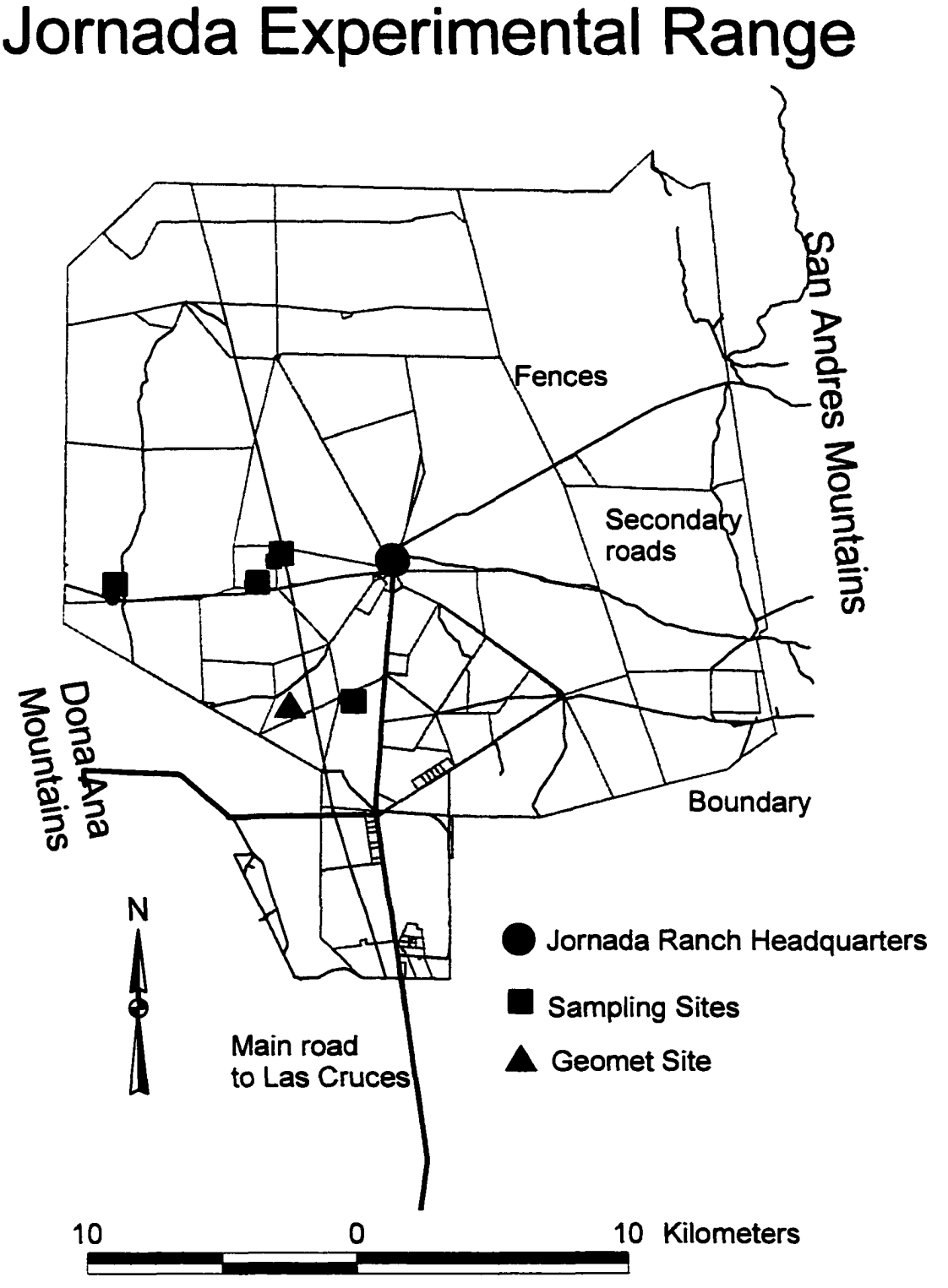

Figure 2-2 Layout of Jornada Experimental Range facilities.

The land has been developed with windmills, stock watering ponds and corrals for livestock management; both sheep and cattle have been grazed in the area except in the exclosures. The area is believed to be representative of the semi-desert grassland designated as the Chihuahuan Desert, stretching from eastern Arizona across New Mexico to western Texas and south to northern Mexico and thus results are applicable to a wide area (USDA, 2002).

A Long Term Ecological Research (LTER) program funded by the National Science Foundation at the JER offered the opportunity to participate in an existing study; this research added the capability to measure the PM_{10} aspects of the wind erosion process. The wind erosion study that is part of the LTER research program has wind erosion sites collocated with historic net primary productivity sites. These existing wind erosion dust collectors and meteorological instruments, along with permission to use the sites and long-term data sets, and the availability of 4-wheel-drive vehicles to drive to the sites and two-way radios for safety were the basis for the decision to perform this research at this location. This infrastructure was essential for conducting the PM_{10} study.

Climate, Geology, Soils and Vegetation

The climate of the JER is semi-arid, with a mean annual precipitation of 24.7 cm. Precipitation occurs primarily in the summer (July through September) and again in the winter (December through February). The growing season is primarily during the summer when precipitation and temperatures are favorable. (USDA, 2002). Wind speeds are highest when storm fronts pass during the

spring months. The impact of the precipitation and wind patterns on wind erosion is that soils are generally dry during the period when wind speeds are highest making them more vulnerable to erosion. In addition, the mesquite plants are in a leaf-off condition that provides less protection than the leaf-on conditions typical later in the year.

Geologically, the JER is a diverse area. The Dona Ana Mountains on the western side of the JER formed through volcanic processes, while the San Andres Mountains on the eastern side formed through fault-block processes. The ancestral Rio Grande was a major of source of river sediment deposits in the area, at one time emptying into a huge lake. When this lake basin was eventually breached, the river cut through these ancestral sediments, creating the confined river valley of the present Rio Grande and leaving behind the deep sandy sediments characteristic of the JER (Gile,1966; and USDA, 2002). In recent times, these sediments were reworked by the wind (Gibbens,1983).

Soils at the JER have almost no humus or organic matter, and there is little change in texture between surface soil and subsoil. Lime content is high in all soil types and leaching has caused the formation of both thick and thin layers of calcium carbonate, also called caliche (USDA, 2002). The deep and thicker layers of caliche are not generally important to wind erosion, except in isolated areas where exposed on the surface, but the thin layers offer a degree of protection to the soil until wind-caused abrasion or animal disturbance breaks the layer (Belnap and Gillette, 1997; and Gillette and Chen, 2001).

The JER has many vegetation types ranging from nearly pure stands of

grass, to savannahs with grass interspersed by shrubs or trees, to nearly pure stands of shrubs. On sandy soils, shrubs or shrub-like plants include honey mesquite, fourwing saltbush, soaptree yucca, and broom snakeweed (USDA, 2002). Extensive dunes have developed in sandy soils dominated by mesquite; these areas are the focus for this study.

Principles of Wind Erosion

Wind erosion potential in arid and semi-arid land can be assessed at many scales crossing orders of magnitude from regional to microscopic. Within this broad range many types of wind erosion and dune formation are possible. This discussion is intended to provide a general overview of the important factors at the different scales. It is not intended to address beach dunes, although some of the principles are the same. It also is not intended to address soil loss as studied by geomorphologists and agricultural engineers. The purpose is to understand the regional scale processes so that the local- and site-scale wind erosion processes can be put into context.

At the regional scale, climate, prevailing winds, vegetation (or lack of vegetation) and a potential source area must combine to produce dry land wind erosion. Regional-scale factors that are favorable for wind erosion include a dry climate; storms with high winds and little precipitation; bare, unprotected ground; and erodible surface material (Shao, 2000). At the subregional scale, the interactions between local winds; topography; and surface roughness due to surface material and vegetation become important in determining the potential of

a specific area for wind erosion (Mulligan, 1995). For development of sand dunes, a sufficient supply of sand must be available. At all these scales there is an interplay between the global- and regional-scale winds, precipitation, and soil particle size. For example, for long range transport, finer-sized particles and sustained regional-scale winds are essential; scavenging of these particles by precipitation cannot be a factor. The sand dunes of the JER meet the all the criteria for dry land wind erosion, and in some cases qualify as a source for long range transport of fine particles.

To further understand how wind erosion occurs, the focus must move from the controlling factors at the regional- and subregional-scales (+1000 km^2) that have formed the deserts of the southwestern United States, to the scale of a study area plot (approximately 50 m x 50 m). Sizes of the soil particles, wind and surface roughness, and amount and orientation of vegetation are crucial to determining the amount of wind erosion at the plot scale.

The size of the particles controls both the modes of movement possible for a given wind speed and the threshold for movement. Three modes of particle movement have been defined, e.g., suspension, saltation, and creep (Bagnold, 1954). Suspension dominates for finer particles less than 70 μm in diameter because their low terminal settling velocities ensure that they remain suspended in the atmosphere for long periods of time, especially if they are lofted well above the ground surface through turbulence (Table 2-1). Terminal settling velocity represents the velocity attained by a particle when the forces of drag

Table 2-1. Examples of modes of movement, particle sizes, and terminal velocities, computed using methods described in Chapter 5. (*assumes spherical particles with a density of 2.6 g/cm^{-3} at 25 °C, 36% relative humidity and 680.4 mm Hg).

Mode of movement	***Soil geometric particle diameter (μm)***	***Approximate terminal velocity****
Long-term suspension	< 20	< 3.1 cm s^{-1}
Example:	10	0.8 cm s^{-1}
Short-term suspension	20 - 70	3.1 - 32 cm s^{-1}
Example:	50	19 cm s^{-1}
Saltation	70 - 500	32 - 365 cm s^{-1}
Example:	100	60 cm s^{-1}
Creep	> 500	> 365 cm s^{-1}

and gravity are balanced. Saltation occurs for the larger particles (of geometric sizes between 70 to 500 μm) that bounce after entrainment by the wind. The impact of these particles creates a splash effect, dislodging additional particles. Particles in the size range of 500 μm and larger roll or slide along the ground; this is defined as creep (Figure 2-3). Sand blasting by the larger particles already in motion is an important factor in the emission of PM_{10} when wind speed would not otherwise be high enough to suspend these particles (Gillette and Walker, 1977; Shao et al., 1993).

Wind erosion is ultimately driven by the transfer of turbulent momentum from the atmosphere to the soil surface (Shao, 2000). A profile of wind speeds measured at several heights above the ground shows the effects of drag with slower speeds near the surface than at the higher, less obstructed levels,

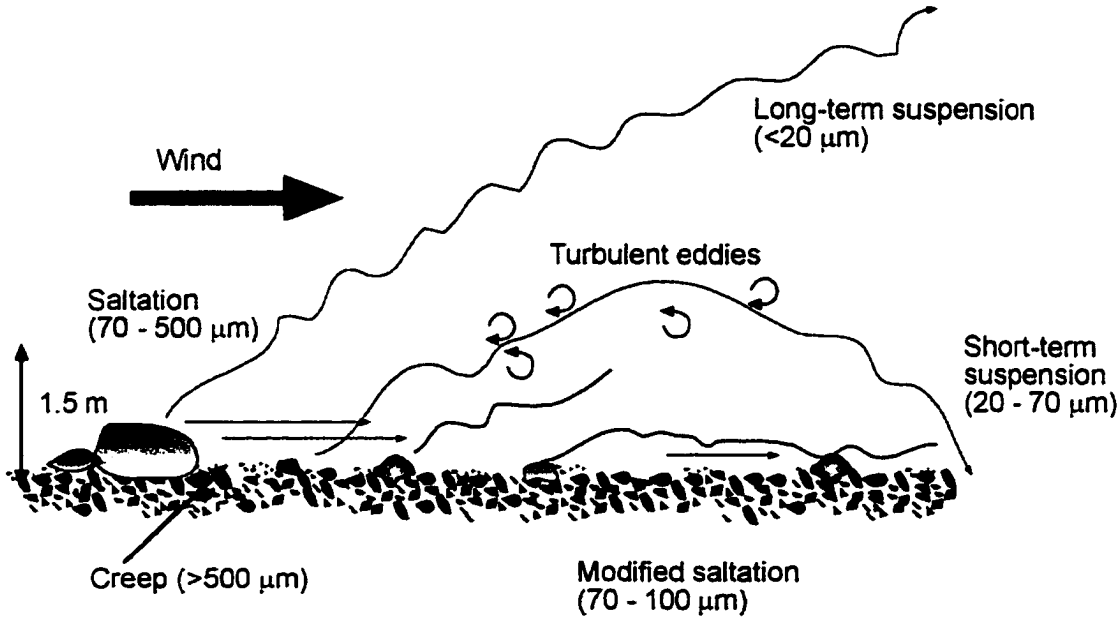

Figure 2-3. Modes of particle movement depend on particle size (Shao, 2000, with kind permission of Kluwer Academic Publishers; and Pye, 1987 with kind permission of Academic Press/Elsevier Science.)

demonstrating this transfer of momentum. To describe this transfer of momentum, a calculated parameter U_*, termed friction velocity, is conceptually defined as

$$U_* = \left(\frac{\tau}{\rho} \right) \qquad \text{Eqn. 2-1}$$

where τ is the shear stress, and ρ is the density of the air. This parameter is not a true velocity. Friction velocity is derived from wind speed data measured at logarithmically increasing heights. It is proportional to the slope of the logarithmic velocity profile.

To understand how friction velocity is calculated, the change of wind velocity with height must be quantified for a specific location. In the lower 50 meters of the atmosphere, turbulent flows dominate, and horizontal wind stresses tend to be constant with height. The laminar flow layer is only a few millimeters thick, and is broken by surface obstructions and their wakes (Shao, 2000). By making some reasonable assumptions,

- momentum is transferred by turbulent mixing of eddies;
- atmospheric conditions are neutral (a parcel of air tends to stay where it is rather than rising or sinking);
- eddies are proportional in size to the height z above the ground; and
- wind speed decreases to 0 at a height $z = z_o$ above the ground,

an expression for the change of wind speed with respect to height can be

integrated to result in the logarithmic wind law:

$$U_{(Z)} = \left(\frac{U_*}{\kappa}\right) \ln\left(\frac{z-D}{z_0}\right) \qquad \text{Eqn. 2-2}$$

where

$U(z)$ = wind speed as a function of height z

U_* = previously defined friction velocity

κ = von Karman constant, typically 0.38

D = the displacement height, and

z_o = aerodynamic roughness height (Hess, 1979).

A positive displacement height indicates that the wind speeds decrease to zero above the surface, minimizing wind effects at the surface. The value z_o describes the capacity of the surface to absorb momentum. To determine U_*, wind speeds measured at different heights z are plotted versus $ln\ z$, resulting in a straight line with a slope of U_* / κ, and an intercept of $(U_* / \kappa)\ ln\ [-d/z_o]$ (Figure 2-4 a, b). Friction velocities and displacement and roughness heights for this study were determined by solving iteratively for the best fit values using 10-minute averaged wind velocities from a 15-m tower with sensors at 5 heights.

Threshold friction velocity is a characteristic of the surface condition defined as the computed friction velocity when particles of a given size begin to move. Different particle sizes respond differently because larger particles present a larger cross-sectional area to the wind, while smaller particles are more affected by wake effects and interparticle cohesion. The range of

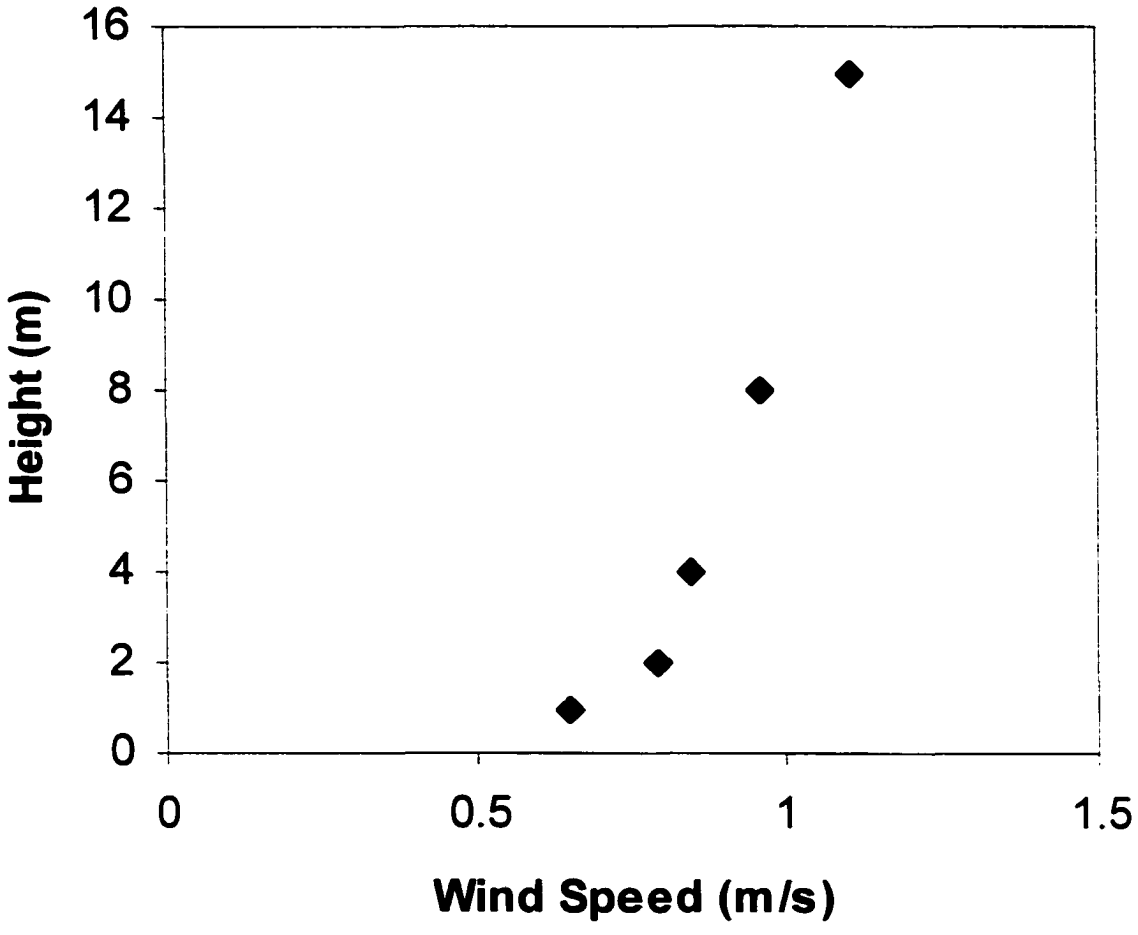

Figure 2-4 a) Typical conditions at MNORT site meteorological tower showing that winds increase logarithmically with height; friction velocity is calculated based on this change in wind speed. Horizontal dashed lines show approximate range in mesquite dune heights.

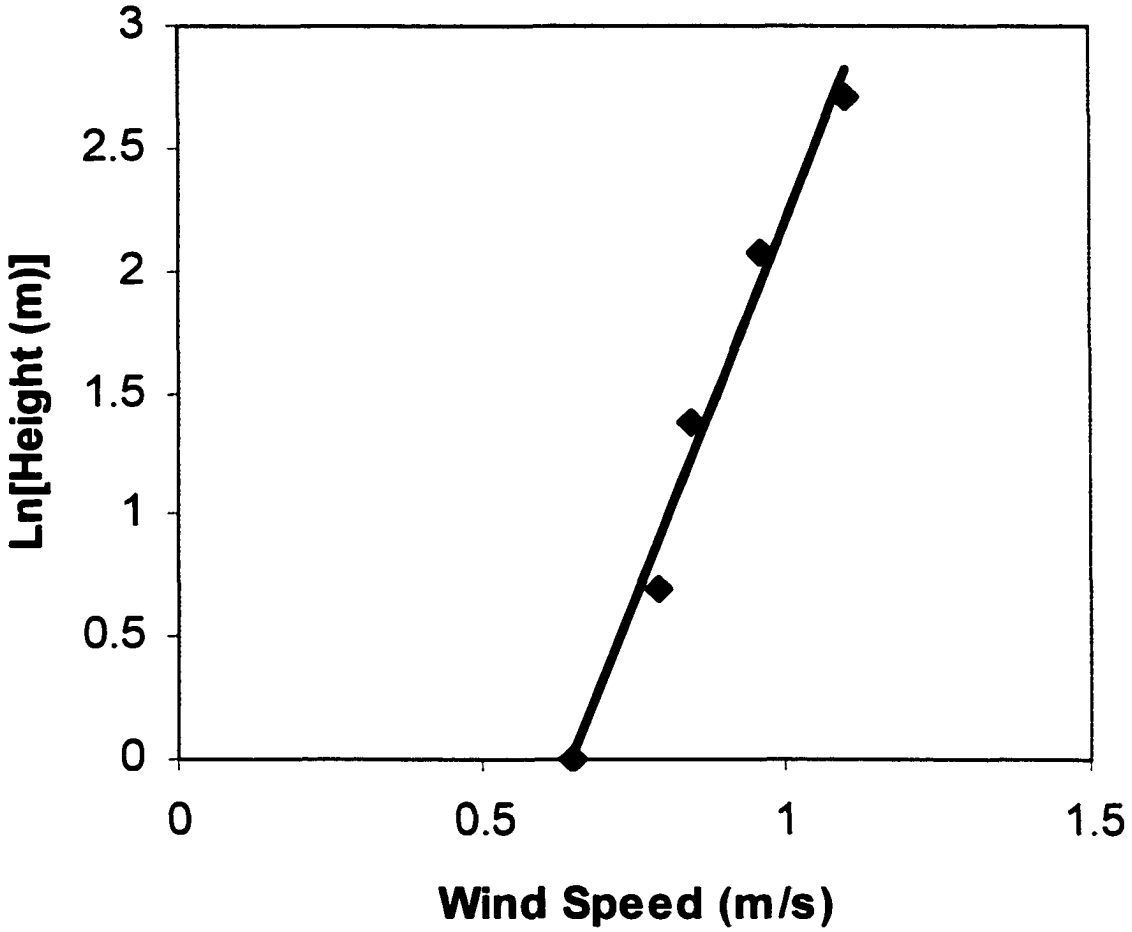

Figure 2-4 b) Same typical conditions at MNORT site meteorological tower with wind speeds measured at different heights z plotted versus $ln\ z$, resulting in a straight line with a slope of U_* / κ, and an intercept of $(U_* / \kappa)\ ln\ [-d/z_o]$.

threshold values (defined by the dashed, u-shaped curve on Figure 2-5) can vary widely with particles with geometric sizes in the 70 to 100 μm range having the lowest thresholds. Threshold velocities for particles with geometric sizes smaller than 10 μm are several times greater than velocities for the larger 100 μm particles (Bagnold, 1954). Since particle-particle interactions are significant, threshold friction velocity is considered a property of the entire surface of particles.

Methods for Particle Sizing

There are several methods for measuring and reporting particle size. The purpose of the data determines which of these is most appropriate (Table 2-2). For the human health perspective, aerodynamic diameters are desirable because this characteristic determines the degree of penetration of particles into the nose, trachea, and lungs. It was on this basis that the U.S. Environmental Protection Agency established the National Ambient Air Quality Standards for particulate matter in terms of particulate matter less than 10 μm aerodynamic diameter (U.S. EPA, 1995). In contrast, for a soil scientist or geotechnical engineer, the sieve particle diameter provides a consistent, easily characterized parameter that is usually determined by sieving for larger-size particles in combination with other techniques for the silt and clay-size fraction of the sample (Das, 1999; Shao, 2000). Two additional particle sizing approaches were used in this study: optical light scattering calibrated to aerodynamic diameters, and spherical-equivalent diameters determined from aerodynamic measurements.

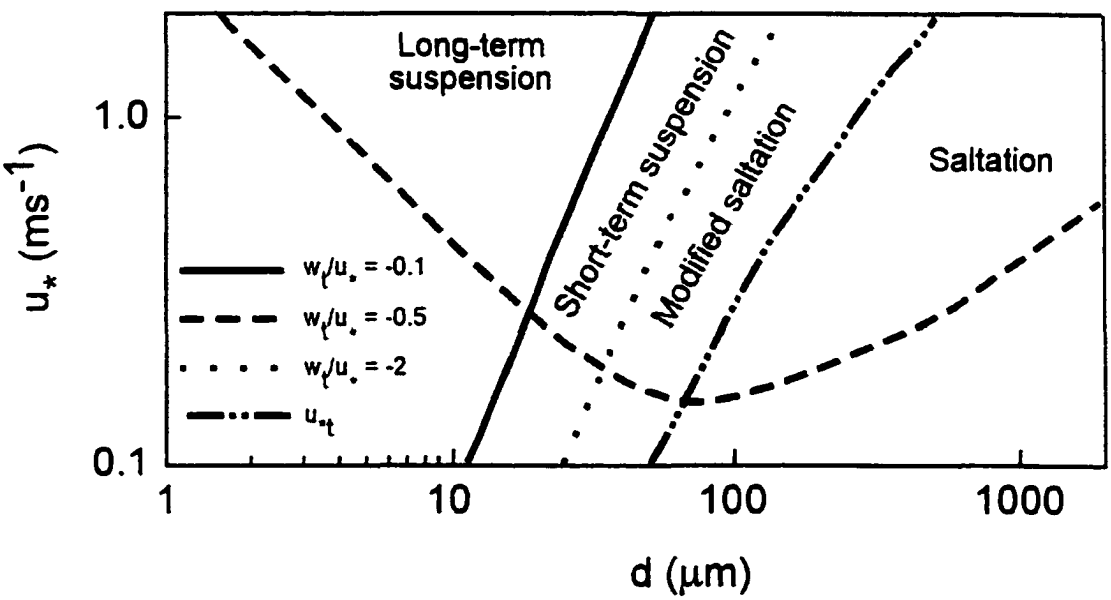

Figure 2-5 Relationship between flow conditions and particle motion (after Shao, 2000, with kind permission of Kluwer Academic Publishers).

Table 2-2. Diameter types, symbols, and definitions used in this study.

Diameter Type	Symbol	Definition
aerodynamic diameter	d_a	equivalent diameter of a unit-density sphere (1 g cm^{-3}) with the same aerodynamic properties as the original particle, e.g., settling velocity (Willeke and Baron, 1993).
equivalent spherical diameter; Stokes diameter	d_{st}	equivalent diameter of a sphere with the same density and Stokes settling velocity as the original particle, e.g., accounts for shape effects (Shao, 2000)
optical light scattering diameter	d_o	diameter based on light scattering properties of individual particles calibrated to the response of nominal unit density polystyrene latex spheres of standard sizes.
sieve diameter, geometric diameter	d_{sieve}	width of minimum square aperture through which a particle will pass (Shao, 2000); doesn't account for shape or density.

Particles of different shapes, but equal Stokes diameters and equal densities, will have the same settling velocity. Soils typically have a specific gravity greater than one, so for a soil particle, $d_a > d_{st}$. The exact relationship between these two diameters depends on particle size. For this study with the size range of interest for particles generally larger than 1μm aerodynamic diameter, the relationship is

$$d_a = 1.61\ d_{st} \qquad \text{Eqn. 2-3}$$

where ρ_p = density of the soil particle, 2.6 g cm^{-3} for this study. This results in

$$d_a = (\rho_p)^{1/2} d_{st} \qquad \text{Eqn. 2-4}$$

The relationship between the geometric (sieve) diameter and the Stokes

diameter was determined empirically to be

$$d_{sieve} = 0.033 (d_{st}^{1.7068}) \quad \text{Eqn. 2-5}$$

or

$$d_{st} = \left(\frac{d_{sieve}}{0.033} \right)^{(1/1.7068)} \quad \text{Eqn. 2-6}$$

with a r^2 value of 0.995 for glass spheres (Gillette and Chen, 1999). For particles of geometric size less than 100 μm, $d_{st} / d_{sieve} > 1$, while for particles of geometric size greater than 100 μm, $d_{st} / d_{sieve} < 1$. In this dissertation, aerodynamic diameters are used in comparisons of results from multiple methods, while customary diameters are used in discussions pertaining solely to one measurement technique.

Methods for Sampling Airborne Dust

Four methods were used to characterize airborne dust at the JER. The sampling approaches can be classified in a number of ways (Table 2-3). Integrated sampling collects a combined sample over a specific time interval such as a dust storm. These bulk samples can be further characterized, for example as in this study, by particle-size analysis. Continuous sampling provides time-resolved information over the same time period, by making recurring measurements at a fixed time interval. Continuous dust sampling was performed using battery-powered instruments that rely on light-scattering from particles to estimate ambient concentrations. These methods are discussed further below.

Table 2-3. Performance characteristics for the airborne particle samplers and monitors used in this study.

Instrument	**BSNE**	**DustTrak™**	**GRIMM™**	**Sensit™**
Measurement method	gravimetric	light scattering for concentration	light scattering	particle kinetic energy
Measurement type	integrated sample with lab analysis	continuous in situ	continuous in situ	continuous in situ for wind speeds above 5 ms^{-1}
Sampling interval	3-5 days, depending on storms and sample collection schedule	1 minute average, 10 s time constant	1 minute	1 minute
Type of inlet	rectangular opening in flow-through chamber	1.2 m Tygon™ tubing with end pointed into wind; with PM_{10} impactor inlet	GRIMM™ standard probe with isokinetic inlet	none
Flow rate (l/min)	not applicable	1.7	1.2	not applicable
Range of particle sizes sampled	< 500 µm geometric diameter	< 10 µm aerodynamic diameter (PM_{10})	0.5 µm to 20 µm aerodynamic diameter, including PM_{10}	> 50 µm geometric diameter
Calibration	standard weights for balance for weighing samples	ISO 12103-1 (Arizona Road Dust)	polystyrene latex standard reference spheres	drop tube of standard height with standard particles
Measurement height and location	fixed	portable, but fixed for this study	portable, as selected by user	fixed
Power source	none needed	batteries replaced every 10-12 hours	battery, recharged overnight	solar-powered battery

Integrated Sampling

Dust samplers, termed BSNEs, (the acronym is for Big Spring Number Eight) were configured with 5 collectors with openings at the standard heights of

5, 10, 20, 50 and 100 cm above ground (Figure 2-6). The collectors have an open inlet that is directed into the wind by an attached wind vane and a screened exit at the upper back (Fryrear, 1986). Once inside the sampler, the dust settles in a collection pan, for removal at a later time. Recent calibration studies have shown that the BSNE has an overall collection efficiency of 35-40%, independent of wind speed, for dust with a geometric median diameter of 30 μm (Goossens and Offer, 2000); and 40% efficiency for particles of geometric size <10 μm (Shao et al., 1993). In this study, the BSNE sampler data will be used to make relative, not absolute, determinations of airborne concentrations. Collectors are typically emptied into labeled plastic bags on a regular schedule, or as in this intensive study, emptied between dust storms. A small paint brush is used to completely brush the inside of the collector clean and move any remaining dust into the bag. Bags containing the sample are weighed using a calibrated balance, and the weight of the bag is subtracted. The sampler must be installed in an unobstructed location so the collector and vane can rotate freely. Because dust is only collected during storms, and sample collection takes place on calm days, the collection events are recorded by date only.

Continuous Sampling

Two continuous monitors were used in this study, the DustTrak™ Aerosol Monitor Model 8520 and the GRIMM™ Fine Dust Monitor Model 106.1. Both these instruments respond to light scattering from particles but they operate in different modes. The two systems are battery operated and both contain a sampling pump; optical system including a laser diode, focusing lenses, and

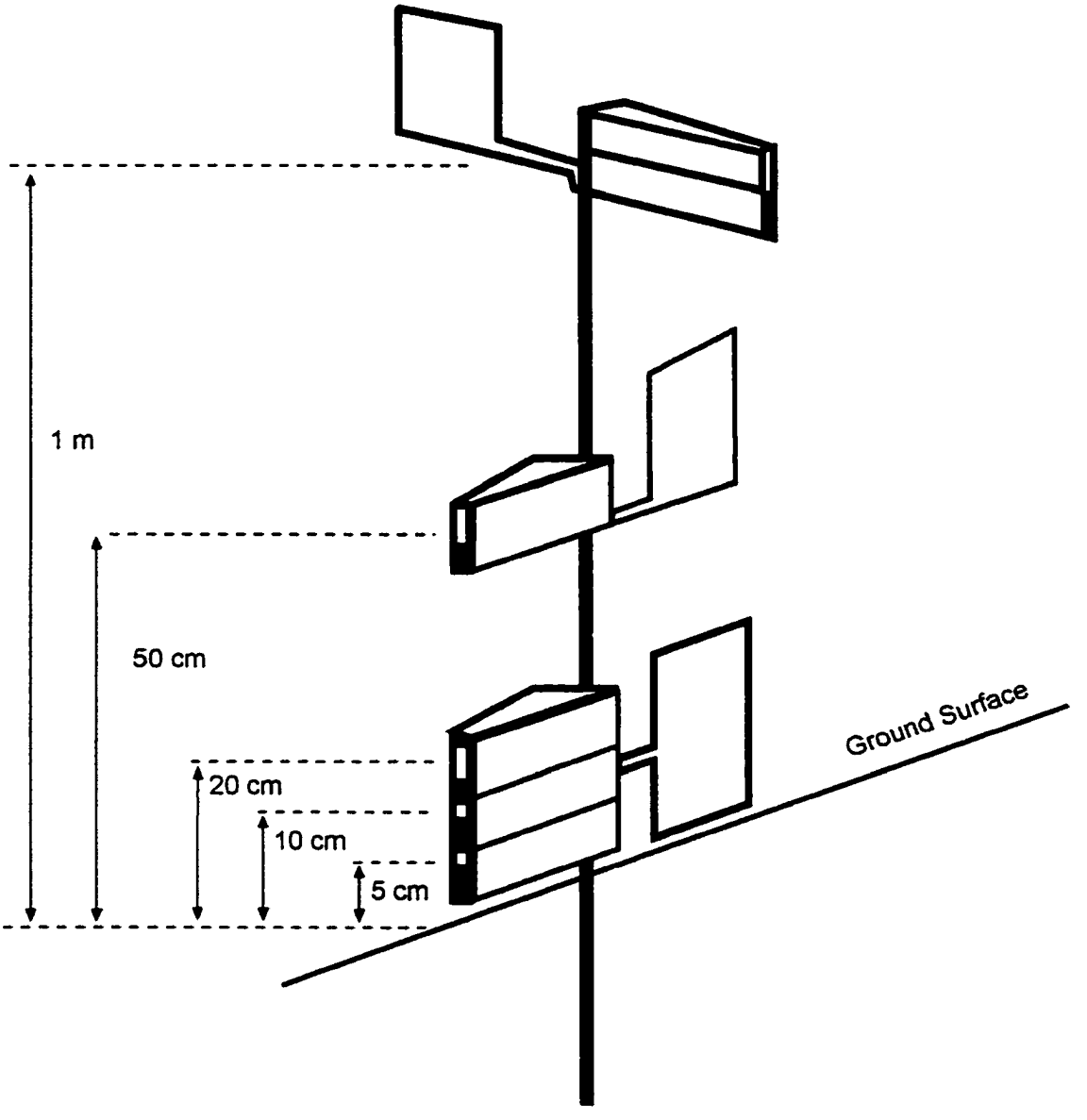

Figure 2-6 The BSNE dust samplers were configured with collectors at 5 heights.

photodetector; filtration system for generating sheath air to surround the optical elements and maintain their cleanliness; and digital data storage with data transfer protocols (Figure 2-7). In both cases, a beam of light shines through the sensing chamber, with the wavelength of the light determining the minimum particle resolution. The amount of light scattered by each particle is detected, and the response is determined by the amount of scattered light. The amount of scattered light depends on particle size, shape, and optical properties (Lehtimaki and Willeke, 1993); this information is interpreted according to the operating mode of the instrument.

The DustTrak™ operates in the photometer mode, responding to the bulk scattering of the particles present in the sampling chamber. The intensity of light assumes an assemblage of particles is present, with the size-distribution referenced to a calibration standard, measuring real-time particle concentration in mg/m^3 per minute (DustTrak™, 2000). An impactor inlet removes particles with an aerodynamic larger than 10 μm. Side-by-side studies with reference sampling methods have shown that the DustTrak™ data correlate well with data from the other methods, but overestimate particle concentration by factors of 2 to 3 for PM_{10} (Chang et al., 2001) and $PM_{2.5}$ (Chung et al., 2001; Yanosky et al., 2002). The GRIMM™ operates in the optical particle counter mode, diluting the sample air so that only one particle is passing through the sensing chamber per measurement. It is calibrated to attribute the intensity of light from each particle to a specific particle-size range, and accumulates this information, providing an

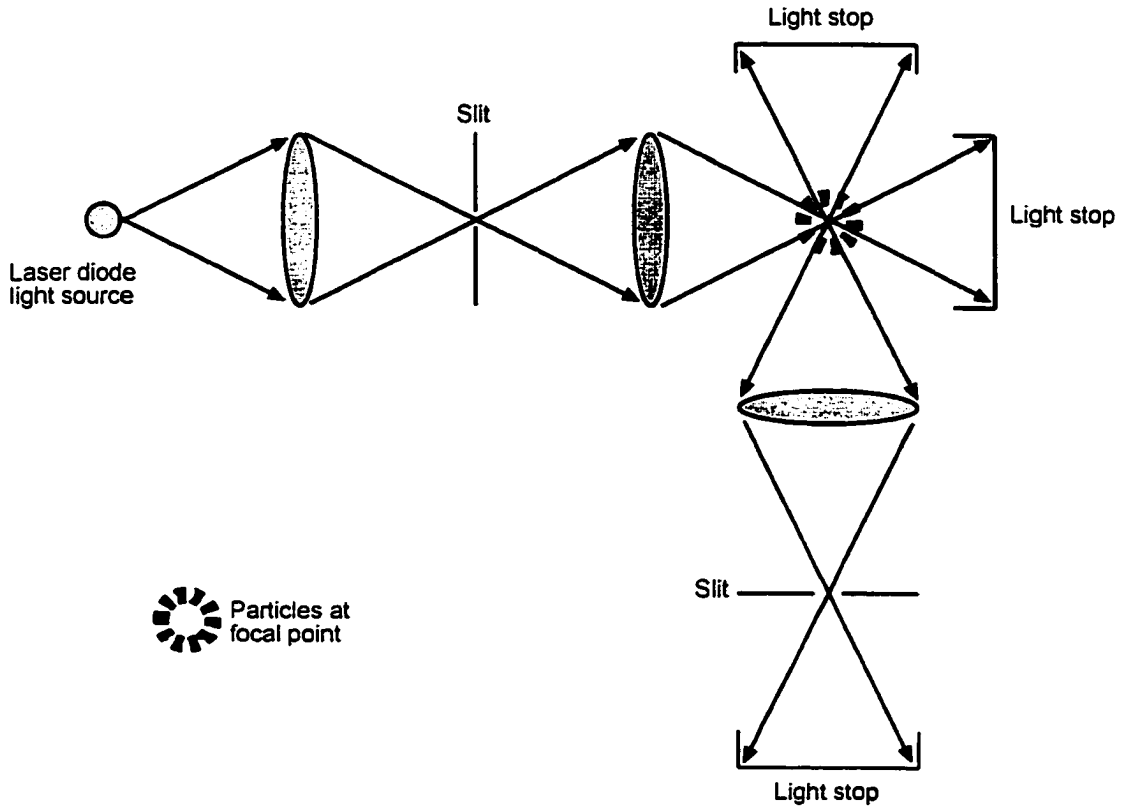

Figure 2-7 Generalized light-scattering detection system of the type used in the DustTrak™ and GRIMM™ monitors.

8-channel particle-size distribution in units of mg/m^3 for a period of one minute or longer as selected (GRIMM Labortechnik Ltd., 1996; Micallef et al., 1998). For this study, the DustTrak™ monitors provided continuous PM_{10} concentrations at fixed locations while the GRIMM™ was used briefly at several locations to gain an understanding of particle size distributions in different settings, maximizing the information obtained from the combination of the instruments.

The Sensit™ measures saltation activity by generating an electronic data pulse for each particle that impacts on a cylindrical piezoelectric crystal mounted vertically near the ground surface (Figure 2-8) (Gillette and Stockton, 1986; Stout and Zobeck, 1996). Data are recorded as average and maximum number of pulses as counts per minute. The Sensit™ is calibrated using a fall tube of known height and particles of known size and density. Impacts from particles of geometric size smaller than 50 μm are not detected (Sensit Company, 2002).

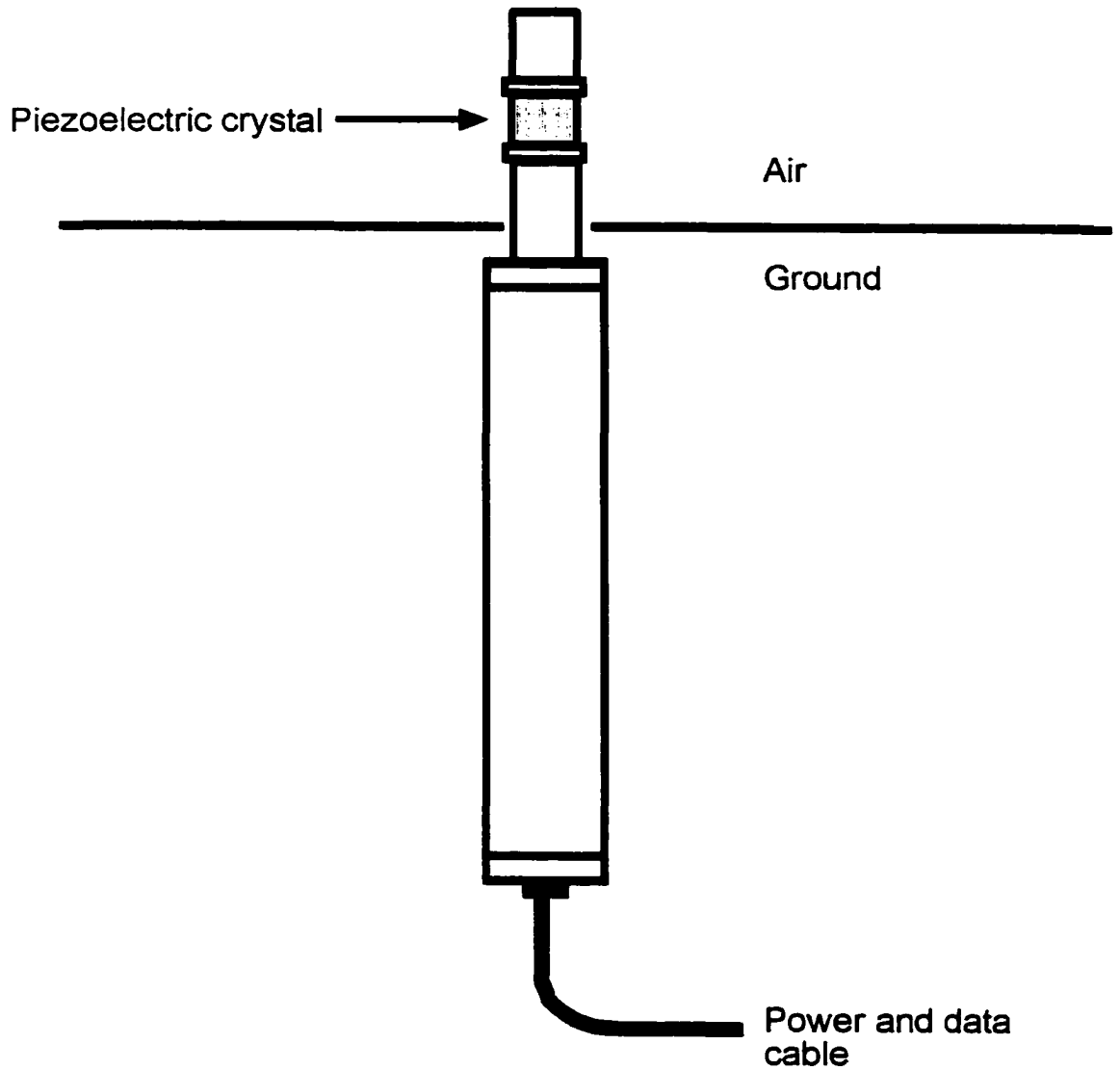

Figure 2-8 The cylindrical Sensit™ detects particle motion near the ground surface. The instrument is 2.54 cm in diameter.

CHAPTER 3

METHODOLOGY

The Methodology Chapter describes the steps followed in conducting this study. Some broader issues that were important during the study including availability of facilities and equipment, and quality assurance are also discussed.

Summary of Tasks

Tasks for accomplishing the study were developed by considering the research questions listed in Chapter 1, the available data from the LTER study, and the instrumentation and measurements that could supplement the available data. Five tasks resulted from this process, focused on producing the information to answer the questions (Figure 3-1). These tasks were:

1. Conduct field sampling during spring dust storms (2000);
2. Conduct laboratory analyses of selected soil and airborne samples (2000-2001);
3. Report the vegetation and soil analysis results (2001-2002);
4. Report the airborne sampling results (2001-2002); and
5. Develop flux models for the aerosol monitoring data (2002).

Tasks 1 and 2 were performed sequentially. The rest of the tasks proceeded in parallel. The details for each task are described in the chapter devoted to it.

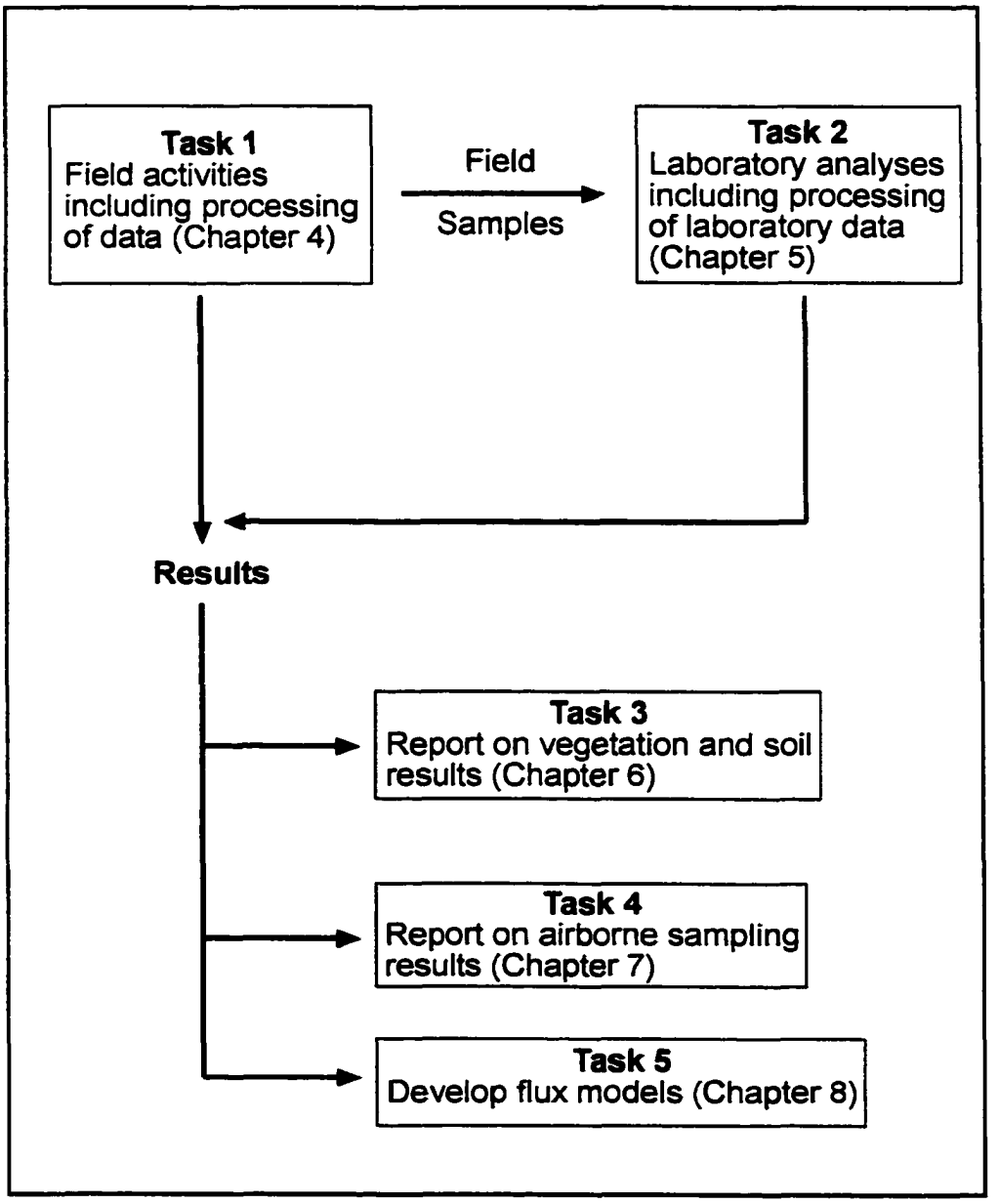

Figure 3-1 The relationships and sequence of the tasks in the study.

Facilities and Equipment

This study depended on using existing instrumentation and facilities at the JER, and at the U.S. Department of Agriculture Big Spring laboratory and fitting the work into existing schedules. In addition, all the equipment used was borrowed for the length of the study. One of the gratifying features of the study was the support received in terms of permission to use these field sites and laboratory facilities, in the loan of equipment for use in the field, and in coordination of schedules so the study could proceed in a reasonable time frame.

Quality Assurance

The quality of the measurements and analysis results was also a concern. This involved thoroughly understanding the scientific principles underlying the techniques being used, documenting procedures and following them consistently, and following maintenance guidelines for the instruments. Written logbooks were maintained for all types of measurements. Field sites and operating instruments were photographed. For continuous instruments, locations and serial numbers were tracked via structured assignment of data file names. For integrated samples, locations and sampling times were recorded using standard format bag labels and in the corresponding data file names. Data sets were duplicated and stored at independent locations. Software for processing data was checked, documented, and saved. Statistical analyses

were performed with widely used and validated SAS™ software. All these features contributed to the overall success of the study.

CHAPTER 4

FIELD SAMPLING

Field sampling for this study was conducted during April 2000. To become acquainted with the JER, the procedures for working there, and to prepare for the intensive April 2000 field work, preliminary site visits were made during 1997, 1998, and 1999. Some samples were collected during these visits; these samples were used as test samples to become familiar with the laboratory analysis procedures. The sections below describe the sites, samples collected, and measurements for the April 2000 field work. The findings of the dissertation are based on the samples and measurements from this field season.

Description of Sampling Sites

Sampling sites are first discussed in the context of area-wide topography, vegetation, and soils. Later in this Chapter, the monitoring sites are discussed from a measurement perspective. The four main monitoring sites for this study are located on a gently sloping plain at an approximate elevation of 1330 m. All the sites are part of the Long Term Ecological Research (LTER) wind erosion study and all the sites are fenced to exclude livestock. Three of these main sites are collocated with the LTER net primary productivity sites, sharing the same names as these sites: MNORT, MRABB, and MWELL (Figure 4-1). The

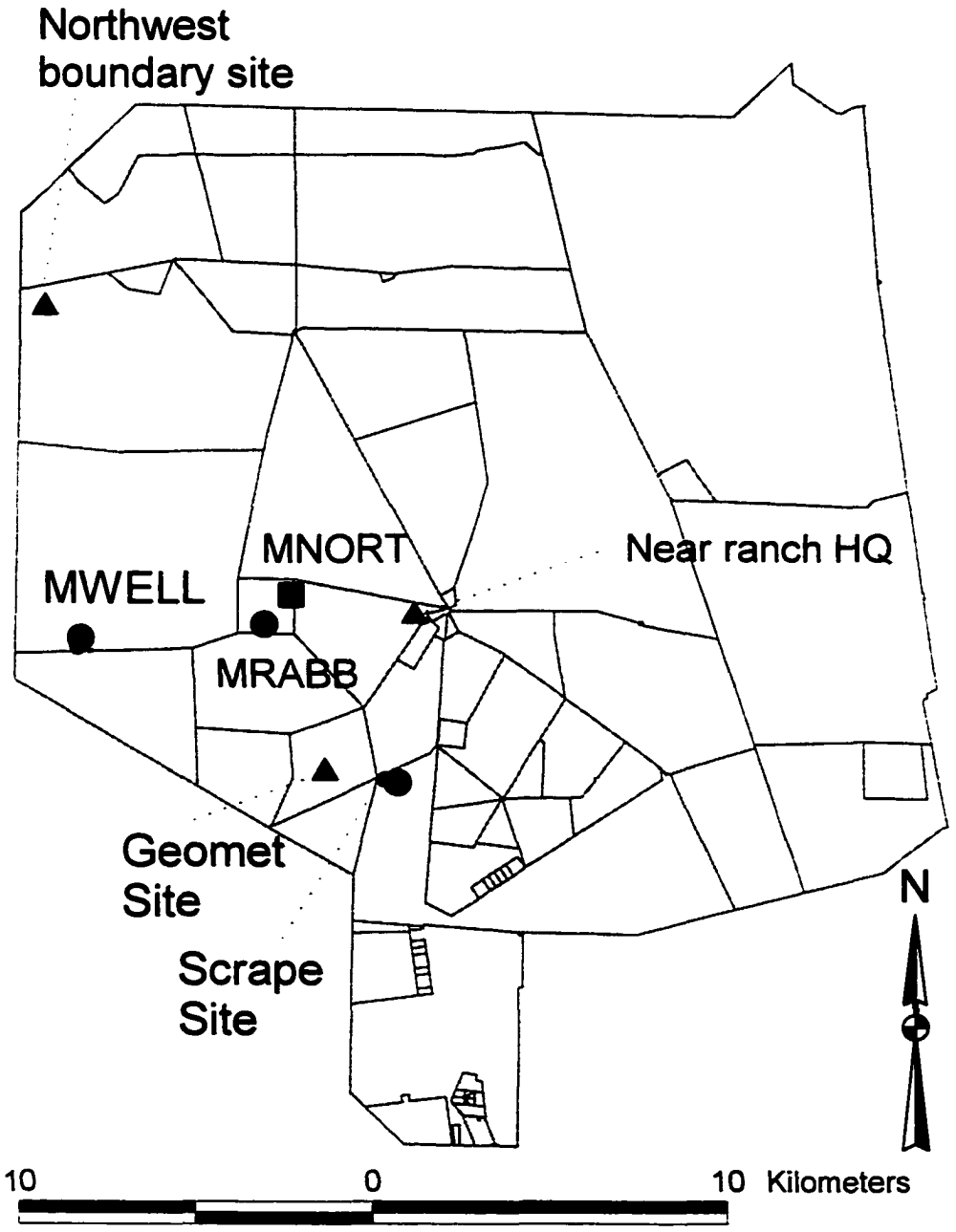

Figure 4-1 Three of the main study sites, MNORT, MRABB, and MWELL, are collocated with LTER net primary productivity sites for mesquite vegetation while the fourth, Scrape site, is a unique vegetation-free area. The triangles denote locations of GRIMM™ measurements conducted for short periods of time on April 18th (Geomet site) and April 19th (Northwest boundary site, Near Ranch HQ site).

naming convention for these sites designates the first letter "M" as the primary vegetation type, in this case, mesquite (Prosopis glandulosa). The remaining 4 letters designate a unique feature of the site, i.e., "NORT" is the northmost location of the mesquite sites; the "RABB" site is near the Rabbit well; and the "Well" site is near the West well site. The MNORT and MRABB sites are located within a historically-maintained grazing exclosure. The fourth main site, Scrape Site, is not a net primary productivity site as it has no vegetation. Measurements were made at all these sites during several dust storms. Three additional sites were sampled briefly to evaluate area-wide concentrations: Northwest Boundary site, Near Ranch HQ, and Geomet site (Figure 4-1). All these sites are located within areas of the JER where mesquite is the primary dominant vegetation (Figure 4-2).

When flying over the Chihuahuan Desert, the stippled appearance of the land indicates the presence of mesquite dunes (Figure 4-3). The bare areas between the dunes, termed "streets" by Gillette, 1997 (pers. comm.) appear much lighter than the dark stems and green foliage that mark the mesquite dunes. Of the all the sites, MNORT has the most clearly delineated streets and the greatest relief between the dune bases and the dune tops, typically 1 - 2 meters. The MRABB site is close to the MNORT site, but the vegetation is more lush; grasses and perennial plants are present in addition to the mesquite shrubs. The site has well-developed dunes. The MWELL site is the western-most of the sites, located on a limestone scarp in a different soil type; the soil

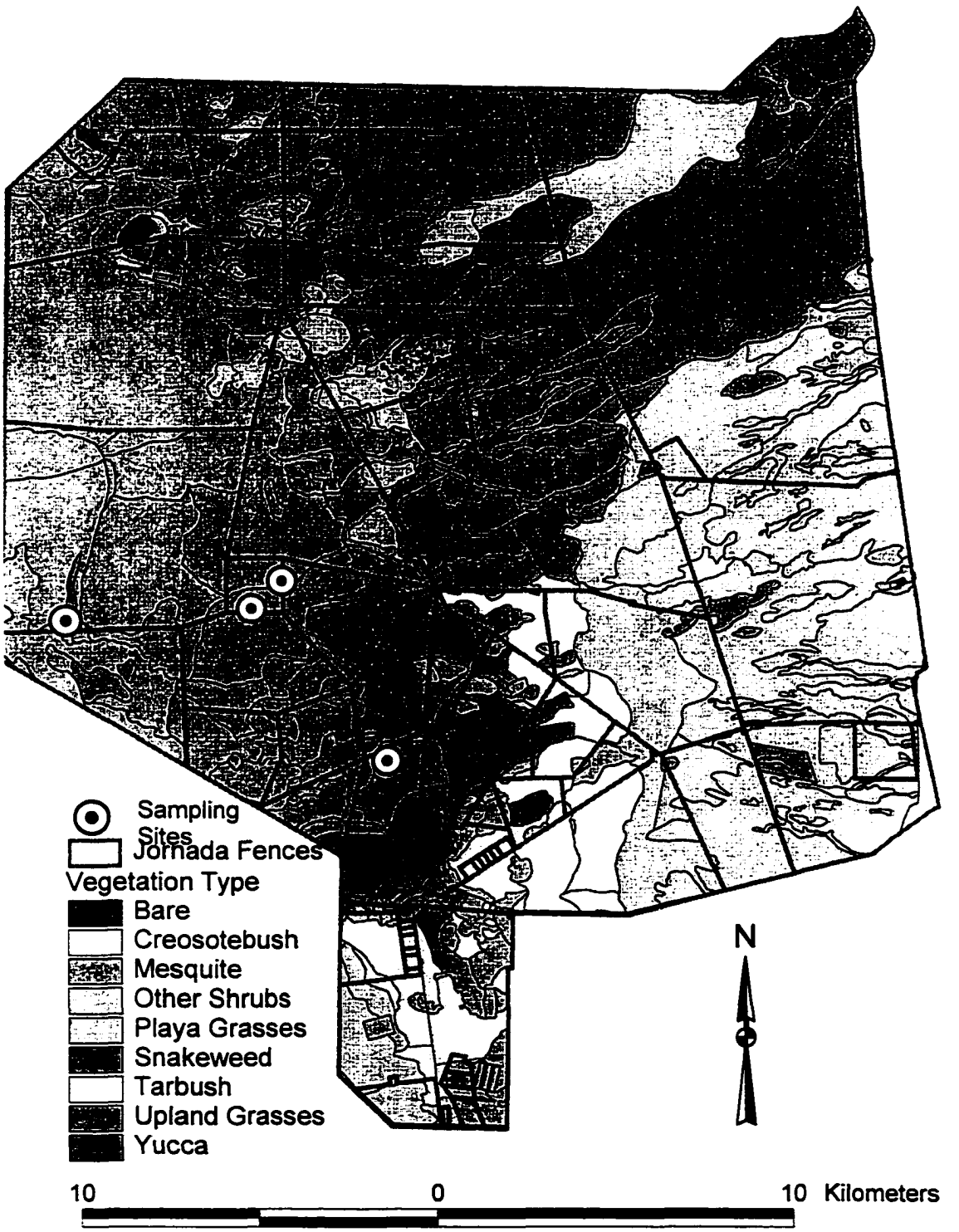

Figure 4-2 Much of the JER plain is dominated by mesquite (Prosopis glandulosa var. glandulosa) while creosote bush (Larrea tridentata) is common in the upland areas.

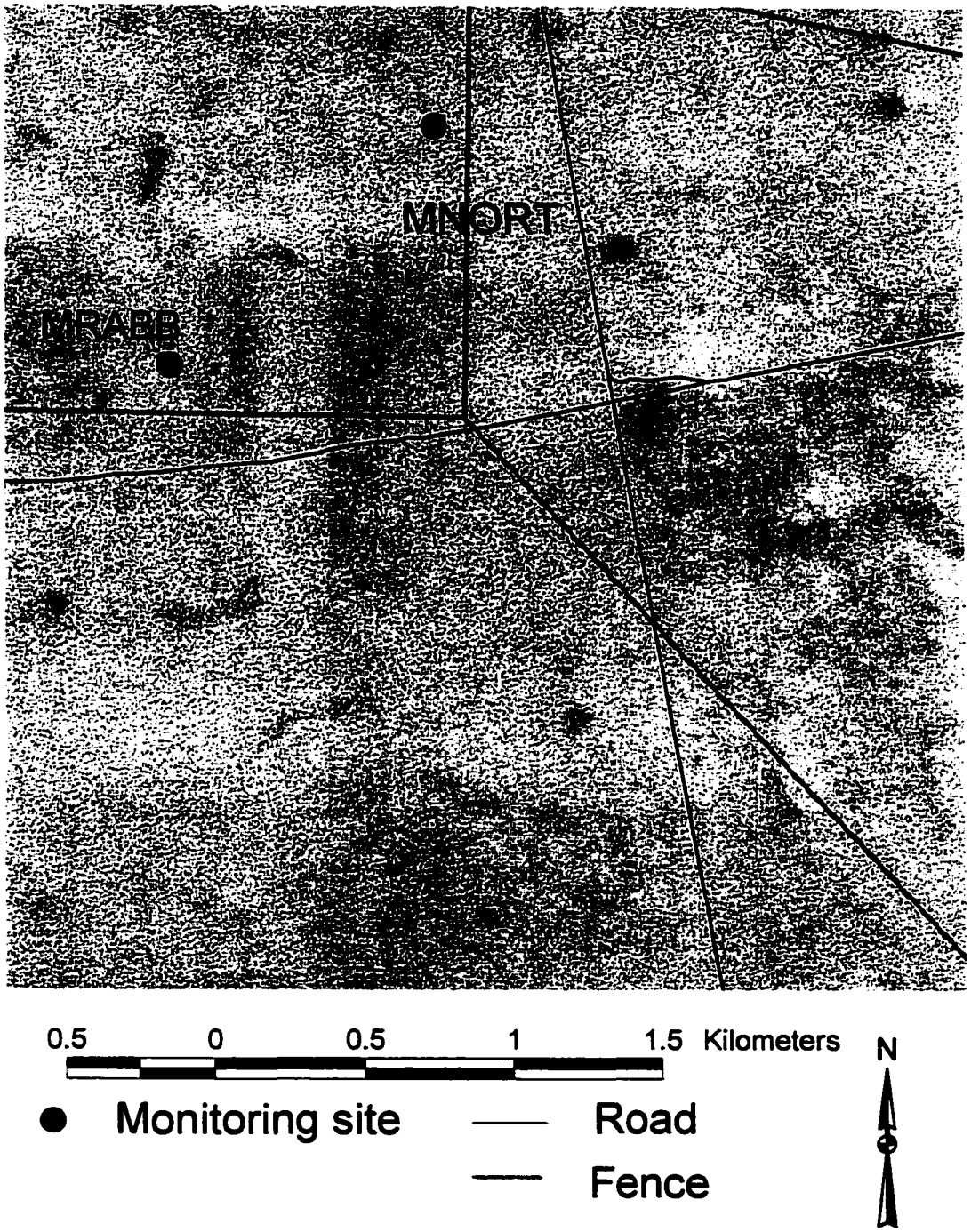

Figure 4-3 The mesquite dunes give the landscape a distinctive stippled appearance and cover extensive areas within the JER. This image was extracted from a larger digital orthophoto quarter quandrant (DOQQ) image with 1-m resolution (see Chapter 6).

appears to be shallower than at the other mesquite sites. While sand deposits are present at the base of the MWELL mesquite shrubs, the dunes typical of the MNORT and MRABB sites are not present. This may be due to the area being at an earlier stage of mesquite encroachment, or it may be due to a combination of factors that are less conducive to dune formation. In 1991, the Scrape Site was graded clear of vegetation and subsequently, it has been treated with a herbicide to maintain it in a vegetation-free state. It serves as a bare (no-vegetation) site for comparison to the more vegetated sites for wind erosion activity. The emissions from this site and the physical mechanisms that control the erosion at this supply-limited site have been described (Gillette and Chen, 2001).

Although the soil types in the JER have many features in common, a number of different soil series have been identified by the USDA Soil Conservation Service (now Natural Resource Conservation Service) and the four main sites are located within three different mapping units (Figure 4-4, Tables 4-1, 4-2). The MNORT and MRABB sites are located within the Onite-Pintura complex, while the MWELL and Scrape sites are located within the Berino-Bucklebar and Onite-Pajarito associations respectively. The terms "complex" and "association" have specific meaning in this context: a soil complex is defined as a map unit of two or more soils that occur in such a complicated pattern that they cannot be shown individually on a soil map at the selected scale, while an association is a group of soils that are geographically related in a distinctive repeating pattern and delineated as a single map unit. The soils in

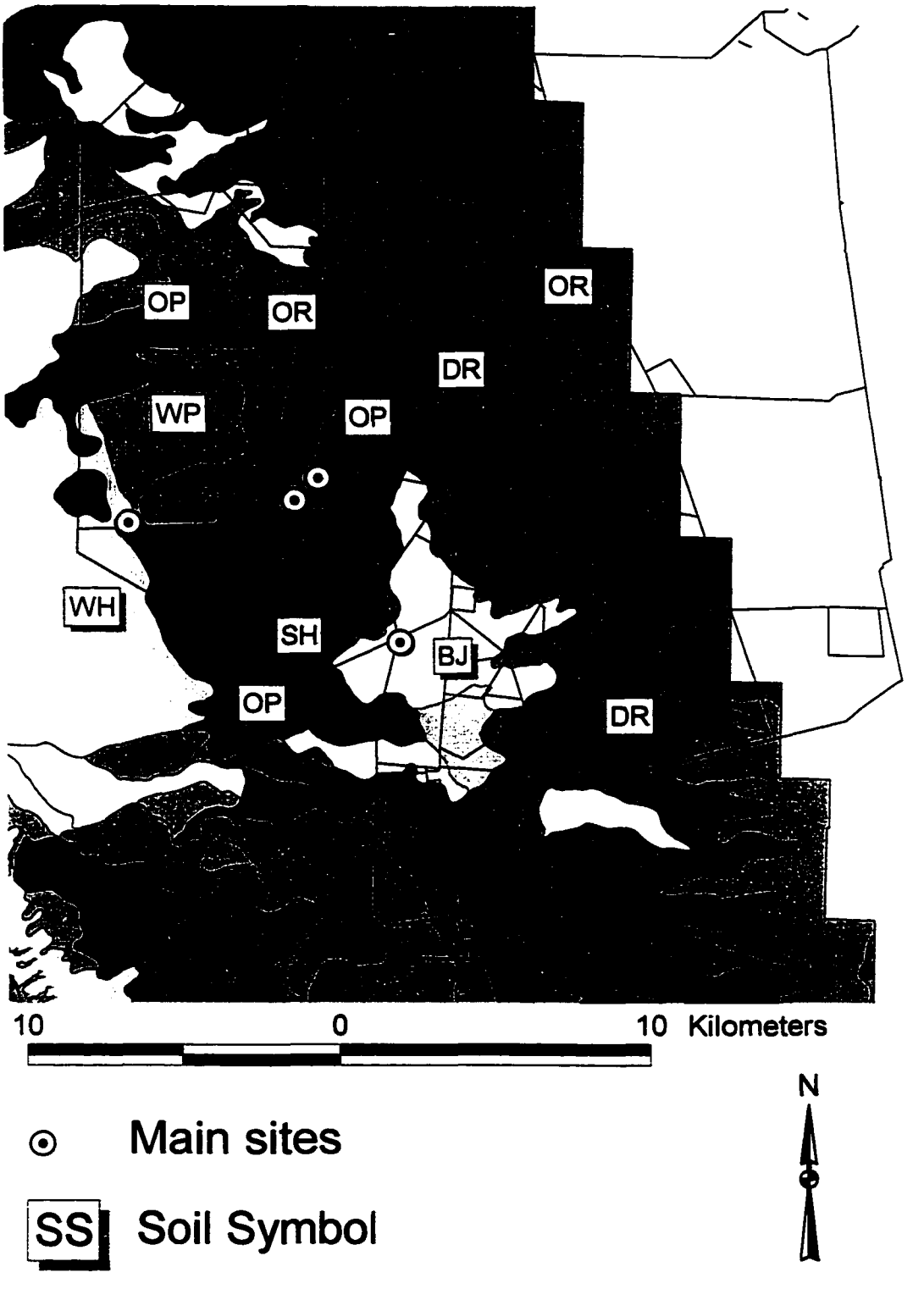

Figure 4-4 The main sites are contained within three different soil groups: Scrape Site–Berino-Bucklebar (BJ) Association; MWELL–Onite-Pajarito (OP) Association; and MNORT and MRABB–Onite-Pintura (OR) Complex.

Table 4-1. Soil Relationships for the main sites (after Bulloch and Neher, 1980).

Summary Information				Percentage less than geometric size of –			
Soil Name and Symbol	Depth of Upper Layer (cm)	USDA Texture	Unified Soil Classification	4.75 mm	2.00 mm	0.425 mm	0.075 mm
BJ: Berino-Bucklebar Association at Scrape Site							
Berino	0-10	Loamy fine sand	SM, SP-SM	95-100	95-100	50-95	10-35
Bucklebar	0-15	Sandy loam	SM, ML	95-100	95-100	60-85	30-55
Dona Ana	0-13	Fine sandy loam	SM	95-100	90-100	60-85	30-50
OP: Onite-Pajarito Association at MWELL							
Onite	0-13	Loamy sand	SM	100	100	50-95	15-35
Pajarito	0-20	Fine sandy loam	SM, SM-SC	100	100	85-100	30-45
Pintura	0-152	Fine sand	SP-SM, SM	100	100	70-95	5-25
OR: Onite-Pintura Complex at MNORT and MRABB							
Onite	0-13	Loamy fine sand	SM	100	100	50-95	15-35
Pintura	0-152	Fine sand	SP-SM, SM	100	100	70-95	5-25

Table 4-2. Descriptive information for map units (after Bulloch and Neher, 1980)

OR: Onite-Pintura Complex at MNORT and MRABB	
Onite Series	--Slightly to strongly calcareous (increasing with depth) loamy sand --The Onite series consists of deep, well-drained soils that formed in alluvium on fans. Onite soils have less than 18 percent clay. --Slopes are 1 to 5 percent.
Pintura Series	--Non calcareous, fine sand --The Pintura series consists of deep, somewhat excessively drained soils that formed in eolian material on broad fans. --Slopes are 1 to 5 percent.
BJ: Berino-Bucklebar Association at Scrape Site	
Berino	--Loamy fine sand with calcic horizon at depths ranging from 20 to 152 cm. --The Berino series consists of deep, well-drained soils that formed in alluvium modified by wind. The soils are on fans, piedmont slopes, and valley floors. --Slopes are 1 to 5 percent.
Bucklebar	--Sandy loam, non calcareous in the upper 0 to 8 inches, then calcareous below. --The Bucklebar series consists of deep, well-drained soils that formed in alluvium modified by wind on fans and coalescent fan piedmonts. --Slopes are 1 to 5 percent.
Dona Ana	--Fine sandy loam, calcareous throughout, slightly calcareous in the upper layers, depth to the calcic horizon ranges from 12 to 30 inches. This horizon is a zone of prominent lime accumulation. ---The Dona Ana series consists of deep, well drained soils that formed in mixed alluvium on fans and piedmonts. --Slopes are 1 to 5 percent.
OP: Onite-Pajarito Association at MWELL	
Onite	--Slightly to strongly (increasing with depth) calcareous loamy sand --The Onite series consists of deep, well-drained soils that formed in alluvium on fans. --Onite soils have less than 18 percent clay. --Slopes are 1 to 5 percent.
Pintura	--Non-calcareous, fine sand --The Pintura series consists of deep, somewhat excessively drained soils that formed in eolian material on broad fans. --Slopes are 1 to 5 percent.

these map units have been described in detail (Bulloch and Neher, 1980). Comparing the uppermost soil layers, the Bernino-Bucklebar association at Scrape Site is comprised of soil series that are calcareous or have a calcareous horizon. This is consistent with findings that identified this site as supply-limited (Gillette and Chen, 2001). The soils at the Scrape site have more coarse material than the other sites and somewhat more fines. However, if the Pajarito series predominates at MWELL, then it would have the most silt/clay among the 4 sites. The amount of silt and clay is important because it has a higher threshold friction velocity than fine sand, and may bind the soil particles into larger, less erodible aggregates. At MNORT and MRABB, the uppermost layer of the Pintura soil series is over 150 cm deep and consists of non-calcareous fine sand. This soil series would likely be supply-unlimited in the wind erosion context and this may explain the difference in the heights of the sand dunes, comparing MNORT and MRABB to the MWELL and Scrape sites.

Instruments and Measurements

The instruments, installation configuration, and measurements used in the study were standardized across all sites when applicable (Table 4-3). As part of the sampling for the LTER Wind Erosion Study, grids with a randomly chosen origin and cells 10 m x 10 m in size were established at each of the main sites. The nodes of the grid were identified with letters in the east-west direction (A, B, C, D) and with numbers in the north-south direction (1, 2, 3, 4, 5). Dust collectors were installed at each of the nodes, except if a substantial amount of

vegetation was present. For example, when a node occurred in a sand dune covered with mesquite bushes, dust collectors were not installed there since these collectors are designed to rotate freely in the wind. The MNORT site was the most intensively monitored location during this study (Table 4-3 and Figure 4-5), with a grid of 14 sand collectors, 1 meteorological tower, 5 masts with wind sensors, and for the intensive, aerosol monitors upwind, on top, and downwind of one mesquite dune. The MNORT site also had a Sensit™ for measuring particle saltation. The MRABB site was instrumented with a grid of sand collectors and meteorological instrumentation including a Sensit™ (Figure 4-6), but a data logger malfunction prevented the recovery of the meteorological and Sensit™ data during the intensive. At the MRABB site, it was not possible to place collectors at many of the grid nodes, so 9 sand collectors were present out of a possible 16. The MWELL site was instrumented with a grid of 15 out of a possible 16 sand collectors (Figure 4-7). The Scrape site was instrumented with three sand collectors for the intensive study period (Figure 4-8).

Table 4-3. Measurements conducted at the main sites during the Spring 2000 intensive; na means not available.

Site/ Measurement	MNORT	MRABB	MWELL	Scrape Site
Airborne sand collector at grid nodes with samples at 5 heights.	2/3 - 4/11 4/11 - 4/16 4/16 - 4/20	2/3 - 4/11 4/11 - 4/16 4/16 - 4/20	2/3 - 4/12 4/12 - 4/17 4/17 - 4/20	3/24 - 4/12 4/12 - 4/15 4/15 - 4/20
DustTrak™	two heights at 3 locations for 4/14 - 4/19	na	na	na
GRIMM™	1-minute averages at many locations during dust storms	na	na	na
Sensit™	4/14 - 4/19	na	na	na
Size distribution analysis for airborne sand	all periods at 5 and 100 cm heights	na	na	all periods at 5 and 100 cm heights
Tower Wind Speeds and Direction	4/14 - 4/19	na	na	na
Tower Temperature Gradient	4/14 - 4/19	na	na	na
Mast Wind Speeds and Direction	4/14 - 4/19	na	na	na
Soil samples	at internodes	at internodes	at internodes	at internodes

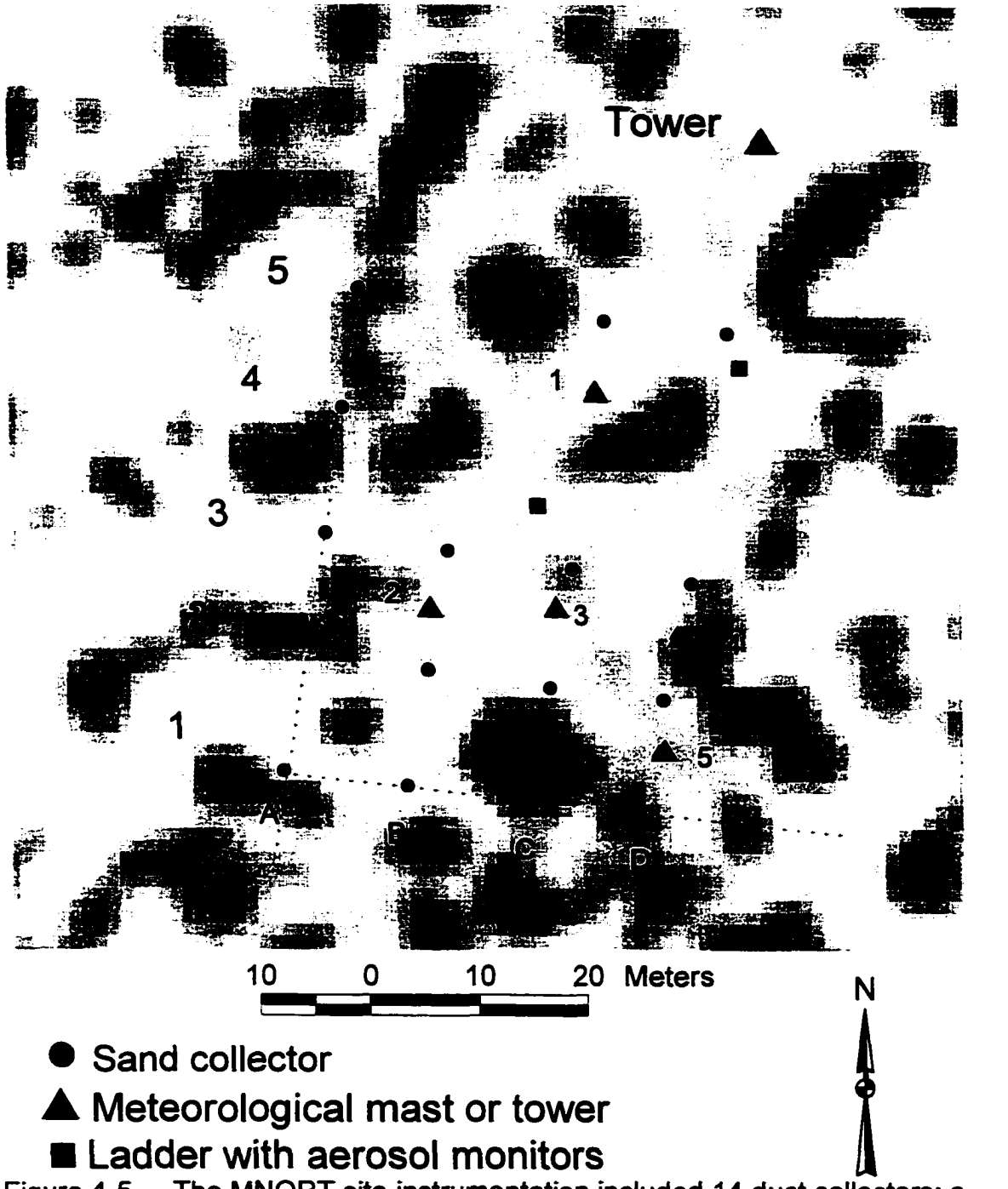

Figure 4-5 The MNORT site instrumentation included 14 dust collectors; a meteorological tower and 5 masts; a Sensit™; and aerosol monitors at three locations along the centerline of one mesquite sand dune. The background image is a digital orthophoto quarter quadrant (DOQQ, see Chapter 6) and the dark areas represent vegetation, mainly mesquite shrubs. The DOQQ resolution is one meter, seen as square 1-m pixels in the photo.

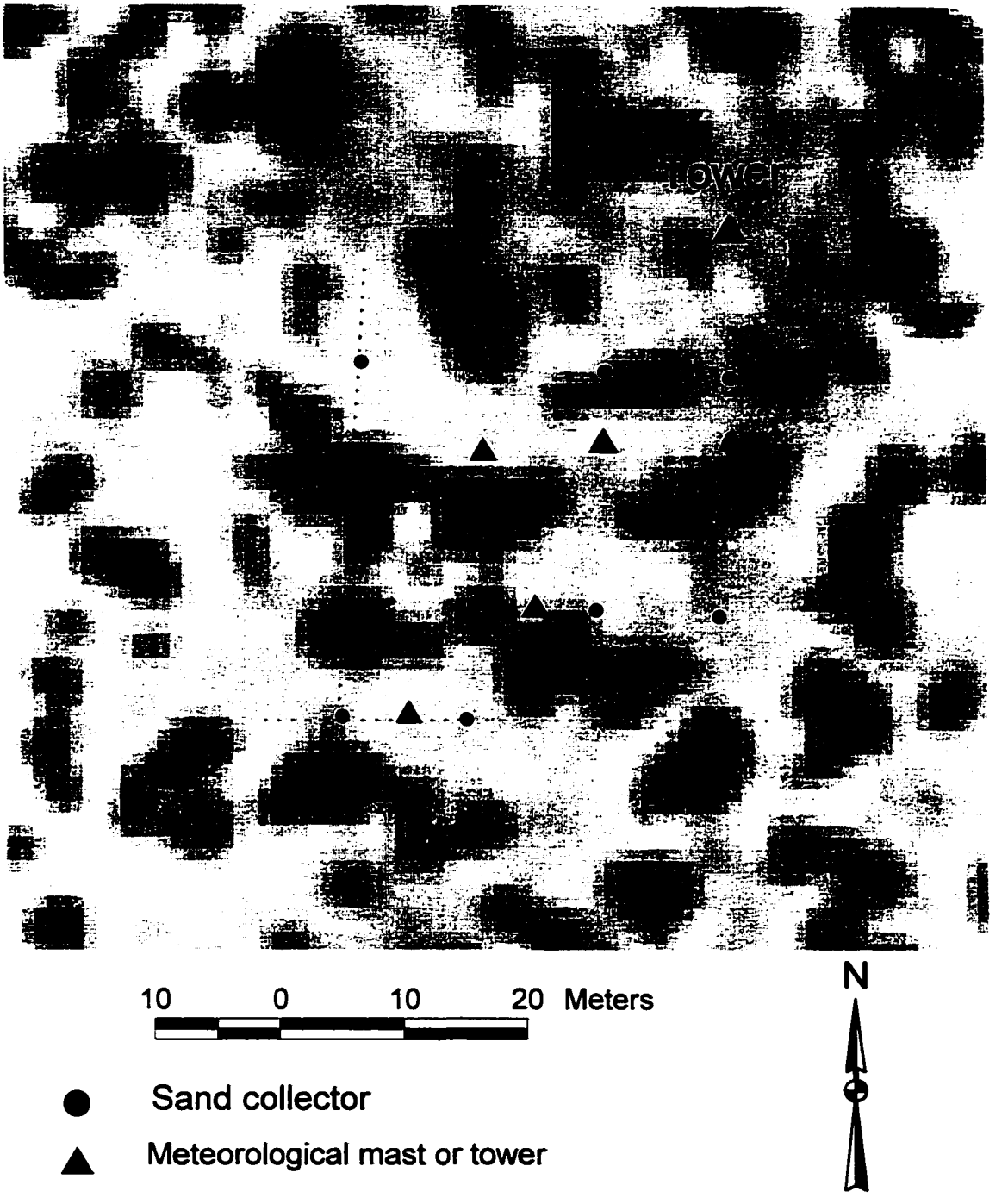

Figure 4-6 The MRABB site instrumentation included 9 dust collectors; a meteorological tower and 5 masts; and a Sensit™. The background image is a digital orthophoto quarter quadrant (DOQQ, see Chapter 6) and the dark areas represent vegetation, mainly mesquite shrubs. The DOQQ resolution is one meter, seen as square 1-m pixels in the photo.

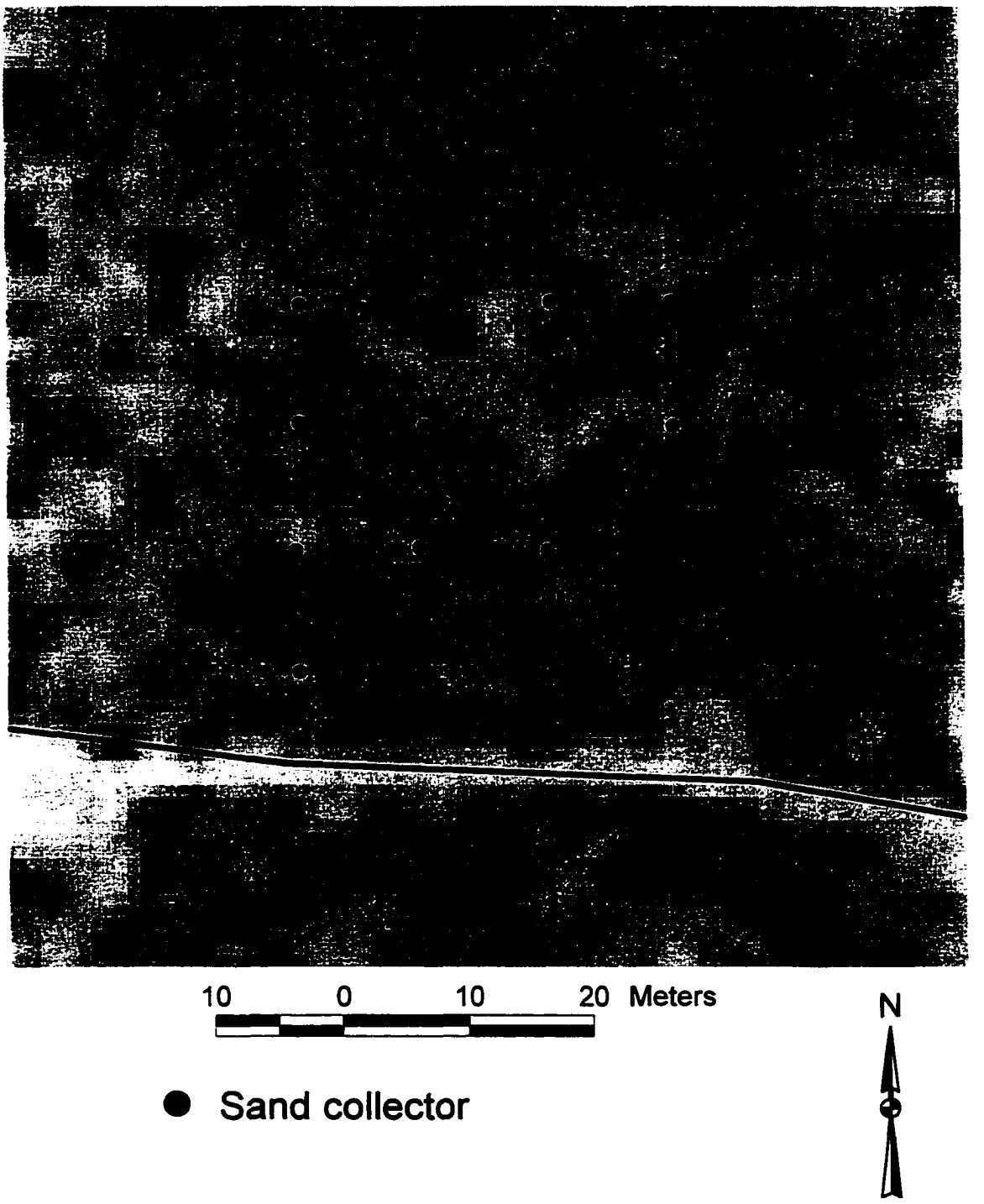

Figure 4-7 The MWELL site instrumentation included 15 dust collectors. The background image is a digital orthophoto quarter quadrant (DOQQ, see Chapter 6) and the dark areas represent vegetation, mainly mesquite shrubs. The DOQQ resolution is one meter, seen as square 1-m pixels in the photo.

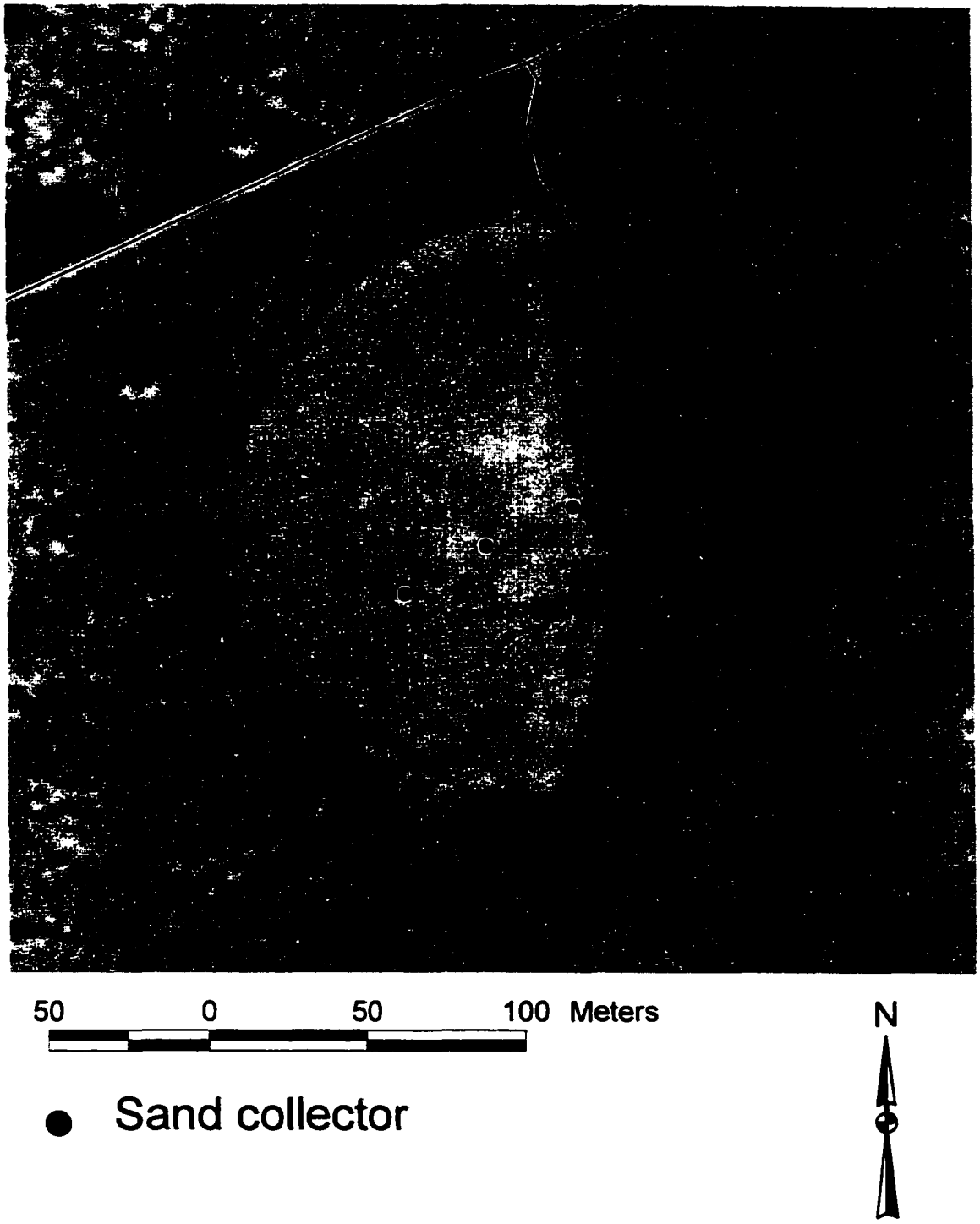

Figure 4-8 The Scrape site instrumentation included 3 dust collectors aligned along the dominant wind direction. The background image is a digital orthophoto quarter quadrant (DOQQ, see Chapter 6) and the dark areas represent vegetation, mainly mesquite shrubs.

Dust and Soil Measurements

Dust Collectors

Samples were retrieved on three occasions from the existing dust collectors at all four main sites (Table 4-3), first to empty the samplers for the intensive period, then to sample two, 2-day storm sequences during the intensive period. All the samples were weighed and stored.

Continuous Dust Measurements

Continuous dust related measurements were conducted at the MNORT site with DustTrak™, Sensit™, and GRIMM™ instruments. Pairs of battery-powered DustTrak™ aerosol monitors were placed upwind, downwind, and on top of a large sand dune, aligned with the long axis of the dune (Figure 4-9). Ladders were used to support each pair of instruments; the ladders were anchored to the ground with stakes for stability (Figure 4-10). The DustTrak™ instruments were secured to the ladder steps with elastic cords. To place the intakes at the desired heights, 1.52 m lengths of Tygon™ tubing were connected to the instrument inlets. The tubing intakes were placed at two heights (1.5 and 3 m) using 2.54 cm diameter metal electrical conduit to support the tubing (Figure 4-11). Sharp bends in the tubing were minimized. The Sensit™ was located very close to and upwind of Mast 3 where it operated continuously during the intensive period, and recorded data when there was sand movement.

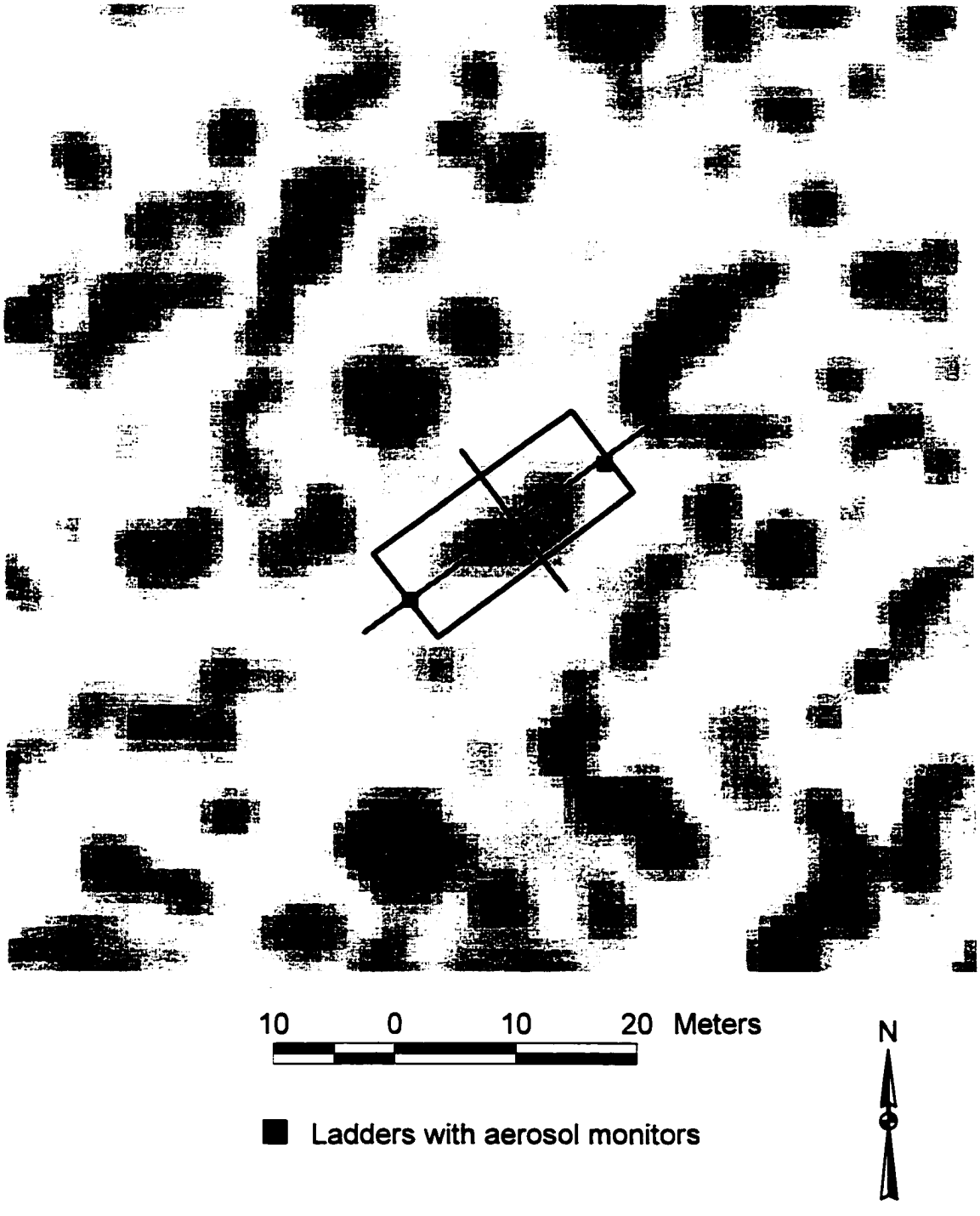

Figure 4-9 At MNORT, the ladders were aligned along the longer dune axis, at locations upwind, in the middle, and downwind of the dune. The background image is a digital orthophoto quarter quadrant (DOQQ, see Chapter 6) and the dark areas represent vegetation, mainly mesquite shrubs. The DOQQ resolution is one meter, seen as square 1-m pixels in the photo.

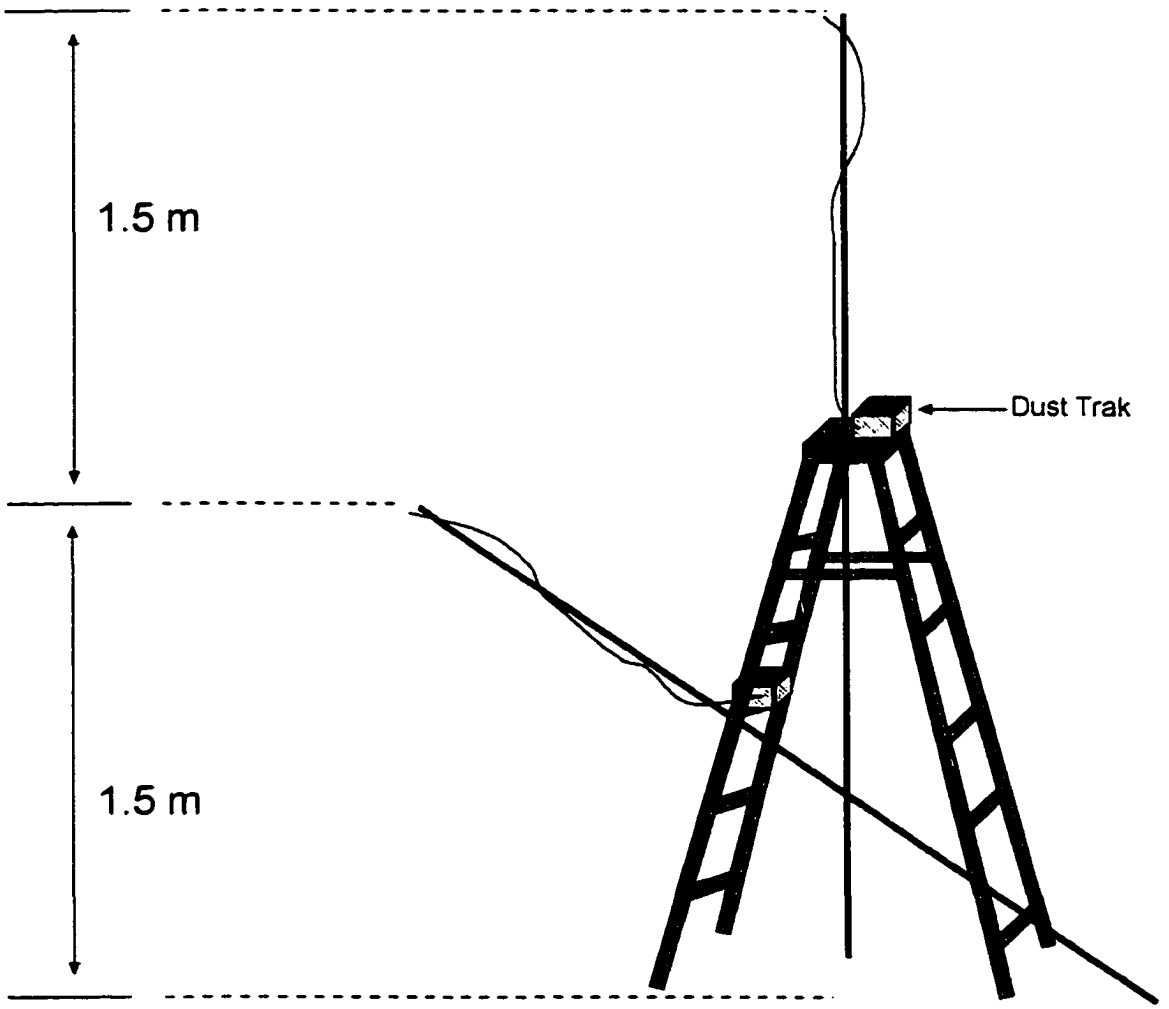

Figure 4-10 Each 1.8-meter-high ladder supported 2 DustTrak™ samplers. The ladders were secured by using duct tape and 0.6 m steel stakes pounded into the ground. The samplers were secured to the ladder with rubber cords.

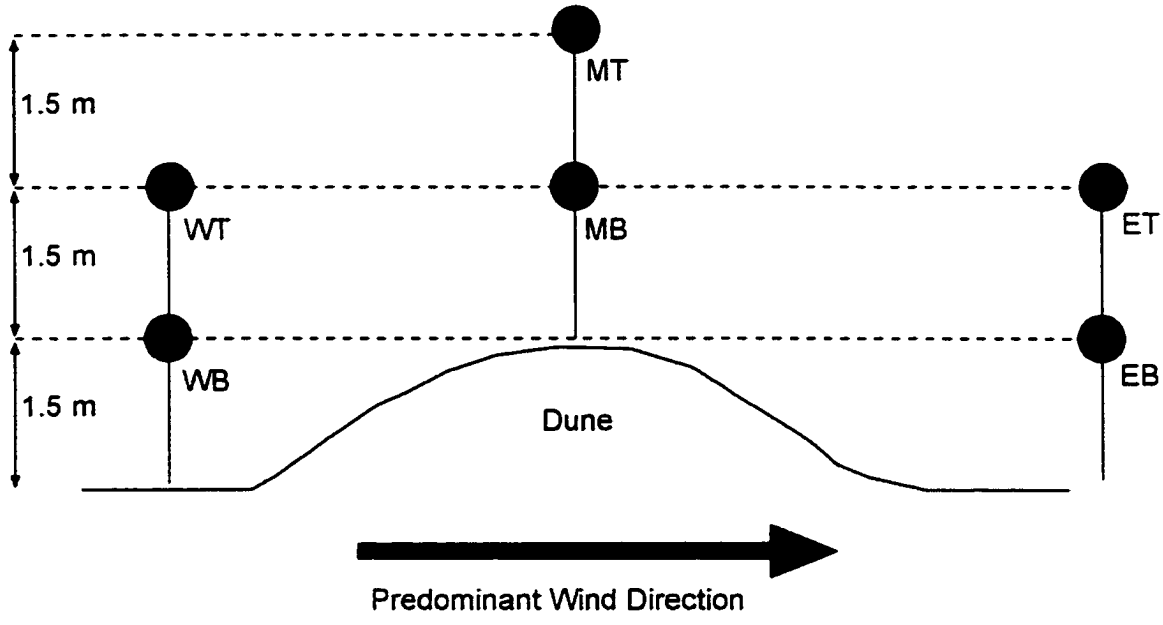

Figure 4-11 Because of the height of the dune, the DustTrak™ samplers were located at three different heights. Although the samplers appear to be aligned vertically in this figure, for each ladder, the lower sampler inlet was approximately 1 m further northwest than the upper sampler inlet. (See Figure 4-10)

The GRIMM™ was used as a portable analyzer during three dust storms and was briefly collocated with various BSNE locations, the DustTrak™ instruments, and selected bushes on the sand dunes. Measurements were conducted briefly with the GRIMM™ in the early evenings of April 18th at the Geomet site and of April 19th at the Northwest boundary, and Near ranch HQ sites.

Meteorological Measurements

Meteorological measurements of wind speed, wind direction, and temperature were made at multiple heights using a 15-m tower and a series of 3-m masts (Figures 4-12 and 4-13). These instruments were solar-powered and recorded data only when a 5 m/s wind speed threshold was exceeded by a wind speed sensor on one of the masts. The Sensit™ was operated on the same data acquisition circuitry and power supply as the masts.

Soil Sampling

Soil samples were collected from locations midway between the grid points, along the grid lines mentioned above. Samples were collected from the upper 1 cm of material using a trowel and dust pan. The 20-cm wide edge of the dust pan was placed at the sample location, and the trowel was used to lift off approximately 4 cm of material along the dust pan edge. Samples were stored in labeled plastic bags. Since there had not been any precipitation for several months, the samples were not dried. If a sampling location occurred in

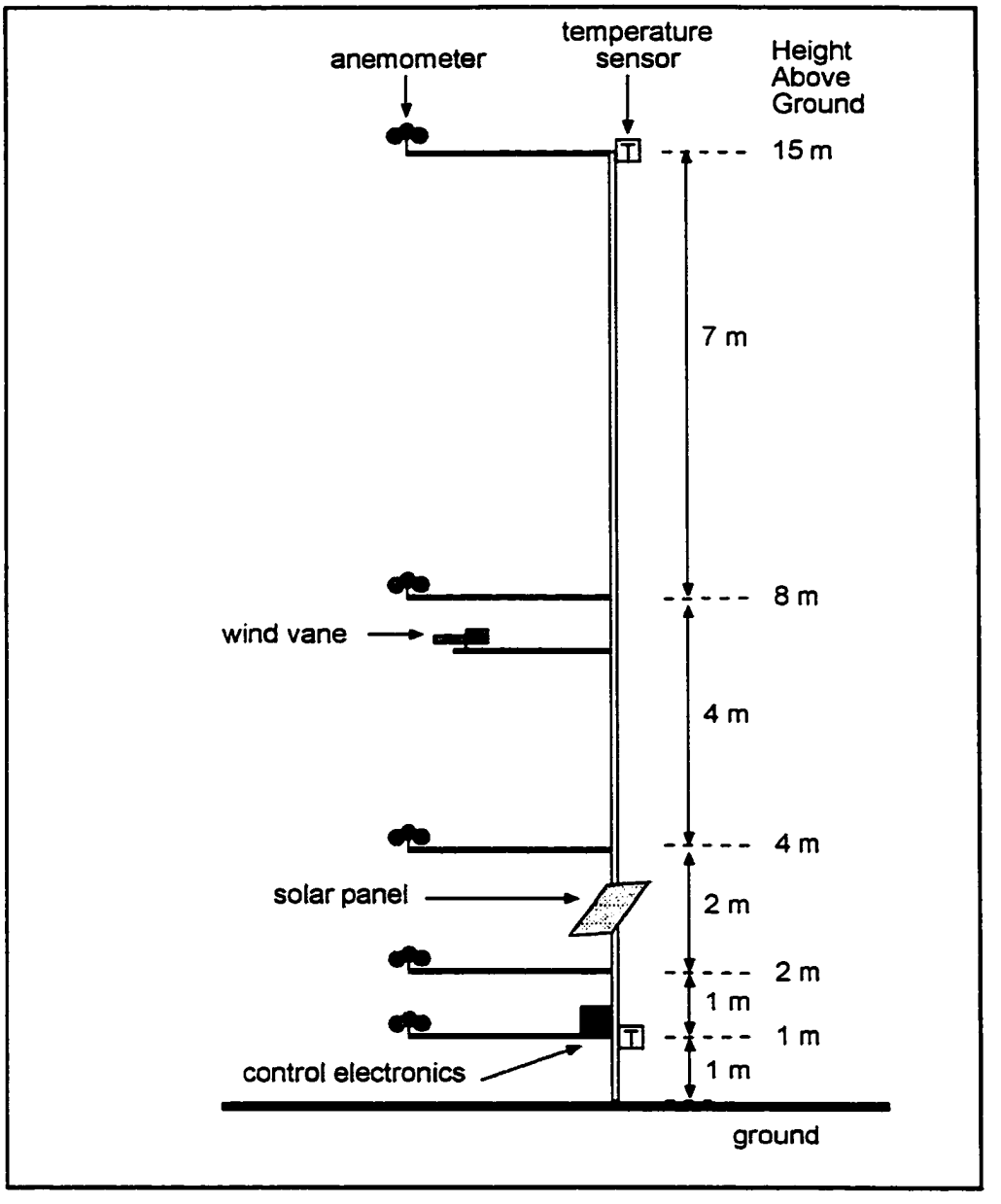

Figure 4-12 With its 15-m height and multiple wind speed measurements, the meteorological tower was designed for determining friction velocities.

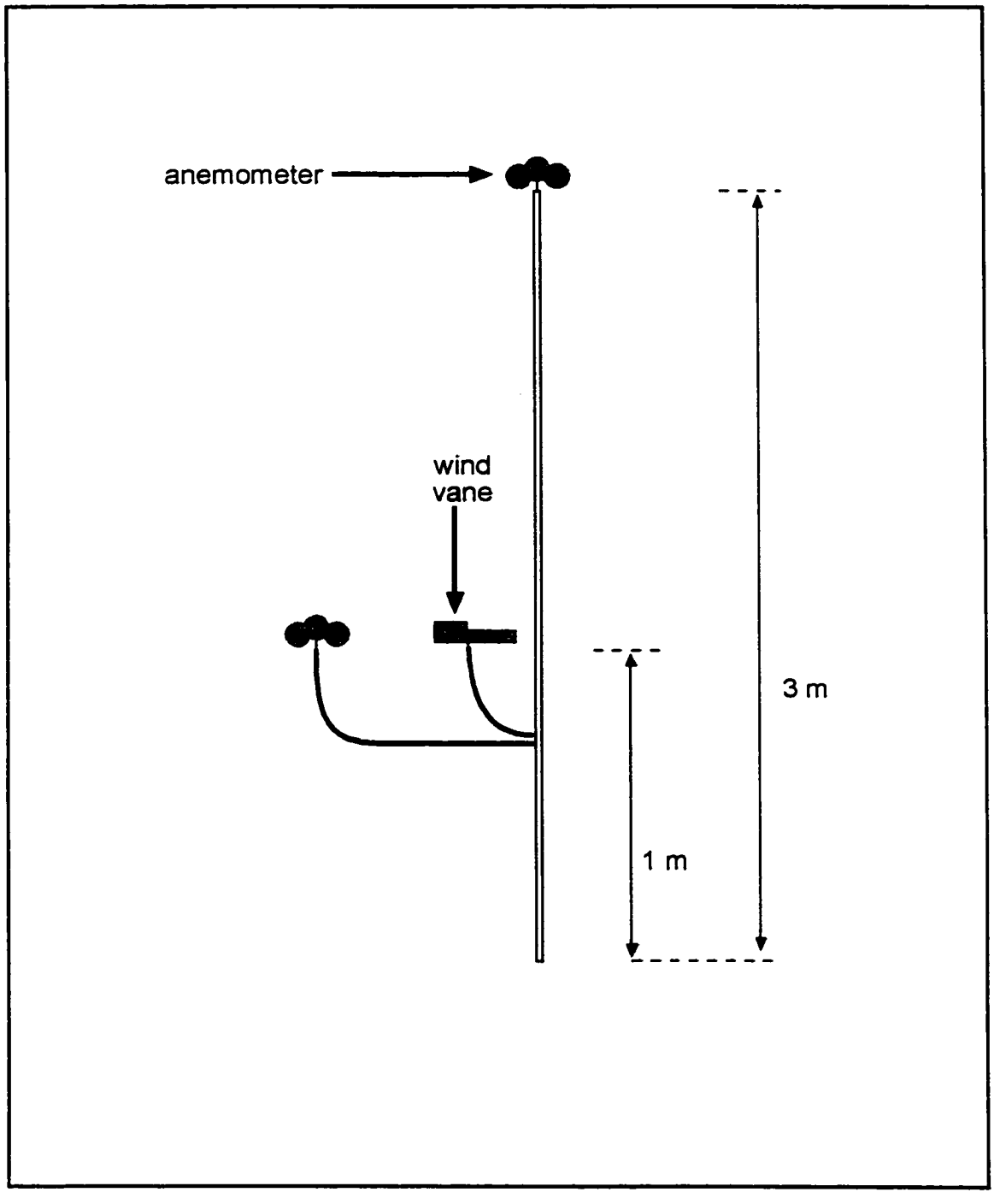

Figure 4-13 The meteorological masts were intended for understanding the microscale winds within the streets of the dune field.

a mesquite bush, the trowel was used to carefully lift out sections of soil and plant debris if present, to sample the equivalent area and depth of soil.

Data Preparation

Data were compiled in Excel™ and QuatroPro™ spreadsheets and checked for accuracy. The continuous monitors provided electronic output directly to spreadsheet formats and files were downloaded from the instruments and saved with descriptive file names. These files were then ready for analysis using the spreadsheets and using SAS™ statistical software.

CHAPTER 5

LABORATORY ANALYSES OF SOIL AND AIRBORNE PARTICLE SAMPLES

In making particle size determinations of soil and airborne particle samples, many options were available including geometric measurements using a microscope or sieves, light scattering measurements with an aerodynamically-calibrated optical particle counter such as the GRIMM™ (described earlier), or aerodynamic measurements. The aerodynamic approach was selected because among the available techniques, this approach accounts for the size, shape, and density of the particles. It is also the best approach for providing consistency with the DustTrak™ measurements (the DustTrak™ has a 10 μm aerodynamic impactor inlet). For this study, aerodynamically-based size determinations were performed at the U.S. Department of Agriculture, Agricultural Research Service's Big Spring Laboratory using their settling tube apparatus, called the Vertical Settling Aerosol Tube (VSAT). A settling tube measures times for sample particles to fall a known distance (Cui et al., 1983; Malcolm and Raupach, 1991). These travel times are then converted into particle sizes using the equations of motion and terminal velocities for equivalent-sized spheres of the same density. Samples analyzed with the VSAT are analyzed with their aggregates intact, and a broad range of equivalent geometric particle sizes is measured, from 10 to 500 μm with one analysis. As

explained earlier, these aerodynamically-based measurements can easily be converted to aerodynamic diameters consistent with other aerodynamic measurement methods. The apparatus, theory and data analysis procedures, and data quality are discussed below.

Apparatus

The most obvious feature of the VSAT was the 2-story tall closet that contained an unsealed, vertical Pyrex™ glass tube, or column, 6.2013 m in height (Figure 5-1). Mercury thermometers were located at the top, middle, and bottom of the column. Ambient pressure was measured with a mercury barometer 1 m above the base of the column. Relative humidity was measured at the top and bottom of the column. (For relative humidities less than 50%, the effect of humidity on air viscosity is negligible.) To perform a measurement, a sample was prepared by splitting the bulk sample using a precision microsplitter to create an aliquot of 0.03 grams that was placed on the release mechanism at the top of the tube. The release mechanism consisted of a glass microscope slide positioned on a small wooden shelf. The slide extended over the lip of the tube and was connected to a solenoid on the end of the slide opposite the tube. A stationary safety-type razor blade was positioned on top of the glass slide, held vertically by a brace. The process was initiated by pressing a button that retracted the slide and simultaneously signaled the computer to start recording times and values from the high-resolution Sartorius™ balance at the bottom of

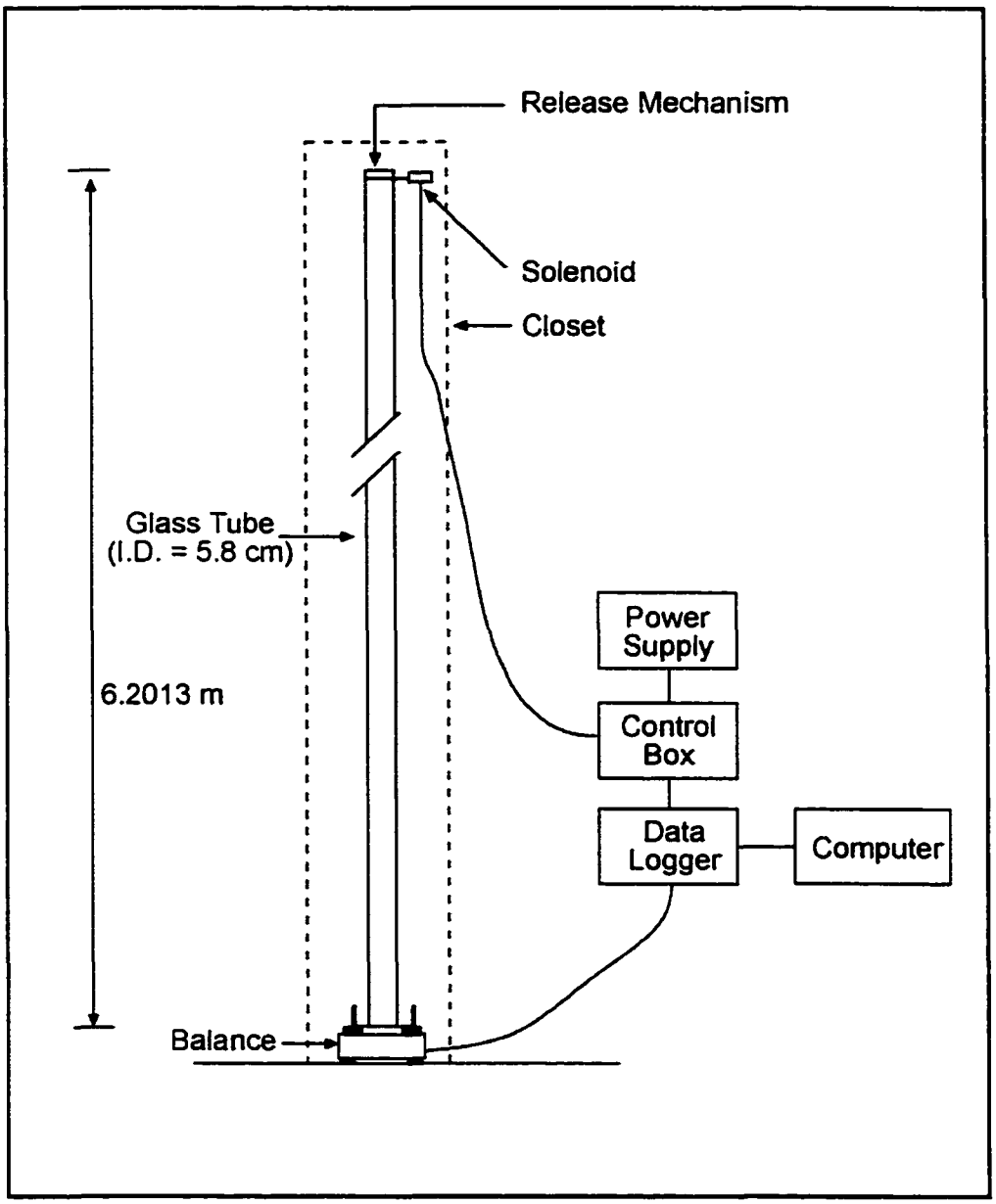

Figure 5-1 The Vertical Settling Aerosol Tube was located in a temperature-controlled closet. The glass fall column was not sealed although the top of the column was enclosed in a small box to prevent dust and turbulence from affecting the tests.

the column. The razor blade served as a scraper as the slide retracted under it, leaving the unsupported sample suspended at the top of the column. A Polonium radioactive source that emitted beta particles to neutralize static electricity was positioned on the release mechanism to minimize this effect on the particles. The particles soon reached their individual terminal velocities, and were collected sequentially in a tared metal cup placed on the balance at the base of the tube. Mass on the balance, steadily increasing as the particles reached the bottom of the column, was measured incrementally at 0.2 s intervals. Typical travel times for particles moving through the column ranged from approximately 2 to more than 800 s, depending on particle size and temperature (Table 5-1). The results of a test consisted of a list of times and weights (Figure 5-2a) that was compared to a list of travel times and equivalent particle sizes adjusted for ambient conditions at the laboratory (Figure 5-2b). These calculations were performed using the Computerized Data Analysis Algorithms (CDAA) explained in detail in the next section.

Table 5.1 Particle sizes and approximate travel times versus temperature for the VSAT for 36% relative humidity, 680.4 mm Hg, and particle density of 2600 kg m^{-3}, determined using CDAA. The typical temperature during the analyses was 25 °C; the other temperatures are provided for comparison.

Geometric particle size	***Travel time (s) 15 °C***	***Travel time (s) 25 °C***	***Travel time (s) 35 °C***
500 µm	5	5	5
100 µm	20	20	20
70 µm	30	30	31
50 µm	48	49	49
20 µm	198	204	210
10 µm	794	808	824

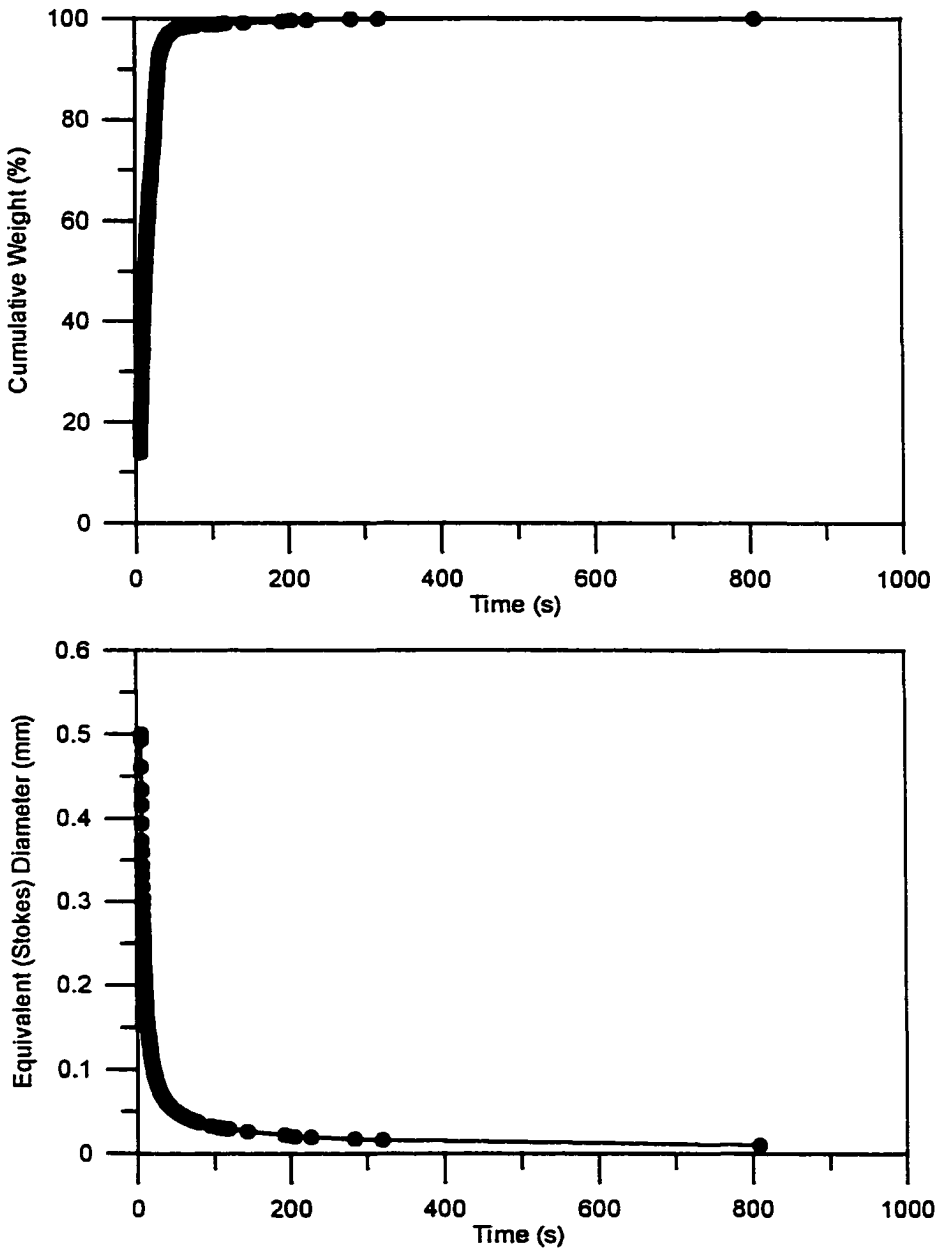

Figure 5-2 (a) Values of cumulative weight and time are recorded on a data acquisition system at 0.2 s intervals (not all data are shown). (b) Travel times for particles ranging in size from 10 to 500 μm are computed for spherical particles of the same density of the soil being characterized, and Stokes diameters are determined by matching the computed with the actual arrival times.

Theory and Data Analysis

The Computerized Data Analysis Algorithms (Appendix 1) were developed from the equation of motion for a particle falling in still air (Chen, pers. comm. 1998). Gravity, drag, and buoyancy are the forces acting on the particle (Roberson and Crowe, 1993; and Fryrear, W., J. Xiao, and D. Gillette, unpublished manuscript and pers. comm., 1998):

$$m\frac{d\vec{v}}{dt} = m\,g\hat{j} - m'\,g\hat{j} - \rho_a \frac{A}{2} C_d\, v^2 \frac{\vec{v}}{v} \qquad \text{Eqn. 5.1}$$

where

m = mass of particle, kg

v = vertical velocity of particle, m s^{-1}

t = time, s^{-1}

g = gravitational acceleration, m s^{-2}

m' = mass of air with the same volume as the particle, kg

ρ_a = density of air, kg m^{-3}

A = cross-sectional area of particle, m^2 and

C_d = drag coefficient for particle.

If the particle is a sphere, then the equation of motion is

$$\frac{d\vec{v}}{dt} = g\hat{j}\frac{(\rho_p - \rho_a)}{\rho_p} - \frac{3\rho_a C_d(\mathrm{Re})}{4\rho_p d} v^2 \frac{\vec{v}}{v} \qquad \text{Eqn 5.2}$$

where

ρ_p = density of particle, 2600 kg m^{-3} for these calculations

$C_d(\mathrm{Re})$ = drag coefficient as a function of Reynolds number and

d = diameter of sphere, m.

The Reynolds number is computed using

$$\mathrm{Re} = \frac{\rho_a v d}{\mu} \qquad \text{Eqn. 5.3}$$

where

μ = absolute viscosity (kg m^{-1} s^{-1})

and the other variables are previously defined.

This equation cannot be solved explicitly so it must be solved iteratively

$$\Delta v = (g(\frac{\rho_p - \rho_a}{\rho_p}) - \frac{3\rho_a C_d(\mathrm{Re})v^2}{4\rho_p d})\Delta t \qquad \text{Eqn. 5.4}$$

where

Δv = incremental increase in velocity

Δt = time increment, 0.001 s

The estimation process starts with $t = 0$ and $v = 0$ and the initial value was calculated. The next value was estimated from the first and so on, until terminal velocity was reached and $\Delta v = 0$ (Chen, pers. comm., 1998):

$$v(t+0.001) = v(t) + (\frac{dv}{dt})_t \qquad \text{Eqn. 5.5}$$

The position, z, of the particle was calculated in a similar manner, starting at z = 0 at the top of the tube, using

$$z(t+0.001) = z(t) + v(t)\Delta t + \tfrac{1}{2}(\frac{dv}{dt})_t \Delta t^2 \qquad \text{Eqn. 5.6}$$

The drag coefficient was estimated using

$$C_d = \frac{24}{\mathrm{Re}} \qquad \text{Eqn 5.7}$$

for Re < 1 and

$$C_d = \frac{24}{\mathrm{Re}} + \frac{3}{\sqrt{\mathrm{Re}}} + 0.3$$

for Re ≥ 1. Eqn. 5.8

Reynolds numbers during these tests vary widely depending on the particle size (Table 5-2). These calculations for position and velocity were repeated until the calculated z exceeded the length of the column, 6.2013 m. The computer algorithm changed the time step when the particle neared the bottom, to calculate the arrival time more precisely (Chen, pers. comm., 1998). These results were accumulated in a table that was compared with the actual arrival times recorded by the VSAT system. Particle sizes and percent of mass for each particle size were determined. The data were then summarized in a variety of ways including size distributions, mean particle size, and skewness and kurtosis of the size distribution. The size ranges used in the distributions were modified from the USDA soil texture size ranges and the sedimentologists' Phi scale (Pye and Tsoar, 1990). All the initial particle diameters were computed as

Table 5-2. Particle sizes, Reynolds numbers, and terminal velocities, determined using CDAA for 25 °C, 36% relative humidity, 680.4 mm Hg, and particles of 2600 kg m^{-3} density.

Geometric particle size	***Reynolds number***	***Approximate terminal velocity***
10 µm	0.0055	0.008 m s^{-1}
20 µm	0.042	0.031 m s^{-1}
50 µm	0.65	0.19 m s^{-1}
70 µm	1.53	0.32 m s^{-1}
100 µm	4.10	0.60 m s^{-1}
500 µm	125	3.65 m s^{-1}

computed as Stokes diameters and were adjusted to aerodynamic diameters for integration with the DustTrak™ and GRIMM™ data (Table 5-3). The nominal analytical range of the instrument was 10 to 500 µm for Stokes diameters and this corresponds to 16 to 806 µm for aerodynamic diameters for particles with a density of 2,600 kg/m^3. However, the presence of PM_{10} could still be estimated from these data distributions.

Data Quality

Traditional quality assurance approaches for environmental measurements generally address precision, accuracy, representativeness, completeness and comparability. In the VSAT context, precision, the amount of agreement among repeated measurements, was assessed by making and analyzing duplicates from the same bulk sample. Twelve samples were analyzed in duplicate, showing differences in the 10% range across the size

Table 5-3. Names for different mineral particle sizes less than 2 mm in various diameters; and corresponding d_a computed using Equations 2-4 and 2-5 ([1]Chen, pers. comm., 1998; [2]Pye and Tsoar, 1990; [3]Bulloch and Neher, 1980).

Name	VSAT Analysis [1] (d_{st}, mm)	Computed Aerodynamic diameter VSAT data (d_a, mm)	Sediment Scale [2] (Phi Units)	USDA Sizes [3] (d_{sieve}, mm)	Computed Aerodynamic diameter, sieved spheres (d_a, mm)
Very coarse sand (VCS)	2.000 to 1.000	3.2 to 1.6	-1 to 0	2.000 to 1.000	1.022 est. to 0.681 est.
Coarse sand (CS)	1.000 to 0.500	1.6 to 0.80	0 to 1	1.000 to 0.500	0.681 est. to 0.453
Medium sand (MS)	0.500 to 0.250	0.80 to 0.40	1 to 2	0.500 to 0.250	0.453 to 0.302
Fine sand (FS)	0.250 to 0.125	0.40 to 0.20	2 to 3	0.250 to 0.100	0.302 to 0.177
Very fine sand (VFS)	0.125 to 0.063	0.20 to 0.10	3 to 4	0.100 to 0.050	0.177 to 0.118
Silt	divided into three parts	divided into three parts	4 to 9	0.050 to 0.002	0.118 to 0.018 est.
Coarse silt (CSILT)	0.063 to 0.020	0.10 to 0.03	4 to 5.64	not identified separately	not identified separately
"VSAT PM_{20}"	0.020 to 0.010	0.03 to 0.016	5.64 to 6.64	not identified separately	not identified separately
"VSAT PM_{10}"	0.010 to 0.005	0.016 to 0.008	6.64 to 7.64	not identified separately	not identified separately
Clay	not included	not included	> 9	< 0.002	<0.018 est.

categories (Tables 5-4 a and b and 5-5). The differences in the values that were measured declined as the particle size decreased for both the cumulative frequency distribution and the particle size categories. This can be partially explained by the relative mass of the larger diameter particles compared to the mass of the sample. For example, a 1-mm diameter particle weighs 1/20 of the nominal VSAT sample, and several of these particles occurring in one sample

Table 5-4a. Differences, mean difference, and standard deviation of differences in cumulative size distributions for duplicate samples analyzed by the VSAT.

Duplicate Number	5% (mm)	16% (mm)	25% (mm)	50% (mm)	75% (mm)	84% (mm)	95% (mm)
1	0.24	0.23	0.18	0.09	0.06	0.05	0.04
2	0.22	0.25	0.26	0.28	0.29	0.02	0.01
3	-0.22	0.01	0.00	0.01	0.00	0.00	0.00
4	0.48	0.27	0.14	0.04	-0.01	-0.02	-0.03
5	-0.12	-0.02	-0.03	-0.02	-0.01	-0.01	-0.01
6	0.27	0.00	0.00	0.00	0.01	0.00	0.00
7	0.00	-0.01	-0.02	-0.01	0.00	0.00	0.02
8	-0.01	0.00	0.00	0.00	0.00	0.00	0.00
9	-0.01	-0.02	-0.01	-0.01	0.00	0.01	0.02
10	0.12	0.11	0.11	0.09	0.06	0.06	0.05
11	-0.09	-0.05	-0.03	-0.02	-0.01	-0.01	-0.01
12	0.21	0.16	0.14	0.11	0.08	0.07	0.06
Mean	**0.09**	**0.08**	**0.06**	**0.05**	**0.04**	**0.01**	**0.01**
Standard Deviation	0.20	0.12	0.10	0.09	0.08	0.03	0.03

Table 5-4b. Differences, mean difference, and standard deviation of differences in for mean size in Phi and millimeter units, standard deviation of mean size in millimeters, skewness, and kurtosis for duplicate samples analyzed by the VSAT.

Duplicate Number	Mean Size (Phi)	Mean Size (mm)	Standard Dev. (mm)	Skewness	Kurtosis
1	-1.43	0.11	0.30	-0.53	-0.19
2	-1.59	0.12	0.43	0.75	14.22
3	-0.07	0.01	-0.09	0.22	-0.23
4	-0.50	0.05	0.84	0.03	-0.34
5	0.18	-0.02	-0.08	0.03	-0.07
6	-0.03	0.00	0.16	-0.24	0.95
7	0.04	0.00	-0.10	-0.19	-0.02
8	0.00	0.00	-0.04	-0.03	-0.08
9	0.04	0.00	-0.14	-0.22	-0.10
10	-1.26	0.08	-0.08	0.20	-0.17
11	0.56	-0.02	-0.15	0.11	-0.11
12	-1.83	0.11	0.07	0.09	-0.06
Mean	**-0.49**	**0.04**	**0.09**	**0.02**	**1.15**
Standard Deviation	0.81	0.05	0.30	0.32	4.13

Table 5-5. Comparison of differences from duplicate sample pairs analyzed by the VSAT when data are classified into size categories.

Duplicate Number	Percent Medium Sand	Percent Fine Sand	Percent Very Fine Sand	Percent Coarse Silt	Percent $VSATPM_{20}$	Percent $VSATPM_{10}$
1	24.03	41.27	-28.45	-37.30	-0.07	0.00
2	76.91	-5.78	-44.77	54.44	-2.67	-0.36
3	9.67	-2.92	-6.62	-0.13	0.00	0.00
4	20.63	-1.93	-28.47	5.12	3.10	1.55
5	-5.91	-11.19	13.03	2.88	0.46	0.46
6	-0.60	5.09	-4.85	0.09	-0.11	0.32
7	-0.05	-5.63	9.66	-4.20	0.00	0.00
8	-0.09	1.61	-0.02	-1.15	-0.23	0.00
9	-0.14	- 4.02	9.65	-5.36	-0.24	0.00
10	0.45	60.97	-3.01	-57.04	-1.37	0.00
11	-0.13	-11.05	-27.49	36.90	2.12	0.00
12	0.58	72.02	24.48	-93.94	-3.49	0.00
Average	**10.45**	**11.54**	**-7.24**	**-8.31**	**-0.21**	**0.16**
Standard Deviation	22.84	29.20	20.85	39.37	1.79	0.48

and not another could significantly change the size distribution. This size particle was also able to bounce out of the collection pan, if the collar was not placed low enough to prevent this.

Accuracy, the amount of agreement of results with an expected value, was characterized by using 3 separate standard sphere materials traceable to National Institute of Standards and Testing (Table 5-6). Four subsamples were analyzed for each of the three sizes of standard spheres, 10 µm, 30 µm, and 1 to 40 µm. These results showed large amounts of clumping of the finer particles into larger aggregates except for the 30 µm sample (Figure 5-3). This same behavior was observed for VSAT analyses for sieved soil samples in similar size ranges. A conversation with the supplier of the standard spheres revealed that the borosilicate spheres tend to clump more than the soda lime glass spheres (J. Vasailiou, pers. comm., 2002). This was consistent with the

Table 5-6. Materials used for accuracy comparisons (obtained from Duke Scientific Corporation).

Test Code Prefix	Catalog Number	Size (μm)	Type	Density g/cm^3	Certificate? (NIST trace-able)	Number of VSAT analyses
T30	9030	30 ± 2.1	soda lime	2.45	yes	4
T10	9010	10.0 ± 1.0	boro-silicate	2.5	yes	4
T140	414	1 to 40	soda lime	2.45	no	4

results from the 30 μm samples, but not for the 1 to 40 μm samples. The clumping problem invalidated the accuracy tests for two of the three samples, while the mean of the 30 μm samples showed good agreement with their certified size. The precision and accuracy parameters discussed above measure overall performance of the system.

Representativeness was a concern for the sample processing including sieving and splitting. These processes were performed slowly to avoid sorting the sample by size unintentionally, or dispersing too much of the sample as airborne dust. Maintaining the fine particles in the sample was a representativeness issue because these size particles were prone to suspension and airborne drift due to their low settling velocity. These particles also had a tendency to adhere to the sample splitter and stainless steel spoon used to transport the sample to the VSAT. The particles were freed by judicious tapping on the splitter and spoon.

Completeness depended on both the selection of the correct test length

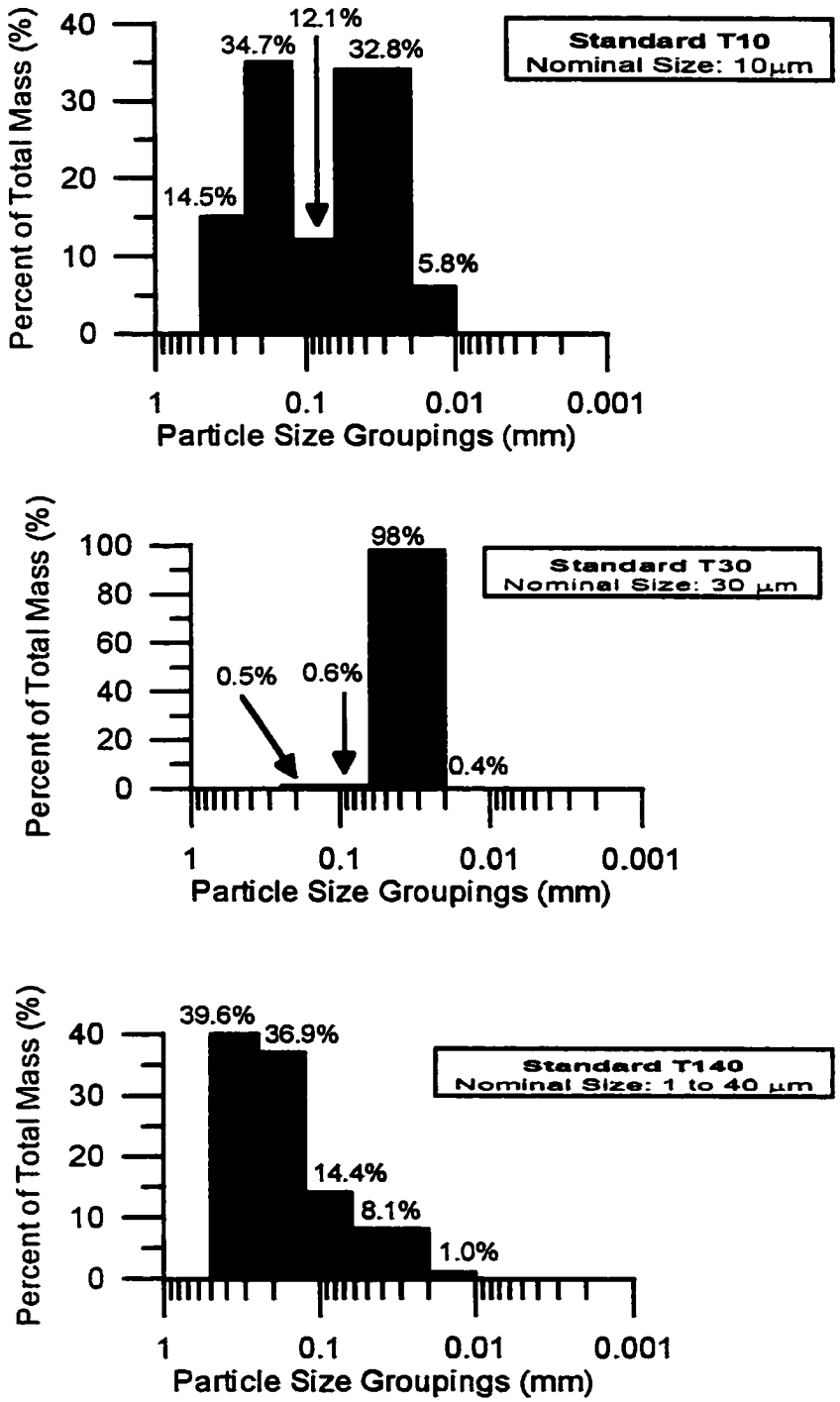

Figure 5-3 Particle size distributions for the 10 µm and the 1 to 40 µm standard samples demonstrate clumping while the 30 µm sample does not.

so all the particles present have time to land on the balance, and on preventing sample loss. Test length was evaluated by estimating the arrival times for the current laboratory conditions (Table 5-1) and then allowing extra time in case the sample contained more fines than expected. Sample loss could occur if some of the sample remained on the spoon, or if some of the sample spilled off the spoon. The most time consuming of these cases was when some of the sample spilled down the column before the test was initiated because then time had to be allowed for the sample to settle. The starting mass of the sample (entered by the analyst) was compared to the accumulated mass as a quality assurance check for sample loss. This starting amount had already been corrected for the amount of sample remaining on the spoon. For samples in this study, the mean sample loss was 9% with a standard deviation of 13%. A criterion of 50% sample loss was used to reject sample results and to rerun a sample if feasible.

Comparability considers possible changes in the measurement system over time. The balance was checked regularly with standard weights and was accurate during the time period of these tests. Stability of the balance during the tests was a concern, as zero drift was observed. The stability of the balance with the sample pan in place was evaluated on 9 occasions by recording balance values when no sample dropped. The variation in the zero measurements over periods of time comparable to regular tests showed several patterns including

- accumulation of material from slight, undetected spillage when a

sample was placed but the intended release did not occur;

- unexplained spikes in values measured; and
- longer-term, unexplained cycles of variability.

These variations ranged from 0.7% to 2.3% of the nominal sample size. A commonly-used criterion for a valid measurement system is that the uncontrolled variability be less than 10% of the actual measurement, and the VSAT balance easily met this criterion for all the zero tests conducted.

CHAPTER 6

RESULTS FOR VEGETATION AND SOIL DATA

This study investigated basic effects of vegetation on soil and airborne particle size distributions, so having reliable maps of vegetation locations was important. Traditionally these maps were prepared manually by having a botanist identify the plant and measure its location on a grid or transect. This process was simplified by using digital orthophoto data, one of the options available from the broader realm of remotely-sensed imagery derived from aerial photography and satellite sensors that have been applied to vegetation delineation in semi-arid rangelands (Peters et al. 1997, Bork et al. 1999) and wind erosion assessment (Lyon et al., 1986). Digital orthophoto quadrangles meld the geometric properties of a map with the image features of an aerial photograph. The distortions caused by terrain relief and camera tilt are removed; and the digital format is compatible with a geographic information system (U.S. Department of the Interior, 1996). In the first part of this chapter, digital photographs are compared to manually-prepared maps to answer

- how do locations of vegetation determined manually compare to locations determined using digital photos; and
- do the vegetation maps demonstrate a system of streets aligned parallel to the predominate wind direction?

In the second part of the chapter, soil particle size distributions are compared for locations with and without vegetation, to answer the question

- how does the soil size distribution vary in bare and vegetated soils?

Determining Locations of Vegetation

Vegetation grids provide information on frequency of occurrence of plant types and their spatial distribution. As part of the LTER study, the vegetation was mapped at each of the main sites during the summer of 1999 (Figures 6-1, 6-2, and 6-3) (Huenneke et al., 2001; Okin and Gillette 2001). A 0.5 m x 0.5 m grid was established that matched the alignment of the sand collectors with margins nominally extending past the sand collector locations to the east and west. Unfortunately, the grid corners were not marked permanently, and were not georeferenced by surveying or global positioning system (GPS) measurements. However, when a sand collector or mast was encountered in the vegetation grid, it was identified along with the vegetation present, so it was possible to confirm the locations of the measurements using independent GPS measurements of these known locations. When a minimum of 4 overlapping known locations were available, it was possible to correlate the locations in the vegetation grid with known GPS locations of the sand collectors and masts using an ArcView™ 3.0 extension for warping feature themes from an unknown datum/projection to a known datum/projection (McVay, 1998). This correlation process was possible for MNORT (Figure 6-4) and MRABB (Figure 6-5), but not

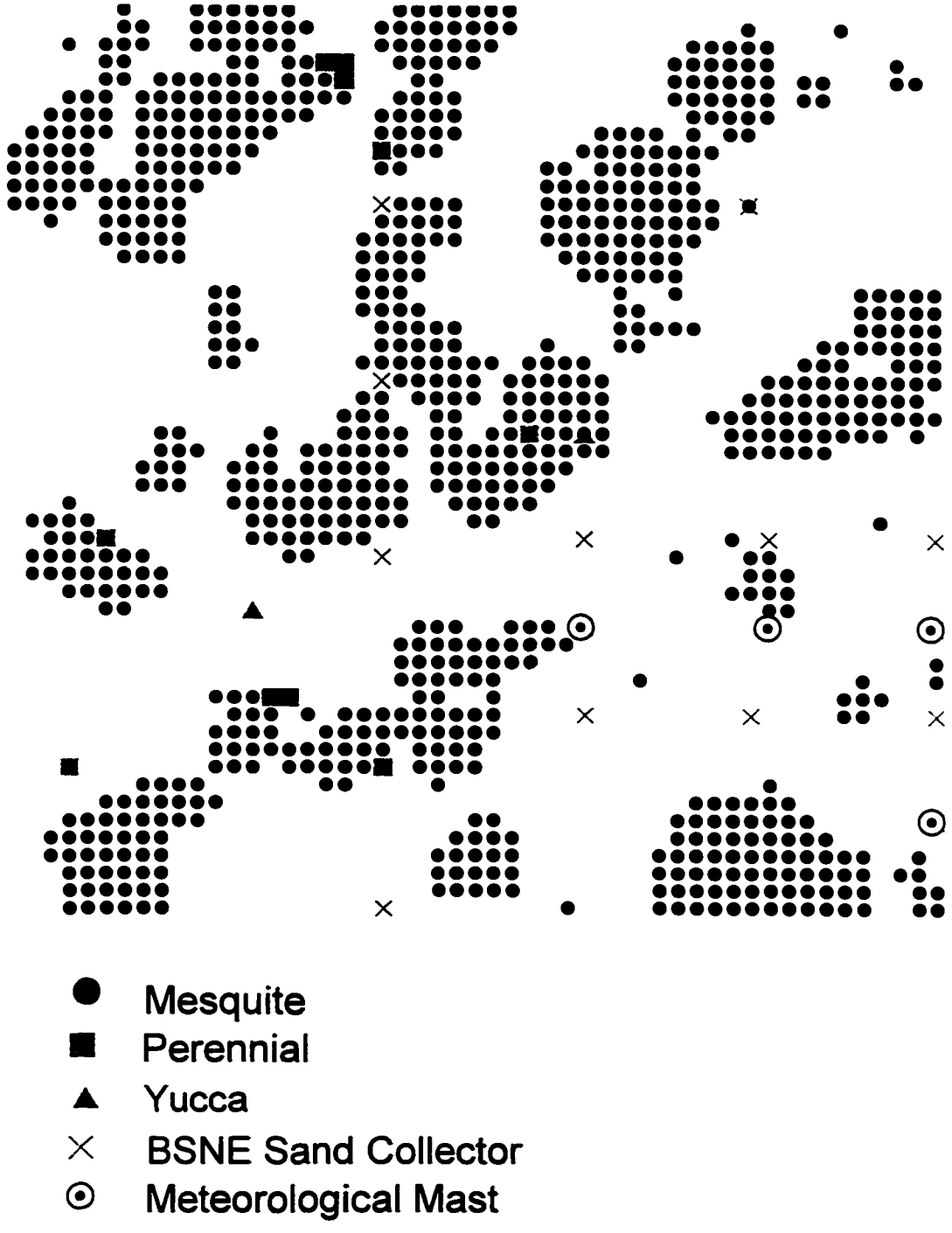

Figure 6-1. Vegetation at MNORT site, mapped manually (courtesy of LTER Wind Erosion Study). The locations of the meteorological tower and one mast were not mapped manually and are not shown.

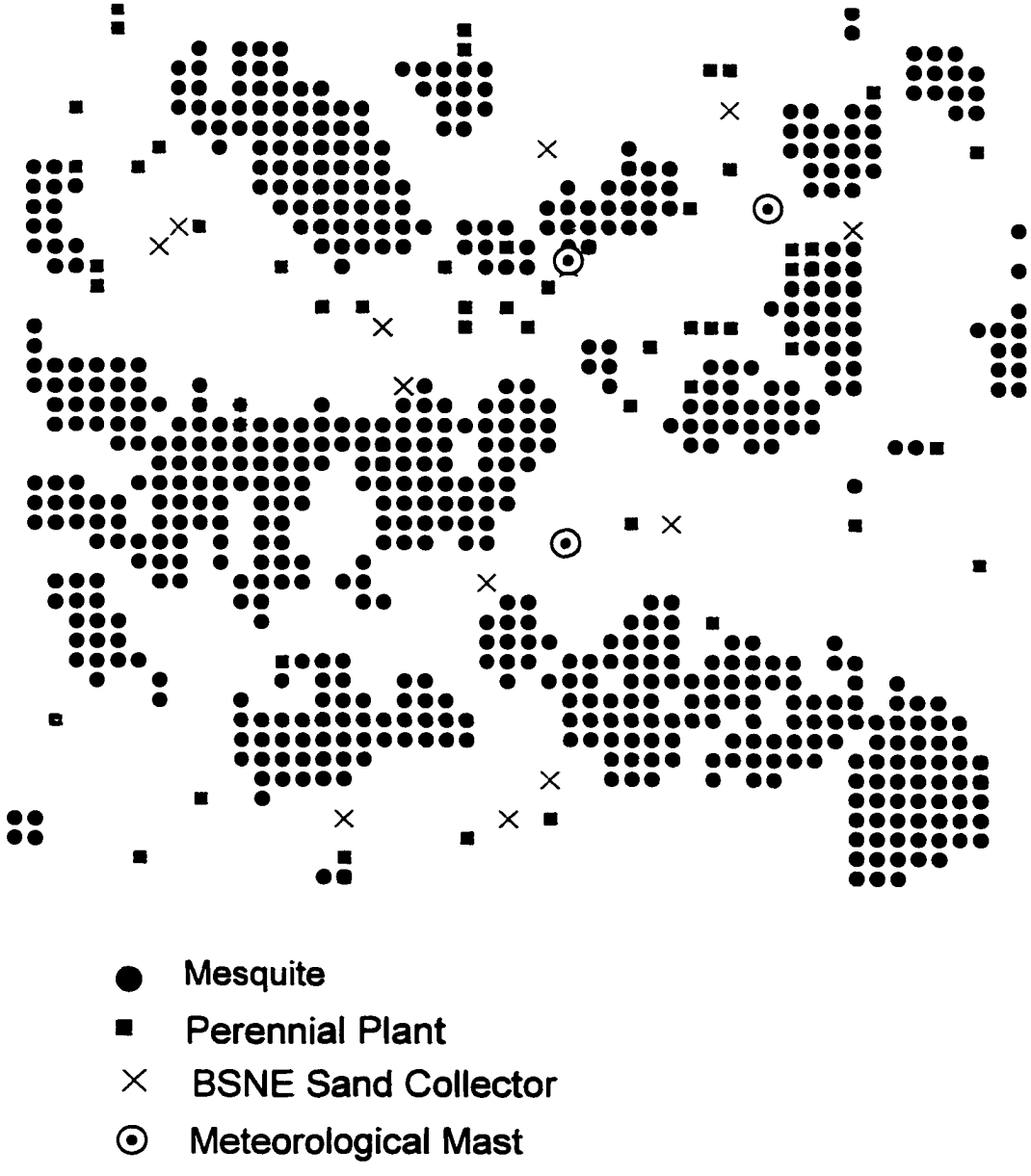

Figure 6-2. Vegetation at MRABB site, mapped manually (courtesy of LTER Wind Erosion Study). The locations of the meteorological tower and two masts were not mapped manually and are not shown.

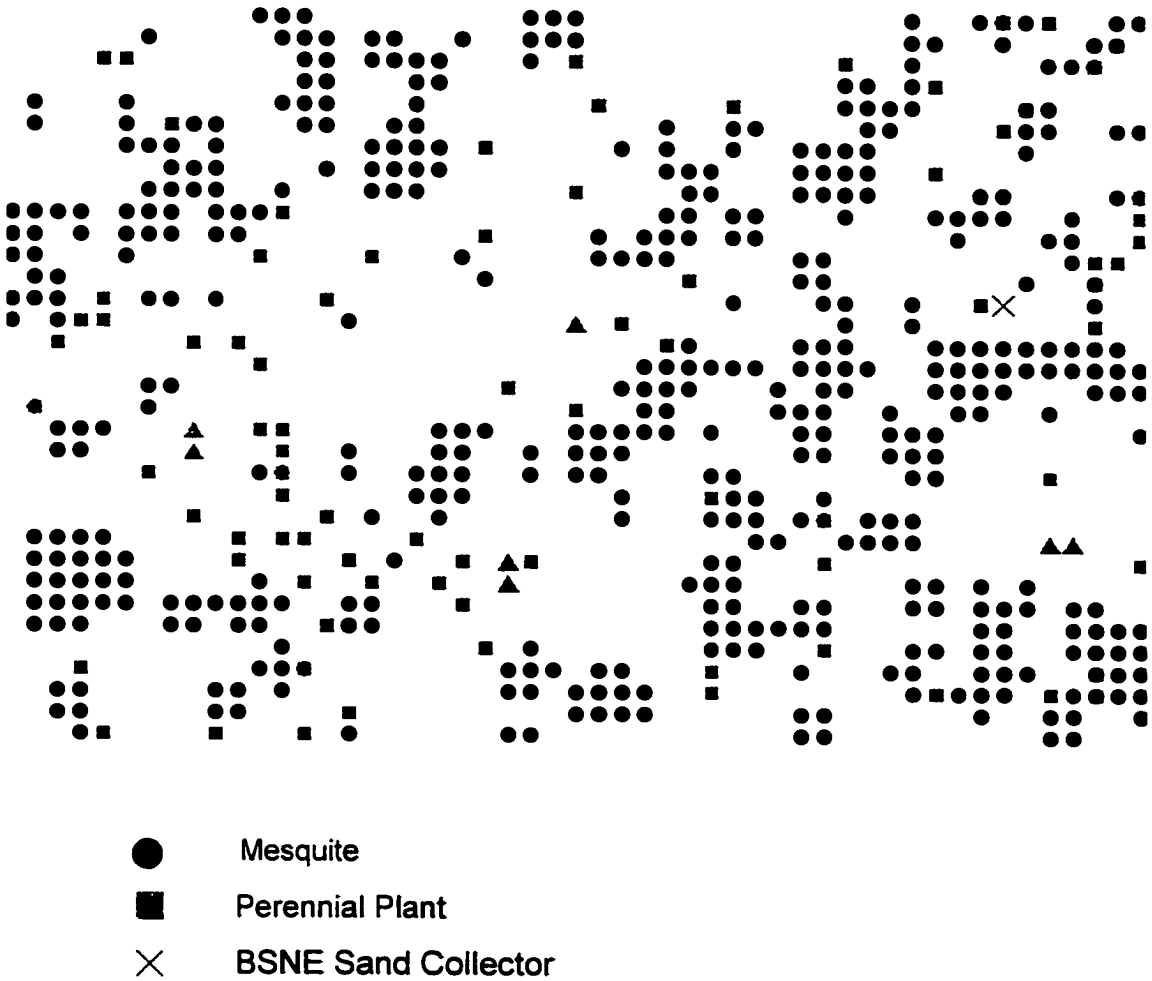

Figure 6-3. Vegetation at MWELL site, mapped manually (courtesy of LTER Wind Erosion Study). Note that only one BSNE sand collector was mapped manually and other collectors are not shown.

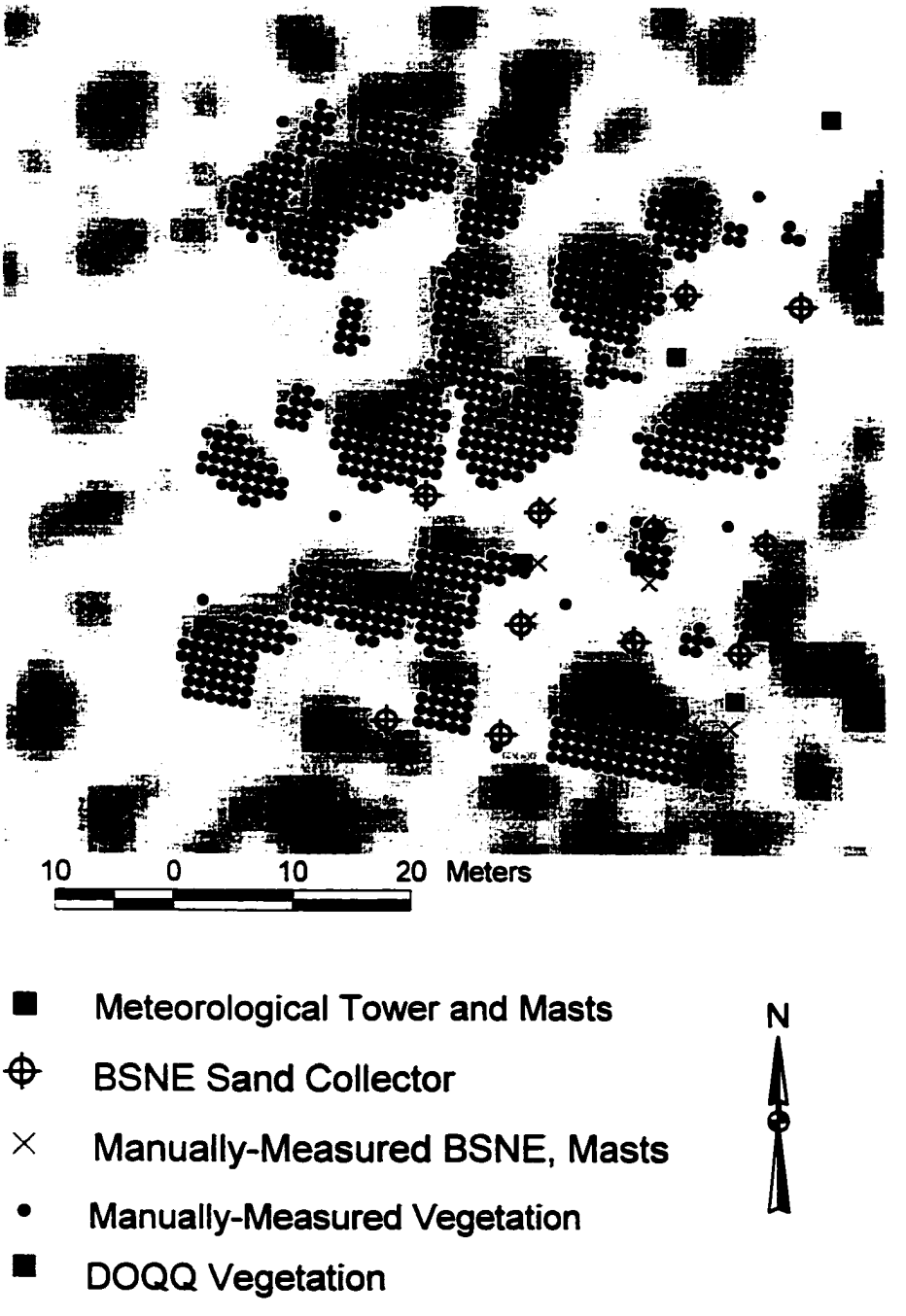

Figure 6-4. Comparison of manually mapped data and the digital orthophoto image for the same area at the MNORT site.

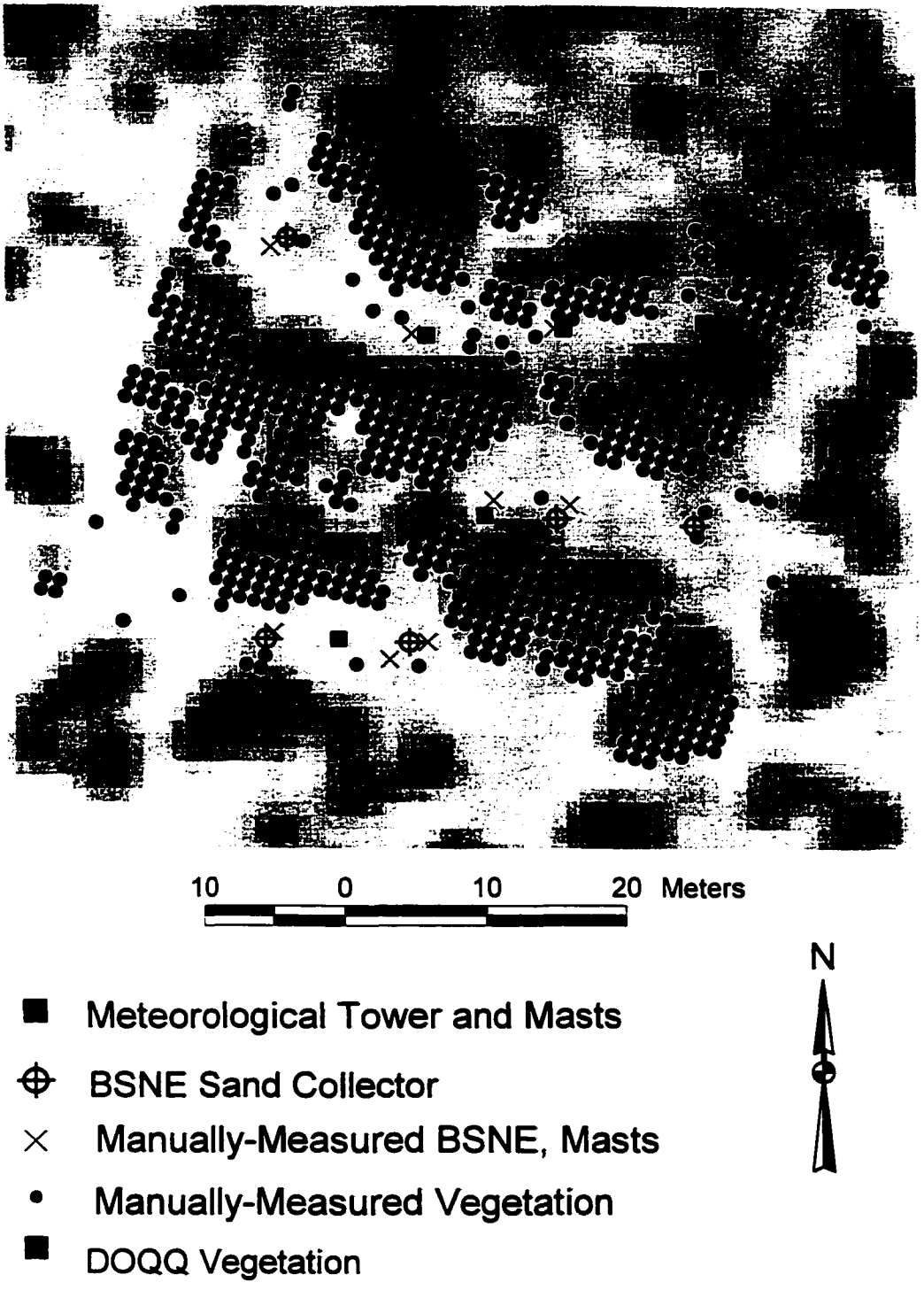

Figure 6-5. Comparison of manually mapped data and the digital orthophoto image for the same area at MRABB site.

for MWELL where only one overlapping point was available. To relate the vegetation positions to predominant wind direction for this study, spatially referenced data were needed. Because of the locational issues, the manually-determined vegetation grids were used for frequency of occurrence and pattern information, while digital orthophoto images were used for georeferenced vegetation information.

The resolution and information content of the digital orthophoto quarter quadrangle (DOQQ) images were compared to the information in the manually-determined vegetation grids. For the JER, DOQQs based on photos from October 1996 were available with 1-meter resolution (Figures 6-4 and 6-5). The patterns shown in the grids compared well although some distortion is present. The differences were attributed to the lack of georeferenced information for the manually-determined vegetation, not to intrinsic differences in the parameters being measured or movement of the vegetation.

The DOQQ cells were indicating the presence of mesquite bushes rather than the other vegetation potentially present, e.g., perennial plants including grass tufts, and yucca. It is possible that because the DOQQs were based on photography in the fall season, that the perennial plants were dry and not green at the time of the photo. In addition, at these study sites the size of a mesquite bush usually exceeded 1 m x 1 m, while the perennial plants and yucca had a footprint of approximately 10 cm x 10 cm. Finally, the mesquite bushes had dark brown and black stems and green foliage that made the plants visible during any time of the year because of the contrast with the lighter sand while

dead grasses and plants were close to the color of the sand. The occurrence of mesquite plants dominated the other vegetation types at the study sites (Table 6-1). For example, at MNORT the other vegetation types are essentially not present. MWELL is notably different, having a higher percentage of barren areas combined with a greater number of perennial plants and yucca. The Scrape site was maintained in a barren state with herbicides. If the emphasis of this study were on the perennial plants and yucca, higher resolution photography for a late spring or summer time period would be needed. If mesquite dunes moved from one year to the next, the study site would have to be photographed on a more frequent basis. In this case, the DOQQs were a good choice for delineation of the primary vegetation, the mesquite.

The digital format of the DOQQs allowed features shown in the images to be compared to known features, based on their brightness. In the case of the Jornada Range, determining the amount of barren, erodible sand was important to understanding and comparing the wind erosion at each of the sites. This was accomplished by counting the number of cells in each the study areas that matched the reflectance (brightness) of the nearby dirt roads. Each DOQQ data set provided reflectance values that were consistent relative to all 1-m pixels in that image. However, these brightness values were not standardized from one DOQQ image to the next, so features known to be equivalent had to be present in each image to perform a comparative analysis. Roads were chosen for this analysis because they were present in each DOQQ image, easily identified, completely clear of vegetation, and consisted of loose, highly erodible sand

Table 6-1. Vegetation types and amounts for main sites (based on manual enumeration data from LTER Wind Erosion Study and analysis of the DOQQs). DOQQ reflectances are measured on a scale of 0 to 255; the red spectral band was used.

Manual Enumeration Results				
Category	MNORT # cells (%)	MRABB # cells (%)	MWELL # cells (%)	Scrape (%)
Barren	7685 (74%)	6437 (77%)	5449 (83%)	(100%)
Mesquite	2691 (26%)	1873 (23%)	1054 (16%)	0
Perennial	10 (~0%)	75 (~0%)	86 (1%)	0
Yucca	2 (~0%)	15 (~0%)	11 (~0%)	0
DOQQ Analysis				
Category	MNORT # cells (%)	MRABB # cells (%)	MWELL # cells (%)	Scrape (%)
Cells of Same Brightness as Dirt Roads	6417 (64%) [reflectances > 214]	4358 (44%) [reflectances > 214]	1876 (19%) [reflectances > 190]	(100%) [reflectances > 214]

typical of the study area. Two DOQQs were analyzed; MNORT, MRABB, and Scrape were in one image while MWELL was in another. The mesquite vegetation absorbs red light so this wavelength was selected for analysis. Using ArcView™ software, each image was converted from a .tif format to a grid format. The roads were examined in the images to determine the range of brightness values on a scale of 0 to 255 for an 8-bit digitization of the intensities. This range was then used to identify grid cells with similar characteristics within a 100 m by 100 m area surrounding each of the sites. Scrape Site had the greatest amount of bare soil, while MWELL had the least (Table 6-1). These

results show less loose, barren soil than the manual enumeration method, except for the Scrape Site. This method may have identified loose soil similar to the road surface, rather than all soil with no plants. The loose soil was expected to be a better indicator of the site erodibility.

The DOQQs were also used to visually characterize the distances from the sand collectors to nearest vegetation and nearest upwind vegetation within a ±20 degree band centered around 240 degrees (Table 6-2). These data were used to examine the vegetation pattern for the presence of streets, and to evaluate the importance of vegetation to the wind erosion process. Just comparing the mean values, the nearest vegetation distances are less than the nearest upwind vegetation distances. These data were evaluated for normality and equal variances and because some of the distributions were not normal and did not have equal variances, comparisons were performed using non-parametric techniques with a one-sided t-test approximation, using the SAS programs UNIVARIATE, TTEST, and NPAR1WAY (SAS Institute, Inc., 1990). These tests confirmed that the nearest vegetation differences are significantly less than the nearest upwind vegetation distance. The results also show that the vegetation patterns are not significantly different from one site to the next, with the exception of Scrape site that has no vegetation. Using the t-statistic as a guide, among the four sites, MRABB and MWELL have the highest probability of being similar (88%). The data show that there is a pattern in the vegetation aligned with the dominant wind direction, but the data do not demonstrate that the length of the streets at the vegetated sites are significantly different from

Table 6-2. One-sided non-parametric t-test approximations were applied for each site to test the null hypothesis that means for distances to nearest vegetation in any direction were significantly less than distances upwind to nearest vegetation for P< 0.05. A non-parametric approach was chosen because it is less sensitive to unequal sample sizes and variances. Additional 2-sided non-parametric t-tests were applied among the sites to test the null hypothesis that means for the upwind distances were different from site to site for P<0.05. Highlights show probabilities that are significantly different at the 95% confidence level. Note that there is no vegetation within the Scrape site.

Comparison of Distances to Nearest and Upwind Vegetation	**Mean Distance to Vegetation (m)**			
	MNORT	**MRABB**	**MWELL**	**Scrape Site**
Number of Measurements	14	9	15	3
Nearest	1.9 m	1.9 m	1.9 m	78 m
Nearest Upwind	16.4 m	9.7 m	9.6 m	78 m
Non Parametric t-test Approximation	**0.00**	**0.00**	**0.01**	0.5
Comparison of Distances to Upwind Vegetation	**Non-Parametric 2-Sided T-test Approximations Comparing Mean Upwind Distances among Sites**			
	MNORT	**MRABB**	**MWELL**	**Scrape Site**
MNORT	-	0.40	0.28	**0.02**
MRABB	0.40	-	0.88	**0.04**
MWELL	0.28	0.88	-	**0.02**
Scrape	**0.02**	**0.04**	**0.02**	-

each other, except for the Scrape site. This is different from the results of Okin and Gillette 2001, that do show differences among expected street lengths among these sites.

To summarize, the manual delineation provided more information on the species of vegetation present than the DOQQs, but the DOQQs provided sufficient information for mapping the mesquite. The digital format of the

DOQQs enabled the calculation of areas similar in reflectance to the dirt roads. Because the roads contained loose soil, the similar areas within the study sites might be more representative of site erodibility. The DOQQs are readily available at low to no cost, cover large areas, and are a practical means for mapping the mesquite dune patterns in the portions of the Chihuahuan desert that are similar to these study sites. The presence of "streets," elongated barren areas aligned with the dominant wind direction, was confirmed statistically at each site. The MNORT site had the longest streets among the vegetated sites, followed by the MRABB and MWELL sites but these street lengths were not statistically different at the 95% confidence level.

Influence of Vegetation on Soil Particle-Size Distributions

In the Chihuahuan Desert, blowing sand settles around mesquite bushes so the dunes are vegetated, while the interdune areas or streets are sparsely vegetated or bare. These streets are the source areas for the dune material. A study based on dune and interdune samples collected from around the world showed that samples from interdune areas tended to be more poorly sorted and to have higher silt and clay contents (Ahlbrandt, 1979). In addition, textural contrasts were present among different positions on the dune (Ahlbrandt, 1979). Langford 2000, points out that nabkha (coppice) dunes have higher organic content than the surrounding soils. He also refers to unpublished data that show that interdunes and nabkhas have distinctly different sand gradations. The interdunes contain much coarser and more poorly sorted sand. He found

that variability due to location on the dune was greater than variability between dunes at the same site.

Soil samples were collected at the MNORT site to assess the effects of vegetation and small-scale geomorphology on soil size distributions, especially the fine-grained component. Visual examination of the street and dune settings revealed differences, for example the streets tended to have a thin layer of rounded quartz particles approximately 1 mm in diameter, while the dune sides and tops did not. To avoid investigator bias in choosing the sampling locations and maintain the randomness established with the grid locations yet avoid the influence of the masts and BSNE support pipes, soil was sampled at midpoints between the BSNE collectors (or midway between the 10-meter grid nodes if a collector was not present). With access limited by vegetation in some cases, this resulted in 23 samples. The locations were photographed and the type of location (street, dune top, or side of a dune) was recorded for each sample when it was collected. The VSAT was used to characterize size distribution of the soil samples using the size ranges discussed earlier.

Statistical tests were applied to evaluate the likelihood that the sample characteristics from the different settings were significantly different. The null hypothesis for each of the cases listed below was that there was no difference between the soil gradations for the different settings. Based on the results in the literature and the physical processes involved, the following hypotheses were tested for each size range and dune setting:

Percent Medium Sand, street>dune top, street>dune side; top<side;

Percent Fine Sand, street<dune top, street<dune side; top>side;

Percent Very Fine Sand, street<dune top, street< dune side; dune top<side;

Percent Coarse Silt, street<dune top, street<dune side; dune top<side;

Percent PM_{20}, street>dune top, street>dune side; dune topside;

Percent PM_{10}, street>dune top, street>dune side; dune top>side.

The VSAT results were grouped according to their location types and the mean and standard deviation for each location type and size category were computed (Table 6-3). These results showed similarities and differences, but there was a considerable range in values in some cases. For example, the streets and dune top settings were the same except that the street was comprised of more medium sand while the dune top had more fine sand. This is consistent with the greater erodibility of this size range. The dune tops and dune sides were similar except the side samples had a higher proportion of medium sand compared to the top while the reverse was true for the fine sand components. $VSATPM_{20}$ and $VSATPM_{10}$ were higher for the top than the dune side samples. The streets and dune sides were similar except for the $VSATPM_{20}$ and $VSATPM_{10}$ that had higher values in the streets. This initial comparison did not provide enough information to decide whether the differences were meaningful or due to chance. To evaluate the probability that a mean abundance in the soil sample for a given particle size range and setting was significantly less than the other means for the same size range, one-sided t-tests and the Shapiro-Wilk test for normality were used with $P<0.05$ (Kvanli, 1988; SAS Institute, 1990). The t-test statistic gives the probability that the difference between the means

Table 6-3. Means and standard deviations for soils collected from MNORT streets, dunes, and dune sides.

Sample Number	Percent Medium Sand	Percent Fine Sand	Percent Very Fine Sand	Percent Coarse Silt	Percent $VSATPM_{20}$	Percent $VSATPM_{10}$
Streets	**n = 11**					
1	62.3	36.7	0.4	0.5	0.1	0.0
2	40.6	50.0	4.7	2.6	2.1	0.0
3	0.0	50.8	42.8	5.1	1.0	0.3
4	70.8	12.3	3.1	10.8	4.6	0.0
5	10.9	51.7	27.3	8.6	1.5	0.0
7	32.7	57.9	7.9	1.4	0.5	0.0
8	17.4	50.0	25.4	4.7	2.1	0.4
10	38.1	44.0	12.5	4.5	0.7	0.2
14	40.2	42.3	12.7	4.8	0.5	0.0
19	6.0	64.8	25.5	3.7	0.5	0.0
22	0.4	65.9	27.3	5.2	0.7	0.4
Mean	29.0	47.9	17.2	4.7	1.3	0.1
Standard Deviation	24.2	14.8	13.3	2.9	1.3	0.2
Dune Tops	**n = 7**					
9	37.2	56.3	2.7	2.0	2.0	0.0
13	0.3	60.1	32.7	5.9	0.9	0.0
15	0.3	80.8	15.3	3.9	0.0	0.0
17	29.1	50.0	13.3	4.7	2.5	0.4
18	20.8	36.7	32.8	8.8	0.9	0.0
20	21.4	60.5	12.9	3.6	2.0	0.0
23	0.3	75.9	19.4	3.8	0.3	0.3
Mean	15.6	60.1	18.5	4.7	1.2	0.1
Standard Deviation	15.3	15.0	11.0	2.2	1.0	0.2
Dune Sides	**n = 5**					
6	0.3	42.4	48.3	8.9	0.0	0.0
11	37.9	39.6	15.1	5.4	2.0	0.0
12	24.5	53.5	19.5	2.8	0.0	0.0
16	0.0	66.0	30.0	4.0	0.0	0.0
21	85.6	12.0	1.9	0.5	0.5	0.0
Mean	29.7	42.7	23.0	4.3	0.5	0.0
Standard Deviation	35.2	20.1	17.4	3.1	0.9	0.0

for each size range is a random effect, assuming that the underlying distribution is normal. Normality was confirmed for the data for each size range and setting except one. In this case, a non-parametric test (NPAR1WAY) confirmed the significance of the t-test result. These statistical tests were conducted with paired data sets; first, streets were compared to dune tops; then dune tops were compared to dune side; and then dune sides were compared to streets (Table 6-4).

In all but two cases the null hypotheses were accepted; the results were not different from chance at the 95% confidence level. In the first case where

Table 6-4. One-sided t-tests, $P<0.05$ were applied to test whether a mean for a given particle size and setting was less than means for the same size range in other settings. Highlights show results that are significant at the 95% confidence level.

Comparison	Percent Medium Sand	Percent Fine Sand	Percent Very Fine Sand	Percent Coarse Silt	Percent VSATPM$_{20}$	Percent VSAT PM$_{10}$
Streets vs. Dune Tops						
Street Mean	29.0	47.9	17.2	4.7	1.3	0.1
Dune Top Mean	15.6	60.1	18.5	4.7	1.2	0.1
t-test	**0.11**	**0.05**	**0.42**	**0.49**	**0.45**	**0.42**
Dune Tops vs. Dune Sides (DS)						
Dune Top Mean	15.6	60.1	18.5	4.7	1.2	0.1
DS Mean	29.7	42.7	23.0	4.3	0.5	0.0
t-test	**0.19**	**0.06**	**0.30**	**0.41**	**0.10**	**0.09**
Streets vs. Dune Sides (DS)						
Street Mean	29.0	47.9	17.2	4.7	1.3	0.1
DS Mean	29.7	42.7	23.0	4.3	0.5	0.0
t-test	**0.48**	**0.29**	**0.24**	**0.41**	**0.11**	**0.02**

the null hypotheses was rejected, streets were significantly different from dunes for the fine sand category with fine sand consisting of an average of 60% of the dune samples and 48% of the street samples. In the second case, streets were significantly different from dune sides for the $VSATPM_{10}$ category, making up 0.1% of the street samples and 0% of the dune side samples. This is attributed to the higher velocity that occurs as the wind lifts over the front edge of the dune, somewhat like wind flowing over the front of an airplane wing. These results suggest that the barren "street" areas were sources for fine sand that is deposited on the dune tops. The results also suggest that the dune sides were scoured by the wind removing $VSATPM_{10}$, and that the dune tops were deposition areas for these particles.

In summary, there were significant differences in the particle size distributions for the samples collected from the streets, dune tops, and dune sides. These differences were significant with percent fine sand comprising a much larger component of the dune top samples compared to the street samples, and percent $VSATPM_{10}$ comprising a larger portion of the dune top samples compared to dune sides. These results are consistent with the results presented by Ahlbrandt (1979) and Langford (2001). Possible reasons for the differences include differences in soil gradation analysis techniques, and a smaller number of samples analyzed.

CHAPTER 7

DUST STORMS: RESULTS FOR AIRBORNE PARTICLE DATA

During the intensive field sampling session from April 11 through 20, 2000, several significant storm events occurred. The storms can be identified by elevated wind speeds and dust measurements. In this chapter, meteorological data, and data for dust based on both integrated and continuous types of measurements for selected periods during the storms are discussed. These data show the characteristics of the storms and help to address the following questions:

- how does particle flux vary in airborne samples collected at various distances from vegetation, and
- what is the threshold friction velocity for PM_{10}?

To answer the first question, dust collector total fluxes were compared and then modeled statistically using data from the four main study sites for two sampling periods. To answer the second question for MNORT site, continuous aerosol monitor data measured at locations around a sand dune were combined with meteorological data to provide insights regarding storm characteristics and PM_{10} emissions.

The protective influence of vegetation for soils in agricultural fields subject to wind erosion has been recognized and studied for many years (Chepil, 1944

and 1957; Bilbro, 1991; Bilbro and Fryrear, 1994). Stockton and Gillette (1990) related sheltering vegetation to threshold velocity, using meteorological data from the Jornada and Yuma Desert Winds Sites operated by the U.S. Geological Survey and a portable wind tunnel in the field. Musick (1990) related plant canopy density, frontal diameter, and height to threshold friction velocity at several field locations including the JER, pointing out that friction velocity increased with increasing canopy density. By knowing the amount of canopy cover, the amount of protection afforded can be estimated. Musick et al. (1996) investigated these relationships in a wind tunnel and discovered that the aspect ratio (plant height divided by diameter) is a critical variable in predicting level of protection. These results were consistent with earlier theoretical work by Raupach (1992) and Raupach et al. (1993), that evaluated the relationship between surface roughness and threshold velocity. Wolfe and Nickling (1996) extended this research further showing shear stress partitioning varies with wind speed and threshold velocity. Measurements of winds over linear sand dunes in the Kalahari desert showed that vegetation had a significant effect on surface roughness (Wiggs et al., 1996). Danin and Ganor (1997) studied the role of a grass in trapping dust, while Lancaster and Baas (1998) investigated the role of vegetative cover on sand transport at Owens Dry Lake in California. Raupach and Leys (1999) are developing and consolidating a theoretical approach to estimating particle deposition to vegetation at the regional and local scales. Gillies et al. (2000) characterized the drag forces and shear stress partitioning under ambient meteorological conditions for a single desert shrub located in an

open agricultural field and connected to a force balance.

Models that predict aeolian processes have incorporated parameters to characterize vegetation. For example, Schwartz et al. (1997) developed a model to predict the effects of agricultural windbreaks on wind erosion. Van Dijk et al. (1999) modeled transport for a transverse dune and showed that growth and burial of vegetation had significant effects on the results. Marticorena et al. (1997) showed that degree of disturbance of the soil surface along with amount of vegetation were important parameters in predicting threshold velocities. Most recently, Okin and Gillette (2001) suggested that the pattern of the vegetation, especially the existence of streets, needs to be included in wind erosion models.

Research has been conducted on threshold friction velocities using instrumented, open-bottomed wind tunnels placed over soil in outdoor settings, for desert soils (Gillette, 1978; Gillette et al., 1980 and 1982); for agricultural soils (Gillette, 1988); for selected sites in Arizona (Nickling and Gillies, 1989); for selected sites at the JER (Marticorena et al., 1997); and for Las Vegas Valley, Nevada (James et al., 2001). Threshold friction velocities have also been investigated using collocated meteorological towers and dust sensors (Holcombe et al., 1996; Gillette et al., 1996 and 1997, Lancaster and Baas, 1998; and Gillette and Chen, 2001). In addition, thermal infrared remote sensing data combined with Medium-Range Weather Forecast data has been used to compute threshold velocities for locations over the Sahara Desert in Africa, with good success (Chomette et al., 1999).

Meteorological Data

The intensive field sampling session began with setting up equipment and collecting BSNE samples on April 11 and 12, and continued through April 20 when BSNE samples were collected for the last time during this session. Continuous wind speed and direction sensors were operated through the U.S. Geological Survey Desert Winds program at the Jornada Geomet site that is located within 10 km of and in the same terrain as the four main study sites (Figure 2-2). Meteorological data for a 6-day excerpt from this period showed a diurnal pattern in the wind speeds, and elevated wind speeds occurred on April 15th, 16th, 18th, and 19th (Figure 7-1). However these continuous wind data can only be used as general information because the winds are not uniform across the area. For example, the winds measured at the Geomet site on the 16th were not sufficient to trigger the sensors at MNORT.

The MNORT data are summarized for each intensive day time period corresponding to wind speeds higher than 5 m s^{-1} (Table 7-1). Based on mean wind speed, the 18th and 19th were the most active days. Based on number of 10-minute intervals above 5 m s^{-1}, the 18th stands out, with nearly 90 minutes additional windstorm activity compared to the other days. None of the days had a mean wind direction that aligned with the mean direction of the streets, approximately 240 degrees true north, but each day except for the 14th had mean wind directions in the arc of 240 ± 20 degrees. Even the 14th had approximately a third of all the 10-minute interval data occurring within this arc.

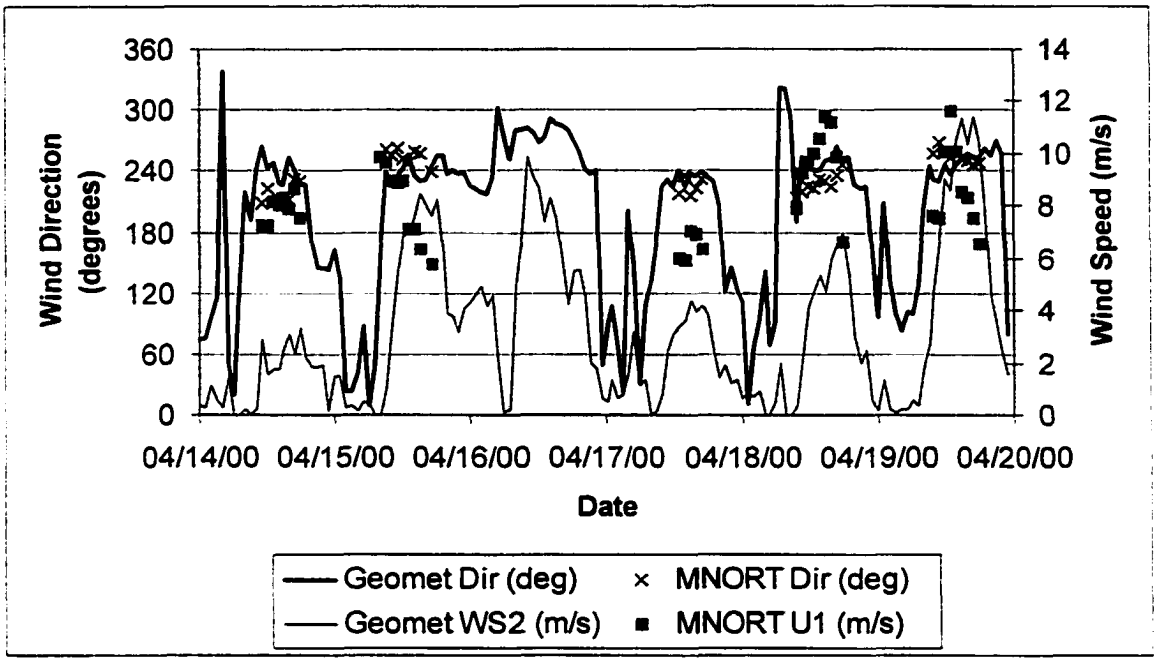

Figure 7-1. The LTER weather station at the U.S. Geological Survey Jornada Desert Winds site provides continuous, hourly averaged wind speed and direction data at a height of 6.1 m; this excerpt is for the intensive field study session. In addition, the 7-m MNORT tower data are shown for comparison. These data are 10-minute averages recorded when the wind speed is greater than 5 m/s. In this graph, hourly-averaged values are represented by continuous lines, while the 10-minute average data are represented by points.

Table 7-1. Basic statistics for the dust storm intensive periods, based on the 7-meter anemometer at MNORT with a threshold of 5 m/s. *The wind directions are referenced to magnetic north. Streets are oriented between 220 and 260 degrees true north.

Date, Time	Mean Wind Speed (m/s)	Wind Speed Std. Dev.	Mean Wind Dir.* (deg.)	Wind Dir. Std. Dev.
4/14/2000 11:10-18:00	7.9	0.5	217	10
4/15/2000 8:40-17:20	8.1	1.5	254	7.4
4/18/2000 10:20-18:50	9.6	1.5	227	9.5
4/19/2000 10:20-18:20	8.9	1.6	254	6.4
Date, Time	Number of 10-min periods for Wind Speed > 5 m/s	Number of 10-min periods for Wind Speed > 7 m/s	Number of 10-min periods for Wind Speed > 9 m/s	Number of 10-min periods for Wind Speed > 11 m/s
4/14/2000 11:10-18:00	28	26	1	0
4/15/2000 8:40-17:20	28	23	10	0
4/18/2000 10:20-18:50	41	39	31	11
4/19/2000 10:20-18:20	32	30	17	5
Date, Time	Number of 10-min periods for Wind Direction in the Range of 220-260 Degrees*			
4/14/2000 11:10-18:00	10	10	1	0
4/15/2000 8:40-17:20	20	16	6	0
4/18/2000 10:20-18:50	34	32	27	9
4/19/2000 10:20-18:20	25	24	15	5

Dust Collector Results

Each of the dust collectors had samples available for two sampling periods, labeled Periods A and B (Table 7-2). These time periods were not strictly comparable because when other field monitoring activities were taking place, it was not possible to retrieve all the BSNE samples from the four main sites in one day. In these cases, samples were retrieved on subsequent days. However, personal observation during the collection periods determined that significant erosion activity occurred during the windy periods, and not when only a light breeze was present. Each of the sampling periods included the same high-wind times when wind erosion was occurring for all the sites and thus the samples are believed to be comparable for wind erosion activity.

The dust collector data were considered from several perspectives at a station location, both as mass collected at a specific height, and then as a total horizontal flux over one meter from the ground upwards. Data for mass at each of the 5 heights were corrected for the size of the inlet area to yield data in the form of grams collected per square cm opening. These data showed a

Table 7-2. Dates for integrated BSNE sampling during the intensive session.

Sand Collectors	Start Date--Period A	End Date--Period A / Start Date--Period B	End Date--Period B
MNORT	4/11/2000	4/16/2000	4/20/2000
MRABB	4/11/2000	4/16/2000	4/20/2000
MWELL	4/12/2000	4/17/2000	4/20/2000
SCRAPE	4/12/2000	4/15/2000	4/20/2000

consistent, declining mass-with-increasing-height relationship (Figure 7-2). This pattern, due to the entrainment of particles from the surface through aerodynamic effects, particle bombardment, and/or other surficial mechanical disturbances during periods when the wind was above the threshold friction velocity, appeared to be the same regardless of the overall wind speed for the four main sites. For example at MNORT site, the amount of mass collected during Period A was one tenth the mass collected during Period B and the corresponding overall friction velocities were 67 and 81 cm/s respectively. The sand collector data demonstrate the decline in particles collected with height in both cases. This relationship has been demonstrated in studies in numerous locations (Fryrear 1986, Fryrear and Saleh 1993) and in wind tunnels (Butterfield 1999). Horizontal flux from a local surface source can be estimated at each sand collector station from the mass collected at 5 heights using the relationship:

$$q(z) = C_o \exp(C_1 z + C_2 z^2) \qquad \text{Eqn. 7-1}$$

where C_o, C_1, and C_2 are fitted parameters; the equation is then integrated vertically from 0 to 100 cm and over time to calculate total flux Q(x) (Shao and Raupach, 1992). Using the convention described by Gillette and Chen 2001, the quantity q is the mass passing through a plane 100 cm in height and 1 cm in width oriented to be perpendicular to the surface and to the wind. The quantity q has units of mass/unit width/time. The total flux Q(x) has the units of mass per unit width. Once all the station total fluxes were calculated, they were averaged

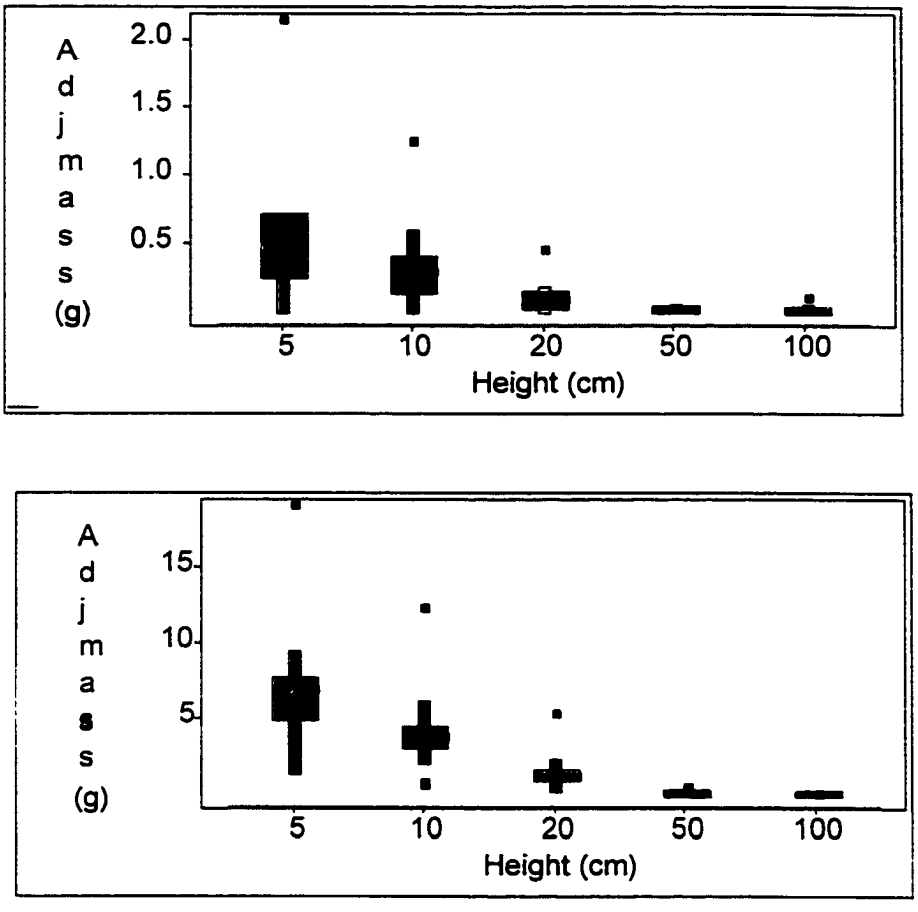

Figure 7-2. Sand collector data for MNORT site for Period A (top) and Period B (bottom) plotted versus height. The variable "Adj mass(g)" refers to the collected mass normalized for the area of the collector intake. The decline in mass with height was present at all the sites. The horizontal line in the middle of the large box represents the 50th percentile or median. The bottom and top edges of the large box represent the quartiles, or the 25th and 75th percentiles. The narrow boxes extending above and below the large box are called whiskers. Whiskers extend from the quartiles to the largest (or smallest) observation not larger (or smaller) than 1.5 times the distance between the quartiles. Extreme data values beyond the whiskers are shown individually.

with other station total fluxes to produce an average total site value (Table 7-3, Figure 7-3) for each period.

In both Periods A and B, the Scrape site has the highest total flux values, followed by MNORT, MRABB, and MWELL. The station-to-station variability is also highest for Scrape site, followed by MNORT, MRABB, and MWELL (Table 7-3 and Appendix 3). Comparing Period A to B shows that 20% higher wind speeds in Period B result in 3 to 10 times higher dust fluxes; this is consistent with the general relationship that dust fluxes are proportional to the friction velocity cubed (Gillette et al., 1997). At least for these two periods of time, this order of the fluxes follows the order of the sites when listed by amount of loose soil with reflectances matching dirt roads as determined from the DOQQs, and the order of similarity of the sites based on the distance to upwind vegetation as determined from the DOQQs, but not the order determined by the manual enumeration of barren soil (Table 6-1). Thus the DOQQs appear to be more useful in evaluating wind erosion potential than a manual enumeration of vegetation. The higher values measured at Scrape and MNORT sites are attributed to more loose sand and longer streets compared to the MRABB and MWELL sites. This is consistent with the findings of Okin and Gillette (2001), that used Fourier transform analysis and geostatistical analysis for the same 3 mesquite sites at the Jornada and determined that the shrub distributions are inhomogeneous at these sites. In their work, the development of streets at each of the sites was ranked with best developed streets at MNORT, followed by MRABB, followed by least developed streets at MWELL. To more fully

Table 7-3. Basic statistics for the sand collectors at the four main study sites. The values for flux represent total fluxes integrated over the height of 100 cm and for the duration of each period (see text for details).

Site and Parameters	**Period A**	**Period B**
MNORT	n =14 (grid)	n =14 (grid)
U* (Tower data)	67 cm/s	81 cm/s
Minimum flux (g/cm)	0.01 (trace)	26
Maximum flux (g/cm)	34.9	348
Mean flux (g/cm)	*10.0*	*119*
Standard Deviation (g/cm)	8.6	75
MRABB	n = 9 (grid)	n = 9 (grid)
Minimum flux (g/cm)	0.01 (trace)	0.1
Maximum flux (g/cm)	10.7	93
Mean flux (g/cm)	*1.7*	*25*
Standard Deviation (g/cm)	3.4	28
MWELL	n=15 (grid)	n=15 (grid)
Minimum flux (g/cm)	0.01 (trace)	0.1
Maximum flux (g/cm)	8.1	22
Mean flux (g/cm)	*3.2*	*9.1*
Standard Deviation (g/cm)	2.7	7.5
SCRAPE	n=3 (all on one line)	n=3 (all on one line)
Minimum flux (g/cm)	50	287
Maximum flux (g/cm)	126	536
Mean flux (g/cm)	*94*	*412*
Standard Deviation (g/cm)	40	125

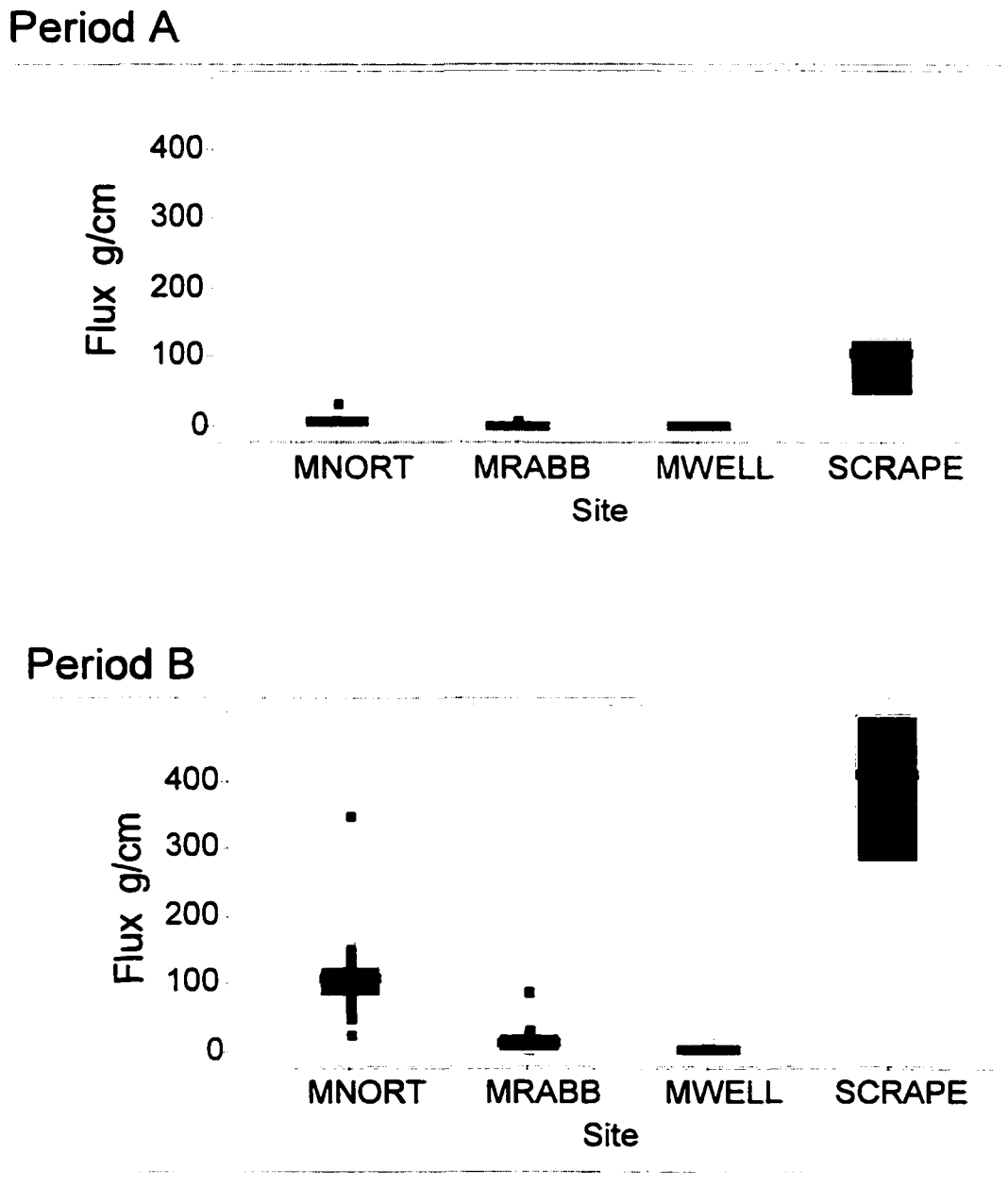

Figure 7-3. Comparison of flux means and quartiles for each of the main sites for Periods A and B. The horizontal line in the middle of the large box represents the 50th percentile or median. The bottom and top edges of the large box represent the quartiles, or the 25th and 75th percentiles. The narrow boxes extending above and below the large box are called whiskers. Whiskers extend from the quartiles to the largest (or smallest) observation not larger (or smaller) than 1.5 times the distance between the quartiles. Extreme data values beyond the whiskers are shown individually.

understand the relationship of the measured fluxes (dependent variable) to the distance to upwind vegetation (independent variable), the data were analyzed using SAS™ computer programs, ultimately resulting in two general linear models (SAS Institute, Inc., 1990; Blattner et al., 1999). These models evolved from an exploratory process that first evaluated whether the two sampling periods were from the same or different statistical populations. Because the flux data at each site and for each period were not normally distributed, the difference between the two populations was tested using a nonparametric technique that was not sensitive to the underlying distribution, e.g., the SAS program NPAR1WAY. Periods A and B were significantly different for all sites at the 95% confidence level. This meant separate models were needed for Periods A and B. The next step in developing the model(s) was to evaluate the similarities in the flux data for the two periods. Evaluation of the mean values and results from additional nonparametric testing using NPAR1WAY showed that all the sites were significantly different for both periods at the 95% confidence level with the exception of MRABB and MWELL (Table 7-4). With this information, within each period, several general linear models were evaluated for goodness of fit using the R-SQUARE parameter (PROC GLM in SAS, SAS Institute, Inc., 1990), with all sites treated individually and with sites grouped (MNORT with Scrape; MRABB with MWELL). The best models were with the data grouped.

Previous empirical work showed that flux was proportional to (upwind distance to vegetation)$^{3/2}$ (Gillette and Chen, 2001) and the models were

Table 7-4. One-sided, non-parametric t-test approximations for mean total flux at each site were applied to check whether a selected site mean was less than each of the others. Highlights show probabilities that indicate one mean is significantly less than the other at the 95% confidence level.

Is one mean significantly less than the other?	Period A			
	MNORT n = 14	MRABB n = 9	MWELL n = 15	Scrape Site n = 3
MNORT	-	0.0084	0.0025	0.0100
MRABB		-	0.2401	0.0171
MWELL			-	0.0089
Scrape				-
Is one mean site flux significantly less than the other?	**Period B**			
	MNORT n = 14	**MRABB n = 9**	**MWELL n = 15**	**Scrape Site n = 3**
MNORT	-	0.0010	<0.0001	0.0129
MRABB		-	0.0762	0.0175
MWELL			-	0.0091
Scrape				-

developed using this relationship. As expected, the resulting models show that the windier period has higher flux values, and yet it is possible to have wind erosion fluxes with more moderate wind conditions (Table 7-5, Figures 7-4, 7-5). In the case of Period A, the model has an intercept of zero, while for Period B the Scrape and MNORT portion of the model has an intercept, while the MRABB and MWELL portion of the model has an intercept that is essentially zero. The slope for Period B is about 4 times higher than the slope for Period A. In putting these relationships into context with other field data, it is important to realize that

Table 7-5. Coefficients for flux model. The variable "veg" refers to the distance to the nearest upwind vegetation from the sand collector.

Period = A **R-Square = 0.92**				
Parameter	**Estimate**	**Standard Error**	**t Value**	**Pr > | t |**
$veg^{3/2}$	0.118	0.005	23.44	<0.0001
$veg^{3/2}$ [MWELL/ MRABB]	-0.736	0.028	-2.59	0.0136
$veg^{3/2}$ [Scrape/MNORT]	0.000	-	-	-
Equation: flux = $0.118*veg^{3/2}$ for MNORT and Scrape flux = $0.118*veg^{3/2}$ - 0.074 for MRABB and MWELL				
Period = B **R-Square = 0.91**				
Parameter	**Estimate**	**Standard Error**	**t Value**	**Pr > | t |**
Intercept	86.6	10.4	8.33	<0.0001
$veg^{3/2}$ [MWELL/ MRABB]	-86.9	12.3	-7.08	<0.0001
$veg^{3/2}$ [Scrape/MNORT]	0.00	-	-	-
$veg^{3/2}$	0.426	0.029	14.7	<0.0001
Equation: flux = 86.6 + $0.426*veg^{3/2}$ for MNORT and Scrape flux = -86.9 + $0.426*veg^{3/2}$ for MRABB and MWELL				

the greatest distance upwind from vegetation was approximately 100 m and that full-scale equilibrium for the wind erosion process occurs at distances that are typically 200-400 m downwind of the flux initiation point (Gillette et al., 1996). The initial steady increase of flux with distance occurs because the aerodynamic processes that entrain particles are enhanced by saltation or "bombardment" of the soil surface by the airborne particles leading to an avalanching effect (Chepil, 1957), and this increased saltation of particles leads to an increased roughness

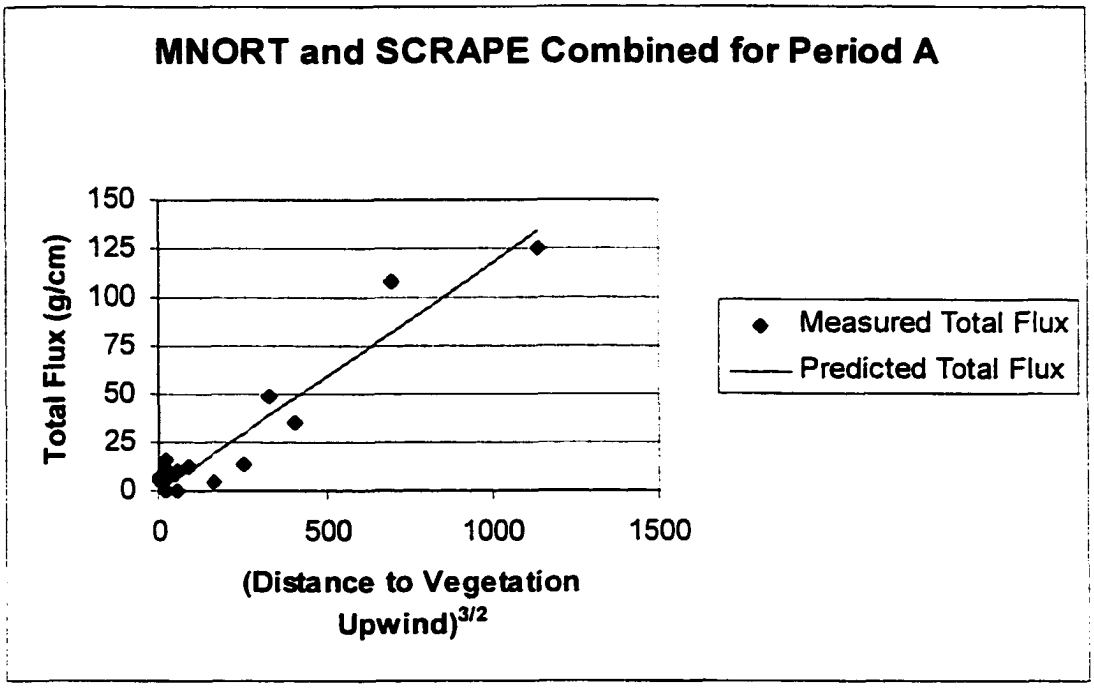

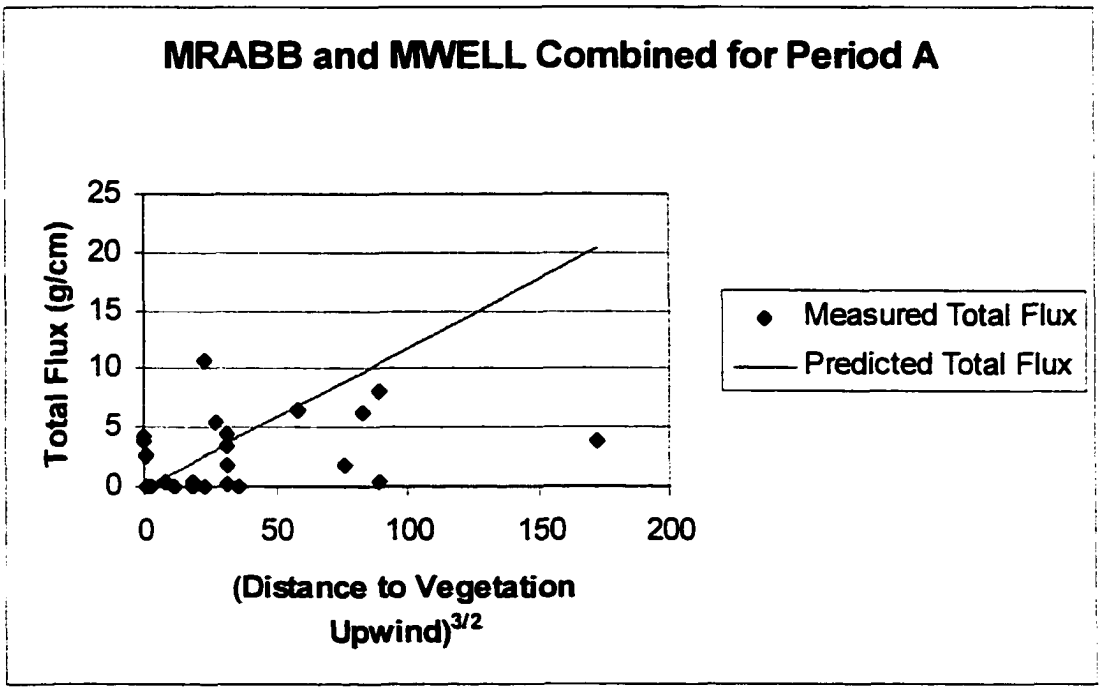

Figure 7-4. Measured and linear model prediction for flux at the four main sites for Period A.

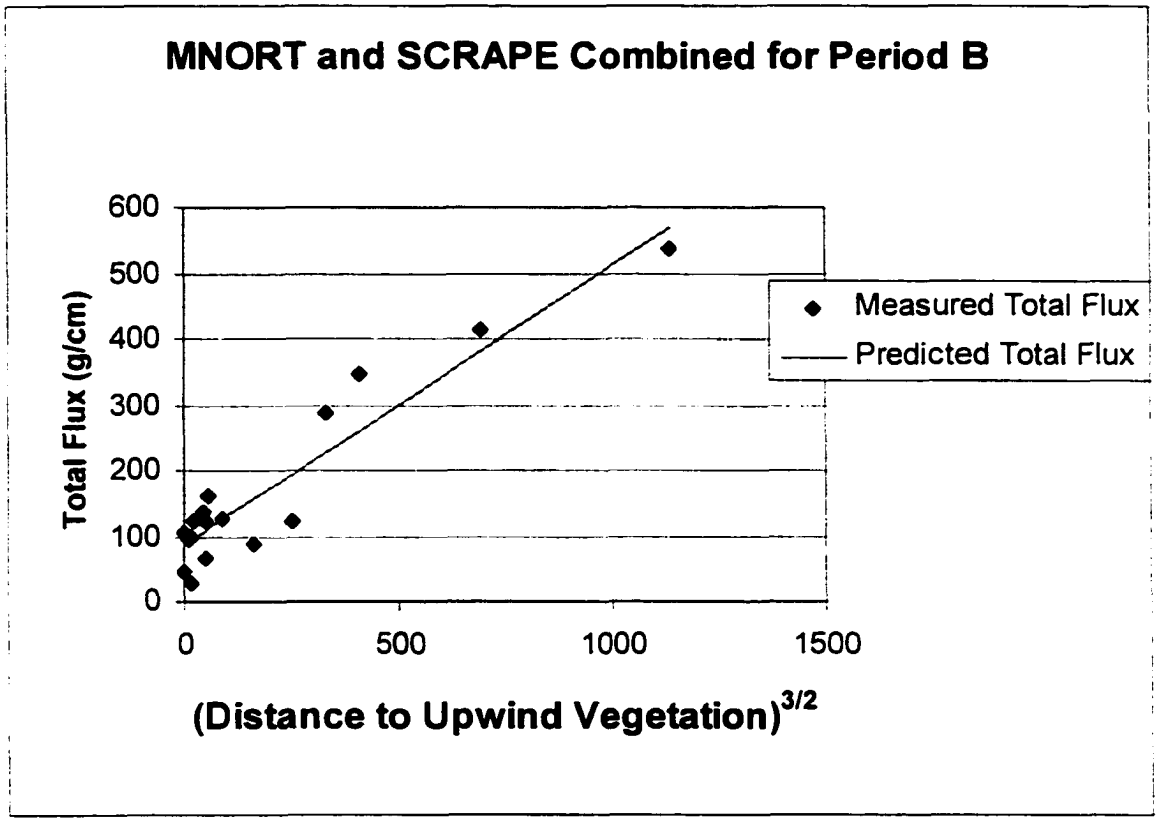

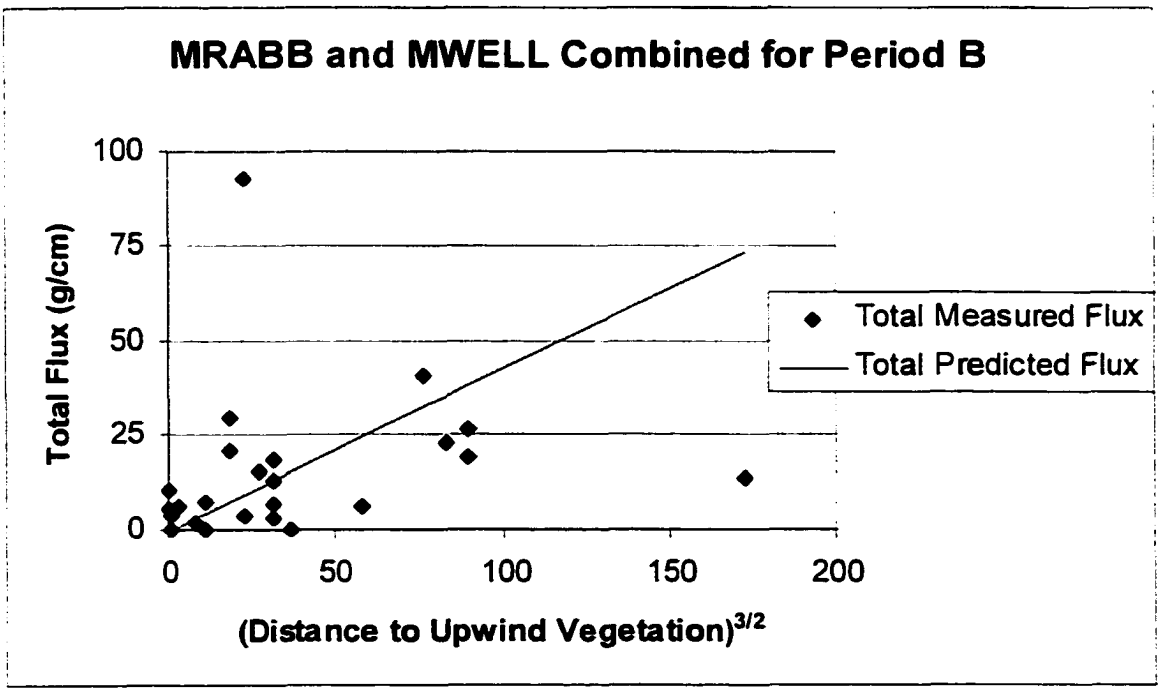

Figure 7-5. Measured flux values and linear model prediction for flux at the four main sites for Period B.

height, with an increase in momentum transfer and even more saltation (Shao and Raupach, 1992; Gillette et al., 1996).

To summarize, the presence of vegetation was a significant factor in protecting the soil surface from erosion. The upwind distance to vegetation along the predominant wind direction was a critical factor in predicting the wind erosion flux measured at randomly selected locations within the mesquite dune landscape, under conditions of both moderate and high wind speeds.

Continuous Meteorological and Aerosol Monitor Results

Meteorological Data

During the intensive field session, the meteorological systems at MNORT on the tower and the masts, including the Sensit™, performed well. Because the data system operated continuously under solar power, and data storage capacity was an issue, the data recorder was designed to record data only when a wind speed of 5 m/s was recorded at the 3-m level on the tower and for one of the masts at the 3.2 m level. When this threshold was reached, then all the parameters including temperature, wind speed and direction and the Sensit™ pulses were averaged and recorded at 10-minute intervals. To match data from other sensors with the meteorological data, it was necessary to average the data to the same 10-minute intervals, 10-minute averages stored by ending times.

Continuous Aerosol Monitor

Data Preparation

The DustTrak™ continuous aerosol monitors were operated in side-by-side configuration in relatively clean conditions for a 6-hour period, and then deployed to measure ambient conditions around the sand dune. Although all the instruments showed generally good agreement during the side-by-side operation, and all the instruments had been calibrated by the manufacturer in the two months preceding the field activities, all the instrument values were corrected mathematically based on the side-by-side measurements. The coefficients used to correct the data are listed in Table 7-6. If a capability for generating homogeneous, standards-traceable, elevated concentrations of fine particles were available, then it would have been possible to better assure and document the performance of the DustTrak™ units. The measurements by the DustTrak™ units can be best considered as relative measurements that have been referenced to each other.

Table 7-6. DustTrak™ correction equations based on side-by-side measurements.

Instrument	Equation	R-Square
Unit 5 =	1.4644 * Unit 0	0.91
Unit 5 =	1.1522 * Unit 2	0.94
Unit 5 =	0.9246* Unit 3	0.95
Unit 5 =	0.9391* Unit 4	0.94
Unit 5 =	1.1834* Unit 6	0.92

The DustTrak™ units were mounted on the ladder supports and operated whenever when a wind storm was forecast and dusty conditions were evident. To standardize the data processing, the same unit was placed in the same location for most events. Each unit had a unique serial number that happened to end in the digits 0, 2, 3, 4, 5, 6, so this was a convenient and permanent way to refer to the instruments. When each instrument was installed, the date, its location, and test number was entered into a log book. The instruments operated on disposable batteries; battery life was often 12 to 14 hours, but for complete dependability, 6 hours was more realistic. The instruments were operated without any environmental protection from temperature change. Over a 6-hour period, temperatures and battery performance were relatively consistent, and the data presented here are from these initial periods of operation. After field use, the units were returned to a clean setting and the DustTrak™-recommended maintenance checks for flow, filter changing, and cleaning were performed. All the units operated according to specifications during the intensive field session. The DustTrak™ units have internal clocks and internal data storage capabilities. The clocks were synchronized to the National Institute of Standards and Technology radio station WWV using transfer standards and relative differences between the DustTrak™ clocks, the GRIMM, and the standard were recorded and corrections performed. Data were recorded on a minute-by-minute basis, with a 10-s time constant, averaging 6 readings to record the minute average. After the units were returned from the field, the data were downloaded, and were stored on a lap-top computer. The proprietary

software provided by the manufacturer was used for checking the completeness and quality of the data after it was downloaded, while the actual processing for interpreting the data was performed using Excel™ and SAS. Data processing involved the use of both 1-minute and 10-minute averages. The 10-minute averaged data were compatible with the meteorological tower and mast measurements.

Dust Storms

DustTrak™ samplers were operated during 5 periods that covered the more dynamic parts of four storms. Excerpts selected for further analysis from these longer operating times focused on periods when concurrent data were available from all the samplers; these were nominally 6 hours long (Table 7-7). Two types of graphs are provided for each of these selected periods: one set displays 10-minute data from all the DustTraks™ along with friction velocities (Figures 7-5 to 7-8); while the other displays the 1-minute data from each DustTrak™ instrument separately (Appendix 4).

As might be expected from the dust collector data, the DustTrak™ PM_{10} data fall into two categories. The storms on April 14th and 15th were relatively small, while the storms on April 18th and 19th had 10-minute concentrations that were a factor of 10 higher. Still the overall appearance and length of the storms is similar.

The relative positions of the individual instruments is important to explaining what mechanisms are acting; e.g., a local source for PM_{10} can be inferred if the bottom instruments are measuring higher concentrations than the

Table 7-7. Dates and times for continuous DustTrak™ sampling at MNORT during the intensive session. The gap in the data on April 18th occurred when batteries were changed between two 6-hour periods.

Date	Start Time	End Time
4/14/2000	14:50	20:39
4/15/2000	11:00	16:59
4/18/2000	12:20	18:19
4/18/2000	18:51	23:59
4/19/2000	12:00	17:59

top instruments, while a middle- or long-range source can be inferred if the top instruments have the higher concentrations (Table 7-8). Of course, the decreasing gradient of the dust collector data with height at all the locations for all the wind storms measured shows some local production is likely during each storm so the comparison is to determine relative importance. The dune itself seems to have had differing effects on the DustTrak™ data collected at the mid-dune and downwind locations (for example, compare April 14 and April 15). For evaluating the possibility of middle-range transport of PM_{10}, the upwind (Upwind Top and Upwind Bot) instruments are probably the best choice. The height of the middle top instrument may have placed it in a separate regime that was well above the activity at the lower heights and more indicative of longer-range transport than the other top instruments. In fact, it measured lower concentrations than the other top instruments in three of the four storms. This is especially noticeable on April 14th and 18th. On April 19th, it measured some of the highest values, suggesting that long range transport may have been an

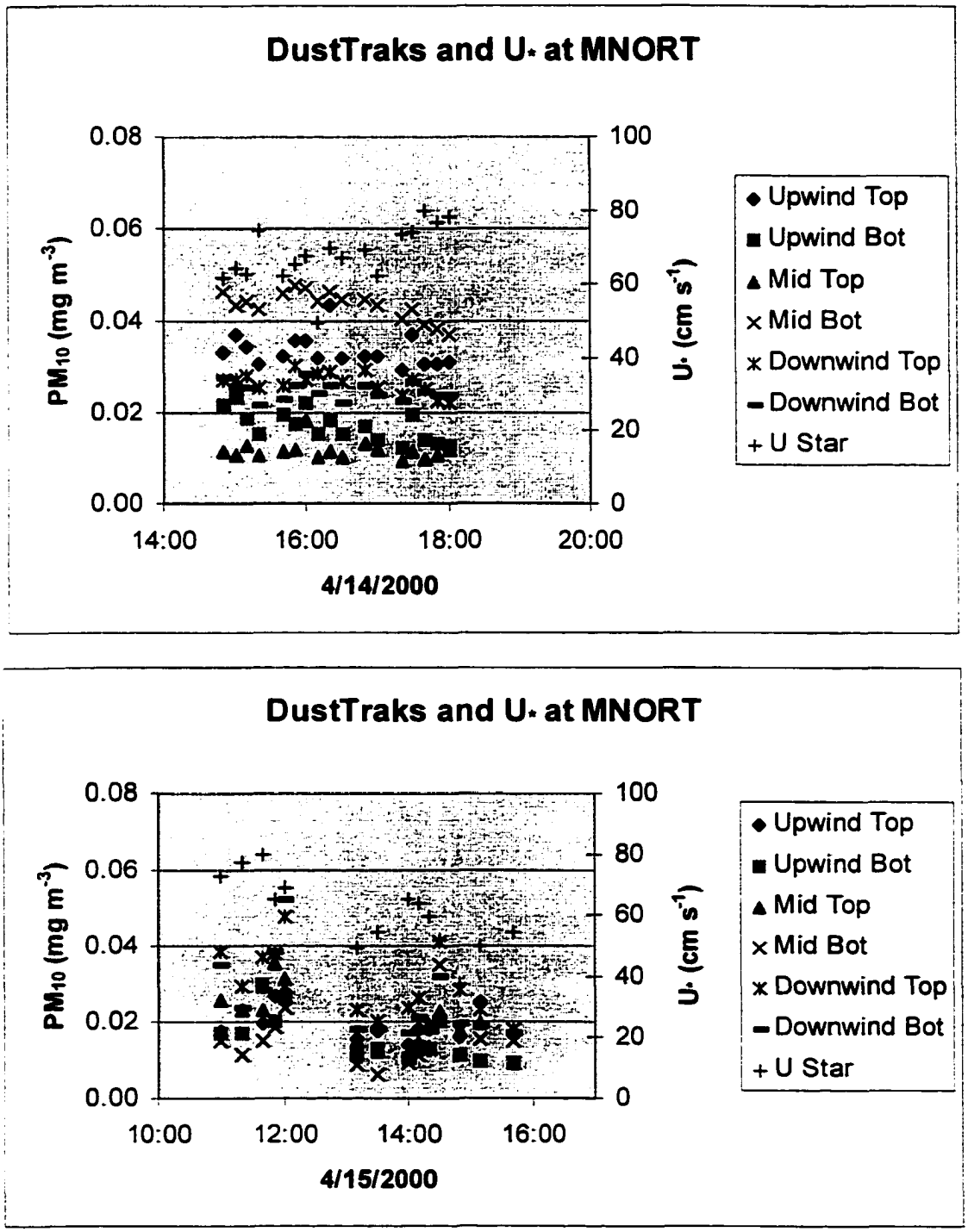

Figure 7-5. Data for the windy periods of April 14 and 15, 2000 with DustTrak™ data and the corresponding friction velocities, U* (U Star).

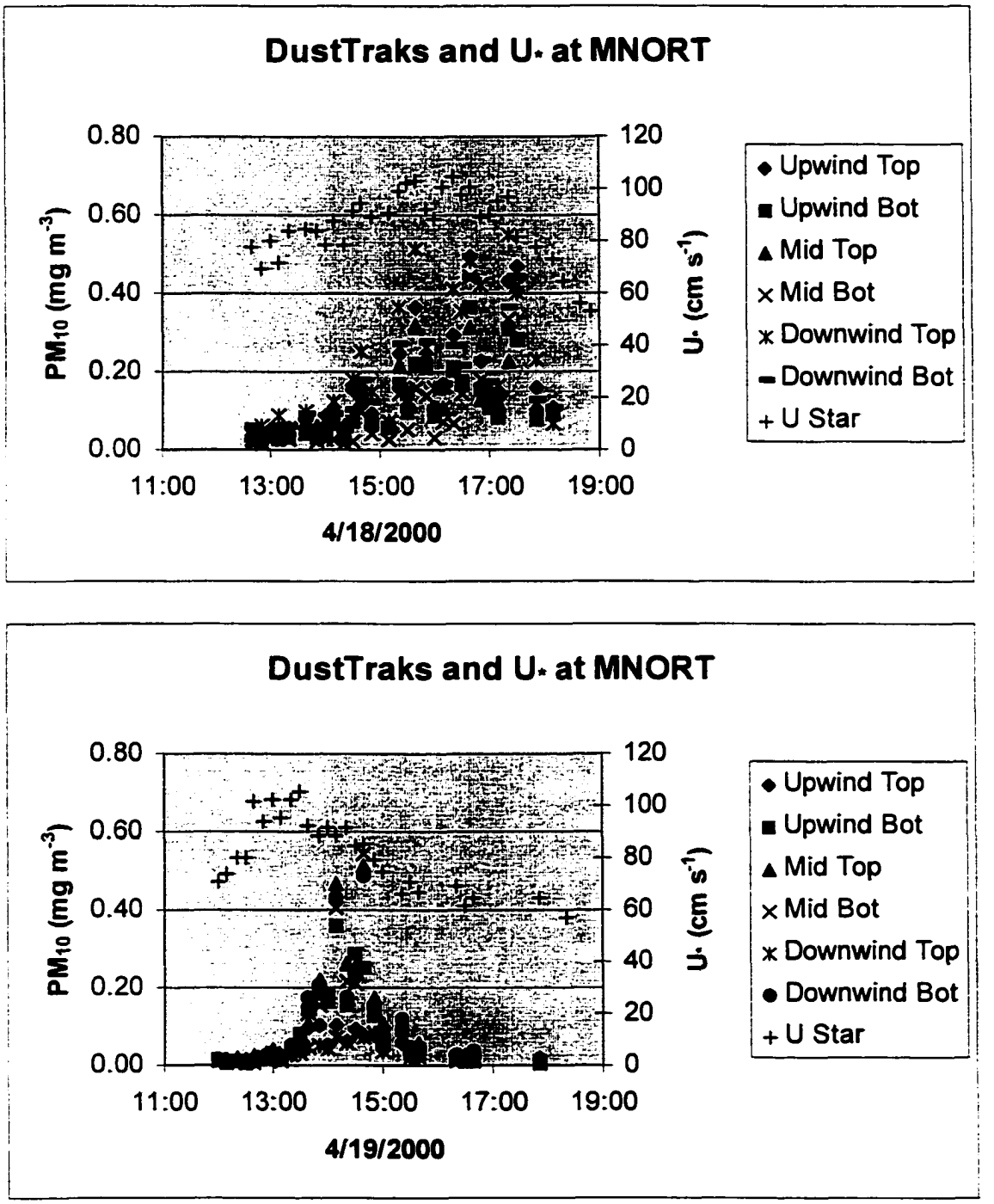

Figure 7-6. Data for the windy periods of April 18 and 19, 2000 with DustTrak™ data and the corresponding friction velocities, U* (U Star).

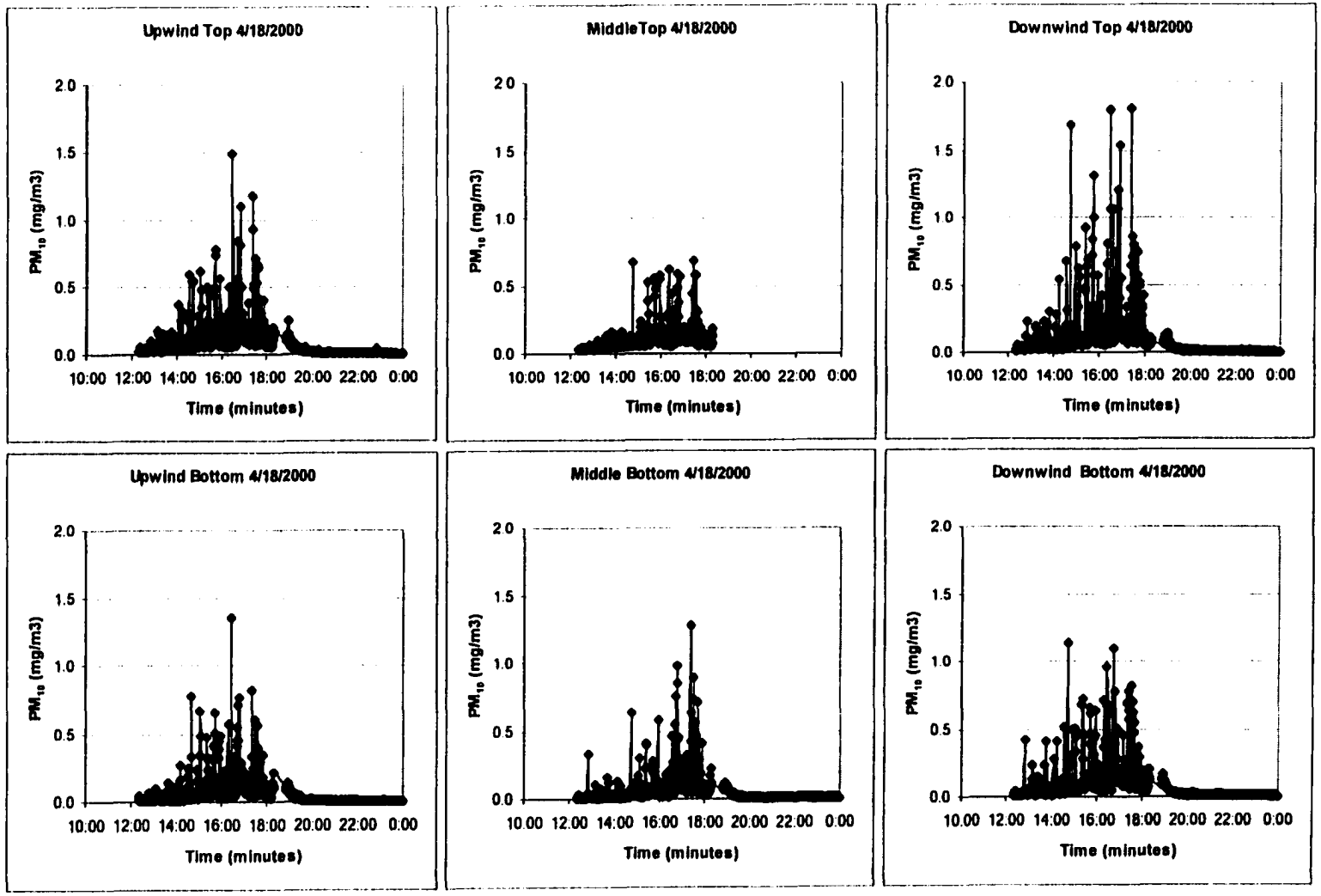

Figure 7-7. The individual DustTrak™ data for April 18, 2000 for each location at the dune site versus time, arranged on the page to suggest the spatial relationships of the instruments.

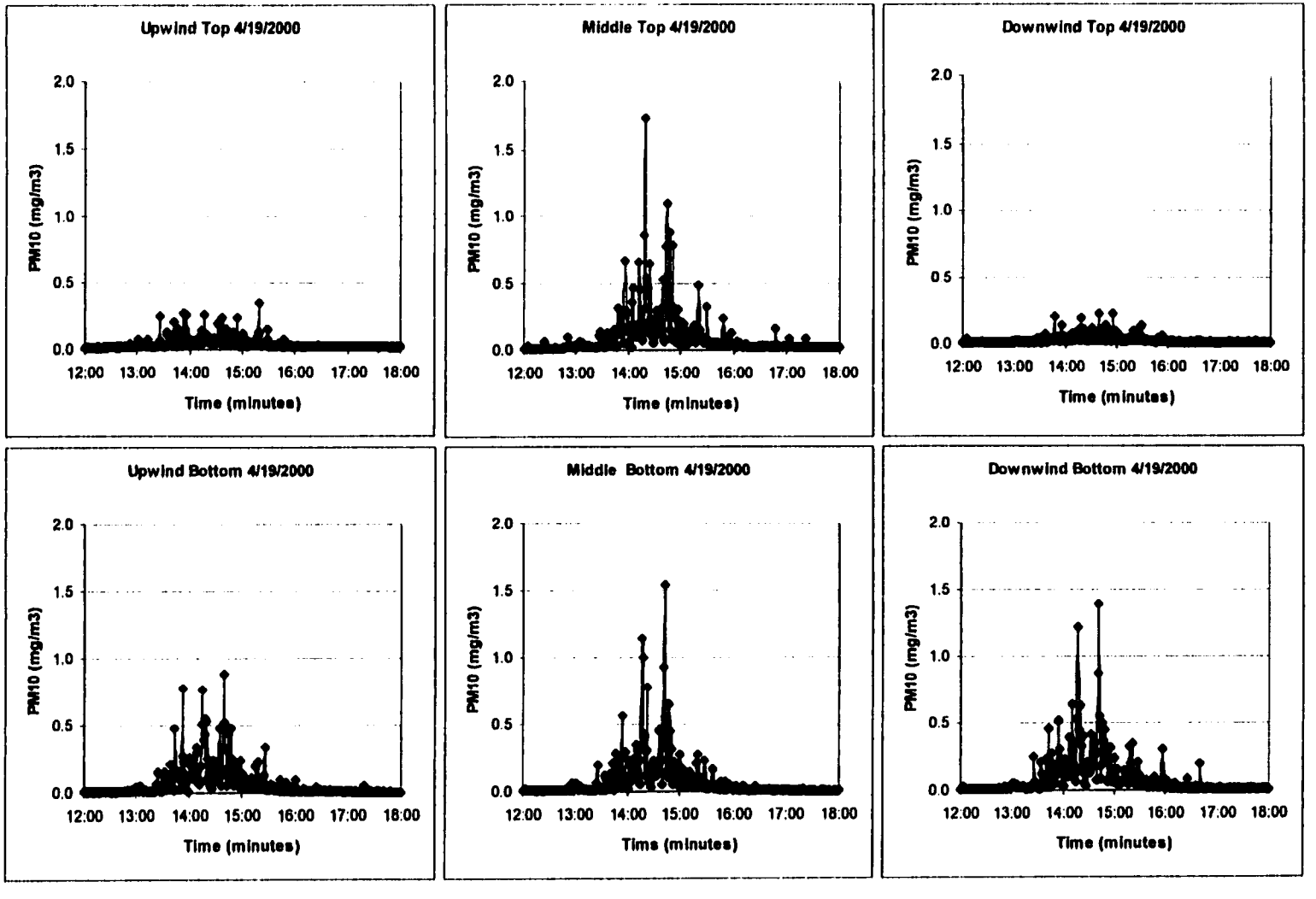

Figure 7-8. The individual DustTrak™ data for April 19, 2000 for each location at the dune site versus time, arranged on the page to suggest the spatial relationships of the instruments.

influence during that storm. It is also possible that the data were indicative of some upward mixing off the front edge of the dune. Additional measurements of winds and PM_{10} concentrations in future studies would help sort this out.

GRIMM™ measurements were performed on April 18th and 19th at locations upwind and downwind of the dune field (Table 7-8). On April 18th, the Geomet site was visited in the late evening. This site is on the downwind side of and within the mesquite dune field. On April 19th, measurements were made towards the end of the storm at a locations upwind and downwind of the dune area (North of the JER West Entrance and near the JER Ranch Headquarters, respectively). With only one GRIMM™, it was not possible to obtain simultaneous measurements, but the background concentration of PM_{10} seemed to have been approximately 20 $\mu g/m^3$ on the evening of April 19th. There was not enough information of this type to be conclusive.

During the most intense moments of the storms on April 18 and 19, 1-minute values exceeded 1 mg/m^3 at many of the instruments. For comparison, the National Ambient Air Quality Standard for PM_{10} maximum 24-hour standard is 150 $\mu g/m^3$ (U.S. EPA, 2002). This confirms the importance of using respirators and goggles when working in dust storm conditions in the mesquite dune setting.

In summary, significant concentrations of PM_{10} were measured in the dune field at the MNORT site. The relative concentrations measured at the upwind top and bottom instruments were used to suggest whether short-, medium-range transport might be influencing these instruments, while the

Table 7-8. Potential role of middle- and long-range transport to the MNORT site, evaluated by using the two upwind DustTrak™ sensors (Upwind Top and Upwind Bottom, "Bot") and the Middle Top (highest) sensor and comparing the values measured. These values are coded as H = high, M = medium, and L = low based on relative concentrations for the individual storm. [1]10-minute average at 9:00 PM; [2] 7-minute average at 5:42 PM; [3] 6-minute average at 6:29 PM.

Date	Upwind Top/Bot	Middle Top	GRIMM™ (μg/m³)
4/14/2000	M/L: middle range transport	L: no long-range influence	none
4/15/2000	much variability, no pattern	L: no long-range influence	none
4/18/2000	H/M: middle range transport	L: no long-range influence	Geomet site[1]: 48
4/19/2000	L/M: no middle range transport	H: long range influence	North of West JER entrance[2]: 22; and Hill near Ranch HQ[3]: 24

concentrations measured by the middle top instrument in comparison to the others were used to infer possible long-range transport to the site. Evidence for all scales of transport was observed. The effect of the dune on the concentrations measured upwind and downwind was mixed, depending on the storm. Additional measurements of both winds and PM_{10} in future studies would help to resolve this further.

Threshold Friction Velocity for PM_{10} and for Sand

Threshold friction velocity was evaluated using the Sensit™ data for sand movement and DustTrak™ data for PM_{10} (Figures 7-9 and 7-10). Data were combined for all storm periods. The plots were examined visually. For sand movement, the threshold friction velocity appears to be between 60 and 70 cm/s,

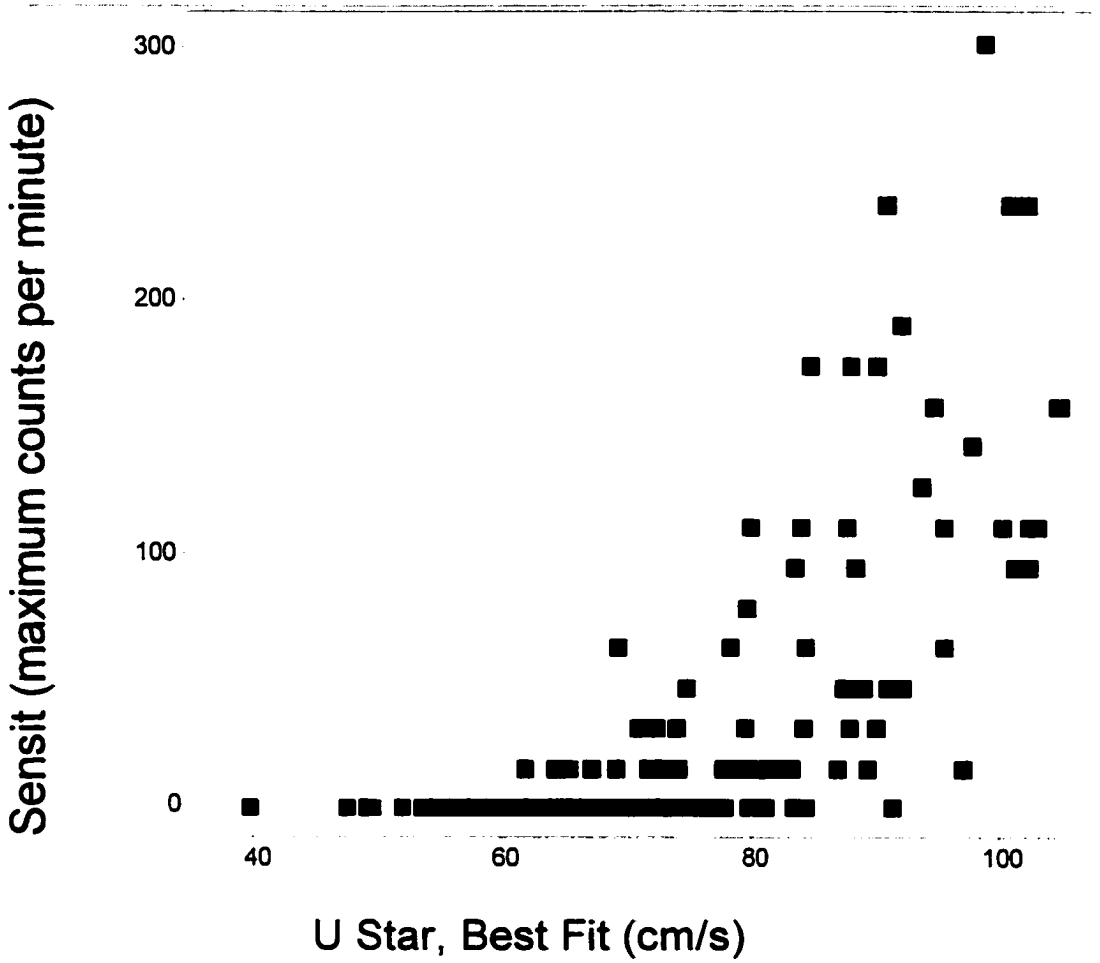

Figure 7-9. Determination of threshold friction velocity based on Sensit™ data for sand movement for the four storms of the intensive session. The threshold friction velocity appears to be between approximately 60 and 70 cm s^{-1}.

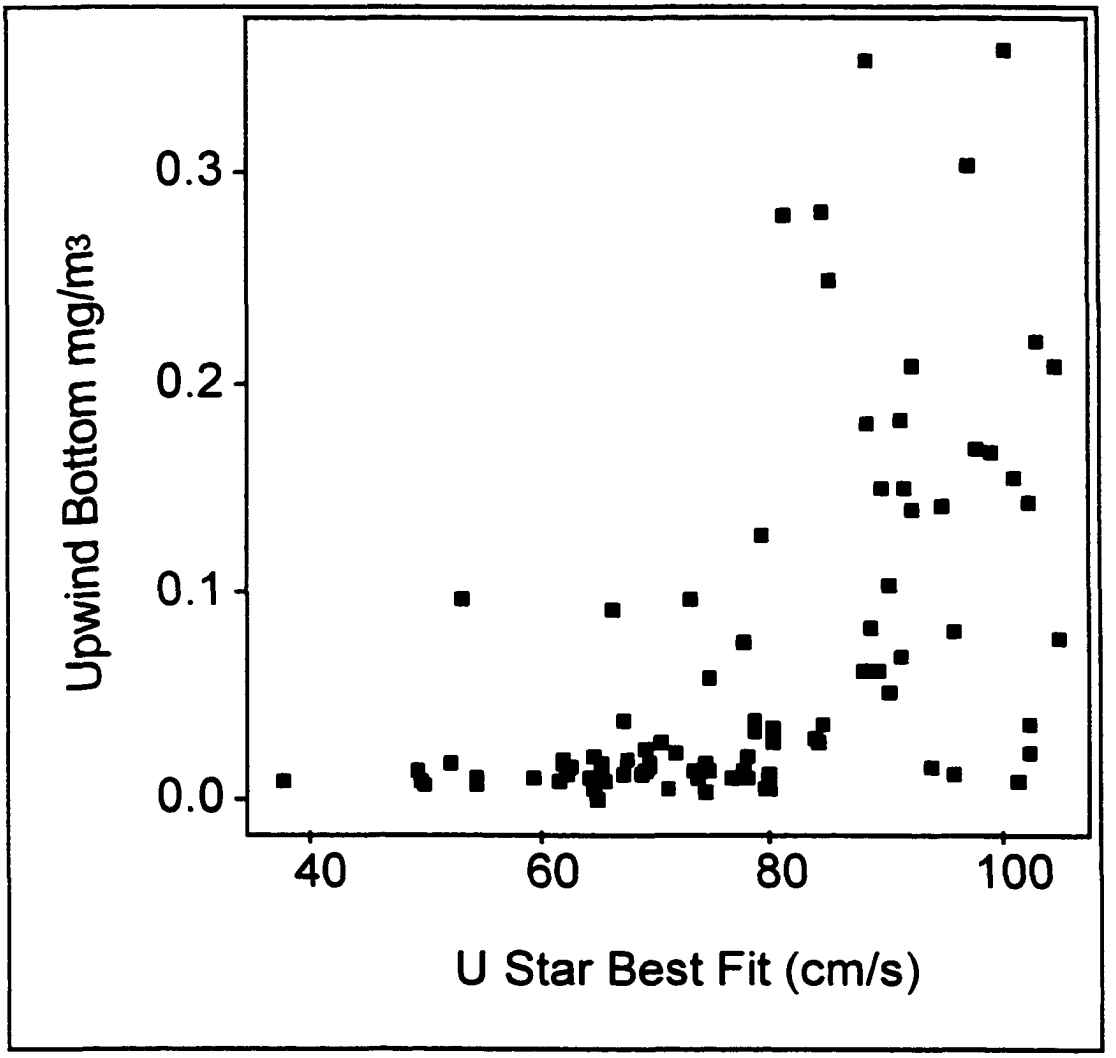

Figure 7-10. Determination of threshold friction velocity based on DustTrak™ data for the upwind bottom instrument for all four storms of the intensive session. The threshold friction velocity appears to be between 65 and 80 cm s^{-1} for PM_{10}. This assumes that the point measured at 0.1 mg m^{-3} and approximately 54 cm s^{-1} is an outlier.

while for PM_{10}, it appears to be between 65 and 80 cm s^{-1}. These values are similar to those previously measured for sand movement at selected locations within the JER using a portable wind tunnel and at the Scrape Site using a Sensit™ (Marticorena, et al., 1999; Gillette and Chen, 2001 respectively). It is not surprising that the two values are similar as PM_{10} is released by sand movement.

CHAPTER 8

FLUX MODELING

To investigate the effects of the dune on the PM_{10} concentrations near the dune, a simple set of flux models was developed and implemented. These models address the remaining question for this study:

- how do PM_{10} concentrations vary upwind and downwind of a mesquite dune?

The model assumptions and input data are described, and the results are discussed in this chapter.

Description of the Box Models

To investigate the behavior of PM_{10} particles near the dune, a set of models based on conceptual boxes was created. All these box models were aligned along the major axis of the dune between the west and east ladder-mounted dust sensors and included the entire dune (Figure 4-9). The first of the models defined the volume of interest around the dune as two rectangular boxes stacked vertically with the upwind and downwind faces centered on the dust sensors at heights of 1.5 m and 3 m (Figure 8-1). Concentrations at the upwind entrance and downwind exit of the boxes were assumed to be uniform across the face of the boxes. Fluxes were computed for both the upwind (West) and

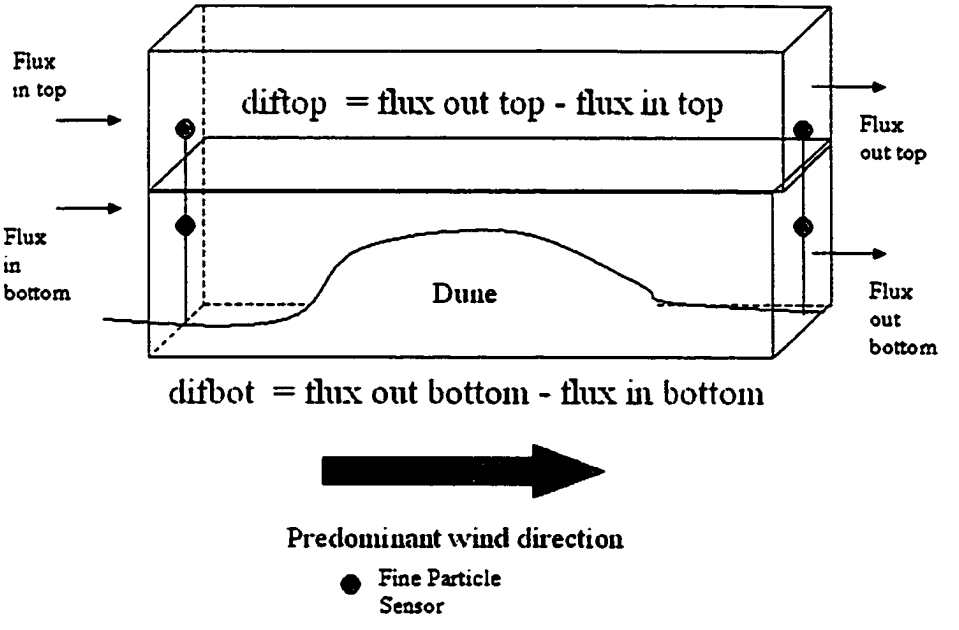

Figure 8-1. The 2-box model encompasses the dune in the lower box and has a second box directly above it.

downwind (East) faces for this 2-box model using the WT and WB sensors for the upwind values and using the ET and EB sensors for the downwind values. For each height box, the downwind flux was subtracted from the upwind flux, giving a net loss (or gain) for that height box as air and particles pass through it over the dune. The other models described below are derived from this 2-box model.

The next model defines the volume of interest by combining the two boxes into one large box, the 1-box model (Figure 8-2). The net fluxes from the two boxes are summed. This large box gives the net impact of the dune on the airstream as measured by all the upwind and downwind dust sensors.

The final model divides the 2-box model at the middle of the dune, creating a 4-box model (Figure 8-3). This model gives the net flux at two levels and for both the front and back portions of the boxes. Unlike the other two models, the boxes are envisioned as tilting up to rise over the dune, and tilting down towards the back of the dune. This configuration is a result of the dust sensors mounted on top of the dune being higher than those mounted upwind and downwind of the dune with the ladders at ground level. The configuration of the ladders and dust sensors is described in Chapter 4, Field Sampling. This shape follows the general form of streamlines over a low hill (Hunt et al., 1988a, 1988b). Hunt's criterion for a low hill was met by this dune.

Input Data Description

In general, flux for these models was calculated using simultaneous wind speed and dust concentration data in the form of 10-minute averages. The

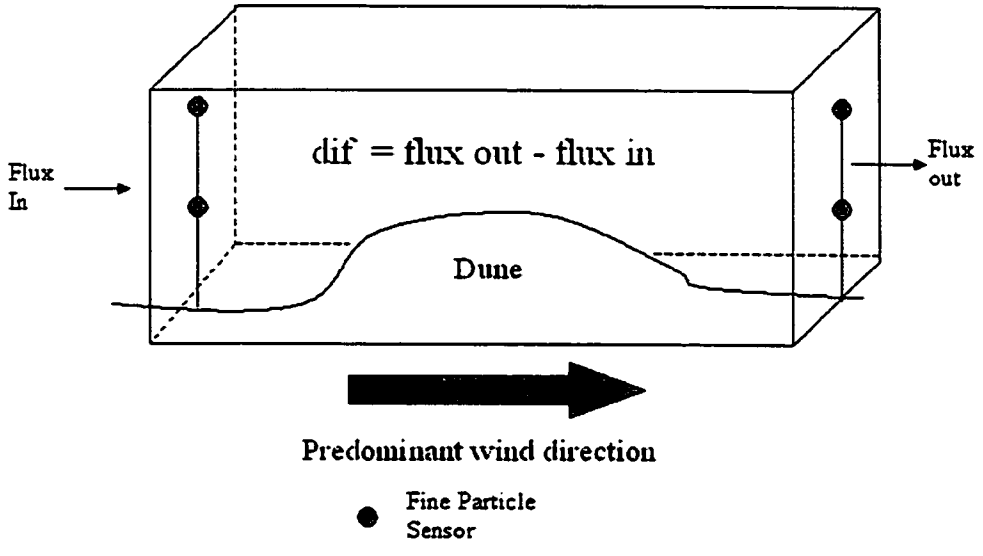

Figure 8-2. The 1-box model combines the two boxes from the 2-box model.

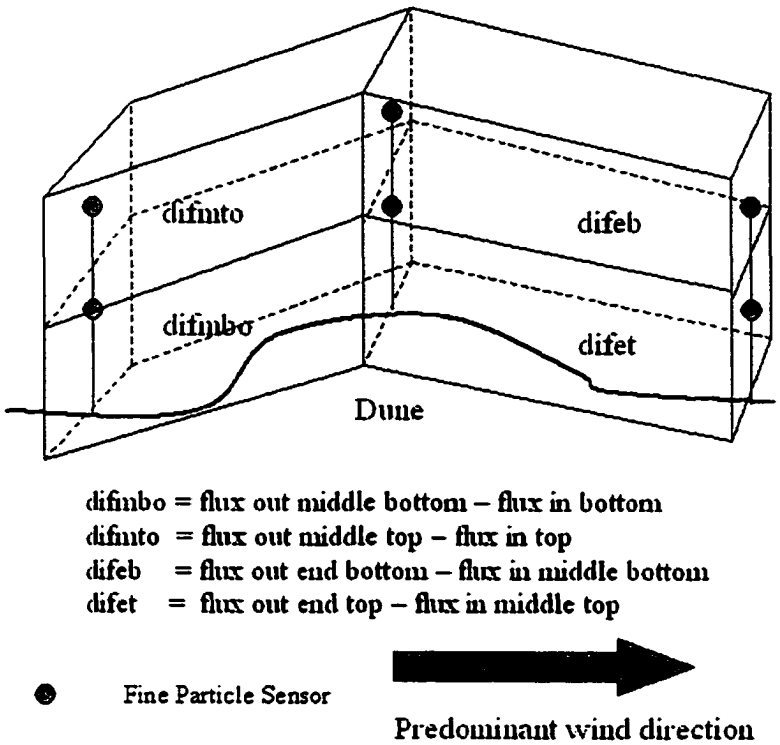

Figure 8-3. The 4-box model has additional faces at the center of the dune.

entrance and exit faces of the box models were chosen to be centered on the various dust sensors, so each of these faces has a corresponding sensor. The meteorological tower and masts were installed previously for a different purpose, and were not aligned with the dune. Still, because of its height the tower is believed to be representative of winds at the higher levels for the entire area. Two basic options were available for selecting the appropriate mast to represent the wind speed upwind and downwind of the dune: a) examine the surroundings of each of the masts in comparison to the corresponding dune setting and choose masts from analogous settings to represent the upwind and downwind dune conditions; or b) choose tower winds at two or three heights as needed to represent the winds at the DustTrak™ locations. Once the wind sensors were chosen, time periods were selected for modeling within a range of wind directions (225 to 245 degrees) to ensure that the wind was actually aligned over the dune.

Model Calculations

The basic equation for flux is

$$Flux\ (mg\ m^{-2}\ s^{-1}) = dust\ concentration\ (mg\ m^{-3}) * wind\ speed\ (m/s)$$

Eqn. 8-1

The flux calculations were performed for all the in and out faces of the box models, and expressed as differences

$$Flux\ difference = flux\ out - flux\ in$$ Eqn. 8-2

The flux for the upwind face (*flux in*) was subtracted from the flux for the downwind face (*flux out*). A positive value means that the amount leaving is greater than the

amount entering; this is a gain from the dune to the air and this represents a loss or erosion of the dune. A negative value means that the amount leaving is less than the amount entering; this is a loss from the air to the dune and represents a gain or deposition to the dune. For the purposes of the model, the conceptual boxes are assumed to have impervious sides and tops, but in reality, losses and gains could be occurring from both the sides and the top. This is particularly likely in the event of long-range transport conditions as suggested for the April 19th data.

Results

Examination of the wind direction data revealed that only two days, April 14th and April 18th, had sufficient data for modeling individually, so all the days were grouped together for analysis. Results for these days are presented with two options for wind data:

- In both options, tower winds were used to represent the corresponding middle dune heights; then
- Mast 3 top and bottom sensors were used for the upwind and downwind side of the dune (Option M3); alternatively,
- The lower two sensors for the tower were used for the upwind side of the dune, and Mast 5 was used for the downwind side (Option TM5).

The data for the model results follow the same format for both the wind sensor options M3 and TM5 (Table 8-1), presenting the results for the1-box model first (dif); followed by the results for the increasingly complex models. For the 2-box model, the variables are diftop and difbot (difference top and difference

Table 8-1. Statistical results for flux differences and propagated errors for both options for wind data. Positive values are indicative of erosion from the dune, while negative values are indicative of deposition. The propagated errors were based on standard deviations for wind speed and the DustTrak™ data; Option 1 used a constant standard deviation for the DustTrak™ data while Option 2 estimated the standard deviation as 10% of the DustTrak™ concentration; both options used a constant standard deviation for the wind speed.

Option M3 n=28	Mean Flux Difference ($mg\ m^{-2}\ s^{-1}$)	Standard Deviation ($mg\ m^{-2}\ s^{-1}$)	Propagated Error Option 1 ($mg\ m^{-2}\ s^{-1}$)	Standard Deviation Option 1 ($mg\ m^{-2}\ s^{-1}$)	Propagated Error Option 2 ($mg\ m^{-2}\ s^{-1}$)	Standard Deviation Option 2 ($mg\ m^{-2}\ s^{-1}$)
dif	0.441	0.628	0.026	0.008	0.210	0.184
diftop	0.200	0.490	0.020	0.006	0.166	0.152
difbot	0.241	0.274	0.017	0.006	0.122	0.113
difmtop	-0.048	0.828	0.020	0.005	0.150	0.132
difmbot	0.119	0.470	0.018	0.005	0.115	0.119
difet	0.248	1.067	0.020	0.006	0.168	0.151
difeb	0.122	0.365	0.018	0.006	0.131	0.131

Option TM5 n=28	Mean Flux Difference ($mg\ m^{-2}\ s^{-1}$)	Standard Deviation ($mg\ m^{-2}\ s^{-1}$)	Propagated Error Option 1 ($mg\ m^{-2}\ s^{-1}$)	Standard Deviation Option 1 ($mg\ m^{-2}\ s^{-1}$)	Propagated Error Option 2 ($mg\ m^{-2}\ s^{-1}$)	Standard Deviation Option 2 ($mg\ m^{-2}\ s^{-1}$)
dif	-0.297	0.546	0.025	0.008	0.195	0.169
diftop	-0.016	0.376	0.019	0.006	0.157	0.142
difbot	-0.281	0.347	0.016	0.005	0.107	0.101
difmtop	-0.103	0.855	0.020	0.005	0.155	0.136
difmbot	-0.033	0.430	0.019	0.006	0.125	0.127
difet	0.087	0.961	0.019	0.005	0.155	0.138
difeb	-0.248	0.525	0.016	0.005	0.105	0.111

bottom). For the 4-box model, the variables are difmto (difference middle top) and difmbo (difference middle bottom); and difeb (difference east bottom); and difet (difference east top). The first two columns provide the mean flux difference, and the standard deviation of the mean flux difference for all 28 cases with suitable wind directions. The results are presented for both wind sensor options, Option M3 and Option TM5, with the DustTrak™ data the same for both options. The large standard deviations indicate significant variability in these mean flux results.

Comparing the flux model results for the M3 and TM5 wind sensor options shows that the choice of wind data for the flux model significantly affected the results. For the M3 option, the mean flux values are all positive except for one while for the TM5 option they are all negative except one. Physically, flux losses for PM_{10} were attributed to deposition, and air parcel expansion and lifting over the dune; while flux gains were attributed to air parcel compression and input from lower layers including erosion of the dune surface. The features of air parcel compression and expansion in proximity to a small hill have been discussed previously (Hunt et al., 1988 a and b). When data from all days that meet the wind direction criterion were combined for the model, the net result was not significantly different from zero. Clearly, to fully understand the mechanisms of dune formation, maintenance, and erosion, wind data for the actual situation modeled are needed.

Propagation of Errors

The flux model incorporates unlike measurements (wind speed, PM_{10} concentrations) and mathematical relationships (multiplying and subtracting these variables), into a modeling framework. Because of this complexity, the effects of errors in the variables on the overall model were not readily apparent. In these type cases, propagation of error techniques are applied (Bevington, 1969). To compute the error associated with the product of wind speed and PM_{10} concentration, the following equation was used:

$$Flux\ error = ((SDWS/(wind\ speed\ (cm/s)/100)**2 + SDDT/(DustTrak^{TM}\ Concentration)**2)*(flux)**2)**0.5 \quad \text{Eqn. 8-3}$$

where *SDWS* and *SDDT* are the standard deviations of the wind sensors and DustTrak™ respectively. To compute the error associated with the difference between two fluxes, the following equation was used:

$$Difference\ error = (Flux\ Error_1**2 + Flux\ Error_2**2)**0.5 \quad \text{Eqn. 8-4}$$

The covariance term that could have been included in both these equations was assumed to be zero.

The values used for the standard deviations were developed from two sources. The value used for the standard deviation of the wind speed (*SDWS*) was 0.05, based on a survey of manufacturer's literature. The data from the side-by-side comparison were used to estimate the standard deviation for the DustTrak™ (*SDDT*). The corrected data (Chapter 7, Table 7-6) were used to compute the differences for each time interval between the individual instrument values and the group mean. The variation of these data with respect to the group mean value for each time interval does not show a trend with ambient concentration (Figure 8-4). However, the side-by-side was conducted during conditions with relatively low ambient concentrations and may not be representative of performance for higher ambient concentrations. Two options were considered. For Option 1, the standard deviation value for *SDDT* was 0.001; for Option 2, the standard deviation value was 10% of the measured *DustTrak™ concentration.*

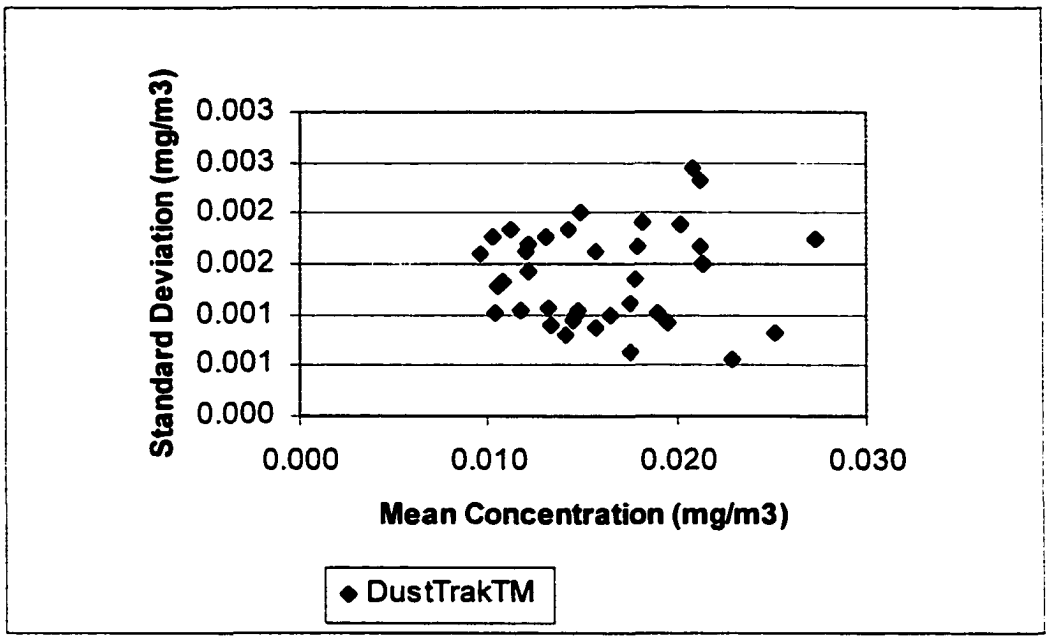

Figure 8-4. Standard deviation of DustTrak™ measurements compared to group mean concentration.

The propagated error values are provided for the constant and 10% options for the DustTrak™ standard deviations. The constant option, Option 1, provided estimates of the flux model error in the range of 10% to 20% of the mean flux differences, except when the means were close to zero. These estimates were lower than those from the 10% option, Option 2, with estimates of 50% to 100% error compared to the flux mean differences.

In summary, flux models were developed and applied for 28 cases when the 10-minute averaged wind data met the direction criteria for aligning with the sand dune. The results revealed the importance of having wind information for the dune being modeled. Error analysis showed that further characterization of the DustTrak™ variability is needed at higher concentrations because while a constant standard deviation yields acceptable results, the 10% option does not.

CHAPTER 9

SUMMARY, CONCLUSIONS, AND RECOMMENDATIONS FOR FUTURE WORK

This final chapter describes the conclusions derived from this study and provides ideas for future work. First, the study is summarized; a discussion of conclusions and recommendations for future work follows.

Summary

The purpose of this study was to investigate the effects of vegetation on soil particle-size distributions and airborne particle concentrations and characteristics, focusing on PM_{10}. This study site was chosen because it had been in use previously, and meteorological instruments and dust collectors were already installed and operating. Aerodynamic size distributions for soil and airborne particulate matter samples collected near and away from vegetation were determined using a settling tube apparatus at the U.S. Department of Agriculture Laboratory in Big Spring, Texas. In addition, 6 continuous aerosol monitors measuring PM_{10} were operated at locations upwind, downwind and on top of a sand dune during two dust storms; and a portable, hand-held dust monitor for determining the size distribution of dust was used to make instantaneous measurements of airborne concentrations at multiple sites near the same dune.

Conclusions

These results contribute to a better understanding of mesquite dune dynamics, and dune contributions to PM_{10} concentrations.

- The locations of vegetation determined using digital orthophotos compared well with manually-determined vegetation locations. This is the only known comparison of these types of data for mesquite vegetation. In future comparisons of this type, the manual vegetation measurement grid should be georeferenced to facilitate comparison with the aerial photography.
- The digital orthophotos were evaluated to determine the amount land area upwind of each of the four main sites with spectral reflectances similar to dirt roads in the area, believed to be a distinctive signature for loose, highly erodible sand. The mean total flux for the four main sites increased with the amount of spectrally-determined erodible soil material; while bare (unvegetated) soil alone did not explain the differences. This is the first time this approach was used and it warrants further development and evaluation.
- Dust collector samples showed that amounts collected and total flux calculated over heights from 0 to 1 meter increased as the distance from upwind vegetation increased for the predominant wind direction. The presence of these bare soil corridors among the mesquite dunes, "streets," had a significant effect on the quantities of sand collected. This is consistent with the "fetch effect" wind erosion theory that predicts greater

erosion with increasing distance downwind (Gillette et al., 1996).

- The threshold friction velocity for PM_{10} emissions was estimated to be between 65 to 80 cm s^{-1} using the continuous aerosol monitors. This is the first time this threshold friction velocity has been measured for PM_{10} within a mesquite sand dune setting. It will serve as a useful reference for other investigators.
- The threshold friction velocity for saltating sand particles was estimated to be between 60 and 70 cm s^{-1}. It is not surprising that the ranges of the threshold friction velocities overlap because saltating sand particles can disturb and release the finer particles. These values are consistent with values measured using a portable wind tunnel on agricultural fields with cloddy sand and cloddy loamy sand (Gillette, 1988) and fall between values measured for desert soils in the undisturbed and disturbed states (Gillette et al., 1980). Wind tunnel measurements at the Jornada showed varying threshold friction velocities depending on aggregate diameter of soil particles (Marticorena et al., 1997); the values determined for the MNORT site were typical of the 0.1-0.2 cm size range measured by these investigators. The threshold friction velocity values are higher than those measured using a combination of meteorological sensors and a Sensit™ at the unvegetated Scrape Site at the Jornada (Gillette and Chen, 2001).
- The results from the soil analyses suggest that the barren areas or "streets" within the mesquite dune areas are sources for fine sand that comprises a large portion of the dune. This is consistent with the idea that the medium

sand particles undergo saltation and are subject to short-range movement, while the fine sand particles can be lofted for short distances. VSATPM$_{10}$ particles were apparently scoured away from the dune sides while the street or long-range transport was a source area for these particles. The dune side particle distributions resembled the streets except for the finer particles, and were not a deposition area for the fine sand. It is possible that the dune sides were an area of wind acceleration and that particles that might otherwise settle in this area were transported to the dune top and beyond. These differences were attributed to deposition on the dune top and to differences in wind flow such as when its speed increases going up the dune side and when it slows passing through the mesquite stems.

- A flux model based on the continuous wind and PM$_{10}$ measurements, for cases when the wind was aligned with the dune axis, showed both losses and gains over the dune, depending on the choice of wind data for the model. The magnitude of the losses or gains was dependent on the wind speed and direction data chosen for the model. In this instance, adapting data collected for another purpose with the associated uncertainties in the wind speeds and directions does not lead to a high degree of confidence in the results. However, the flux model conceptual approach for assessing the flow over the dune is a valuable process that warrants further development.

Recommendations for Future Work

Many ideas for improvements developed as the study progressed. These

are organized below by topic area. It is important to realize that this study relied on using existing laboratory apparatus as a visiting scientist and using meteorological instrumentation and dust collector data from another study in the same location. These facilities and data were essential to the success of this study. These existing capabilities made it possible to focus on the PM_{10} issues and not on building a basic laboratory and monitoring infrastructure. The recommendations provided below are intended to reflect lessons learned in this process, and are not criticisms of these current systems which were intended for other purposes.

Having readily available, standardized methods for determining minimally-dispersed fine particle content in soils and airborne samples is important to the further the understanding of the behavior of these particles. A rapid and preferably field portable method for determining the PM_{10} content of a dry soil sample would have been a big time saver in this study. The combination of a suspension chamber with existing continuous aerosol and dust monitors may be a viable approach. Alternatively the settling tube approach could be standardized. In this case, the problem of fine particles adhering to larger particles during the sample drop needs to be addressed. It is not clear how the clumping condition relates to the concentrations measured in field conditions.

In preparation for settling tube analysis, small plumes of fine particles were observed rising from samples especially in the splitting process. Fine particles also adhered to the inside of the plastic bags that were commonly used to store the samples. Both these processes resulted in a preferential loss of fine particles,

leading to underestimates of their presence. The loss of fine particles due to sample splitting could be assessed by performing this process in a chamber and measuring the concentration during the process. The chamber could be ventilated and the exit air passed through a filter. This would add a safety factor by controlling the PM_{10} particles in the laboratory.

Additional masts located upwind and downwind of dunes collocated with particulate monitoring and combined with vertical velocity measurements would improve the confidence in the wind speed inputs to the flux model. Positioning dust collectors in front, on top, and behind dunes would provide additional data on the influence of a dune on both overall mass collected and PM_{10} content.

Finally, it would be useful to investigate similar settings in other areas of Chihuahuan desert using the same techniques to evaluate the representativeness of these data and their applicability to larger scale modeling efforts for PM_{10} in the desert Southwest.

BIBLIOGRAPHY

Ahlbrandt, T., 1979, "Textural Parameters of Eolian Deposits," Chapter B in A Study of Global Sand Seas, Edwin D. McKee, editor; prepared in cooperation with the National Aeronautics and Space Administration [Reston, Va.]: U.S. Dept. of the Interior, Geological Survey Professional Paper No. 1052; Washington, D.C., pp. 21-51.

Bagnold, R., 1954, The Physics of Blown Sands and Desert Dunes, Methuen and Company, London, 265 p.

Belnap, J. and D. Gillette, 1997, Vulnerability of desert soil surfaces to wind erosion: impacts of soil texture and disturbance, Journal of Arid Environments, Vol. X, pp. 1-17.

Bevington, P., 1969, Data Reduction and Error Analysis for the Physical Sciences, McGraw-Hill Book Company, New York, 336 p.

Bilbro, J., 1991, Relationships of cotton dry matter production and plant structural characteristics for wind erosion modeling, Journal of Soil and Water Conservation, Sept-Oct, p. 381-384.

Bilbro, J., and D. Fryrear, 1994, Wind erosion losses as related to plant silhouette and soil cover, Agronomy Journal, Vol. 86, pp. 550-553.

Blattner, P., L. Ulrich, K. Cook, T. Dyck, 1999, Special Edition, Using Microsoft Excel 2000, Que Corporation, Indianapolis, 1063 p.

Bork, E., N. West, K. Price, 1999, Calibration of broad- and narrow-band spectral variables for rangeland cover component, International Journal of Remote Sensing, Vol. 20(18), pp. 3641-3662.

Bulloch, H.E., Jr., and R.E. Neher, 1980, Soil Survey of Dona Ana County Area New Mexico, United States Department of Agriculture, Soil Conservation Service in cooperation with United States Department of the Interior, Bureau of Land Management New Mexico Agricultural Experiment Station, 177 p.

Butterfield, G., 1999, Near-bed mass flux profiles in aeolian sand transport: high-resolution measurements in a wind tunnel, Earth Surface Processes and Landforms, Vol. 24, pp. 393-412.

Chang, L., H. Suh, J. Wolfson, K. Misra, G. Allen, P. Catalano, P. Koutrakis, 2001, Laboratory and Field Evaluation of Measurement Methods for One-Hour Exposures to O3, PM2.5, and CO, Journal of the Air and Waste Management Association, 51, pp. 1414-1422.

Chepil, W., 1944, Utilization of crop residues for wind erosion control, Scientific Agriculture, Vol. 24(7), pp. 307-319.

Chepil, W., 1957, Width of field strips to control wind erosion, Agricultural Experiment Station, Technical Bulletin No. 92, pp. 1-16.

Chomette, O., M. LeGrande, and B. Marticorena, 1999, Determination of the wind speed threshold for the emission of desert dust using satellite remote sensing in the thermal infrared, Journal of Geophysical Research, Vol. 104(D24), pp. 31207-31215.

Chung, A., D. Chang, M. Kleeman, K. Perry, T. Cahill, D. Dutcher, E. McDougall, and K. Stroud, 2001, Comparison of Real-Time Instruments Used to Monitor Airborne Particulate Matter, Journal of the Air and Waste Management Association, 51, pp. 109-120.

Cui, B., P. Komar and J. Baba, 1983, Settling velocities of natural sand grains in air, Journal of Sedimentary Petrology, 53(4), pp. 1205-1211.

Danin, A. and E. Ganor, 1997, Trapping of airborne dust by Eig's meadowgrass (Poa eigii) in the Judean Desert, Israel, Journal of Arid Environments, Vol. 35, pp. 77-86.

Das, B., 1999, Fundamentals of Geotechnical Engineering, 1st edition, Brooks Cole Publishing Company, Pacific Grove, California, 576 p.

Fryrear, D., 1986, A field dust sampler, Journal of Soil and Water Conservation, 41, p 117-120.

Fryrear, D. and Saleh, A., 1993, Field wind erosion: vertical distribution, Soil Science, Vol. 155(4), pp. 294-300.

Gibbens, R., J. Tromble, J. Hennessy, and M. Cardenas, 1983, Soil movement in mesquite dunelands and former grasslands of southern New Mexico from 1933 to 1980, Journal of Range Management, 36(2), pp. 145-148.

Gillette, D. and T. Walker, 1975, Characteristics of airborne particles produced by wind erosion of sandy soil, high plains of west Texas, Soil Science, Vol. 123, No. 2, pp. 97-110.

Gile, L.H., 1966, Coppice dunes and the rotura soil, Soil Science Society of America Proceedings, Vol. 30, p. 657-660.

Gillette, D., 1978, Tests with a portable wind tunnel for determining wind erosion threshold velocities, Atmospheric Environment, Vol. 12, pp. 2309-2313.

Gillette, D., J. Adams, A. Endo, D. Smith, and R. Kihl, 1980, Threshold velocities for input of soil particles into the air by desert soils, Journal of Geophysical Research, Vol. 85(C10), pp. 5621-5630.

Gillette, D., J. Adams, D. Muhs, and R. Kihl, 1982, Threshold friction velocities and rupture moduli for crusted desert soils for the input of soil particles into the air, Journal of Geophysical Research, Vol. 87(C11), pp. 9003-9015.

Gillette, D.A., and Stockton, P.H., 1986, "Mass Momentum and Kinetic Energy Fluxes of Saltating Particles," pp. 35 - 56 in: Aeolian Geomorphology, Proceedings of the 17th Annual Binghampton Geomorphology Symposium, W. Nickling ed., Allen and Unwin, Boston, 311 p.

Gillette, D. 1988, Threshold friction velocities for dust production for agricultural soils, Journal of Geophysical Research, Vol. 93(D10), pp. 12645-12662.

Gillette, D., G. Herbert, P. Stockton, and P. Owen, 1996, Causes of the Fetch Effect in Wind Erosion, Earth Surface Processes and Landforms, v. 21 pp. 641-659.

Gillette, D., D. Fryrear, T. Gill, T. Ley, T. Cahill, and E. Gearhart, 1997, Relation of vertical flux of particles smaller than 10 um to total aeolian horizontal mass flux at Owens Lake, Journal of Geophysical Research, Vol. 102(D22), pp. 26009-26015.

Gillette, D., E. Hardebeck, and J. Parker, 1997, Large-scale variability of wind erosion mass flux rates at Owens Lake, 2. Role of roughness change, particle limitation, change of threshold friction velocity, and the Owen effect, J. Geophysical Research, v. 102, D22, pp. 25,989-25,998.

Gillette, D., and W. Chen, 1999, Size distributions of saltating grains: an important variable in the production of suspended particles, Earth Surface Processes and Landforms, v. 24, pp. 449-462.

Gillette, D. and W. Chen, 2001, Particle production and aeolian transport from a "supply limited" source area in the Chihuahuan Desert, United States, J. Geophysical Research, 106 (D6), p. 5267-5278.

Gillies, W., N. Lancaster, W. Nickling, and D. Crawley, 2000, Field determination of drag forces and shear stress partitioning effects for a desert shrub (Sarcobatus vermiculatus, greasewood), Journal of Geophysical Research, Vol. 105 (D20), pp. 24871-24880.

Goossens, D. and Z. Offer, 2000, Wind tunnel and field calibration of six aeolian dust samplers, Atmospheric Environment, Vol. 34, pp. 1043-1057.

GRIMM Labortechnik Ltd., 1996, Manual for the Dust Monitor Model 1.104/1.105/1.106, GRIMM Labortechnik Ltd., Ainring, Germany, 43 pp.

Hess, S., 1979, Introduction to Theoretical Meteorology, Krieger Publishing Co., New York, 362 p.

Holcombe, T., T. Ley, and D. Gillette, 1996, Effects of prior precipitation and source area characteristics on threshold wind velocities for blowing dust episodes, Sonoran Desert, Journal of Applied Meteorology, Vol. 36, pp. 1160-1175.

Huenneke, L., D. Clason, E. Muldavin, 2001, Spatial heterogeniety in Chihuahuan Desert vegetation: implications for sampling methods in semi-arid ecosystems, Journal of Arid Environments, Vol. 47, pp. 257-270.

Hunt, J., S. Leibovich, and K. Richards, 1988a, Turbulent shear flow over low hills, Quart. J. Royal Meteorological Society, v. 114, pp. 1435-1470.

Hunt, J., K. Richards, P. Brighton, 1988b, Stably stratified shear flow over low hills, J. Royal Meteorological Society, v. 114, pp. 859-886.

James, D., J. Pulgarin, J. Becker, S. Edwards, T. Gingras, G. Venglass, C. MacDougall, 2001, Development of vacant land emission PM-10 factors for Las Vegas Valley, in: Emission Inventory Conference: One Atmosphere, One Inventory, Many Challenges, May 1-3, 2001, Denver Colorado, Office of Air Quality Planning and Standards, U.S. Environmental Protection Agency downloaded from http://www.epa.gov/ttn/chief/conference/ei10/index.html#ses-5

Kvanli, A., 1988, Statistics, a Computer Integrated Approach, West Publishing Company, St. Paul, 935 p.

Lancaster, N., and A. Baas, 1998, Influence of vegetation cover on sand transport by wind: field studies at Owens Lake, California, Earth Surface Processes and Landforms, Vol. 23, pp 69-82.

Langford, R.P., 2000, Nabkha (coppice dune) fields of south-central New Mexico, U.S.A., Journal of Arid Environments, Vol. 46, pp. 25-41.

Lehtimaki, M. and Willeke, K., 1993, Measurement Methods, pp. 112-129 in Aerosol Measurement Principles Techniques and Applications, K. Willeke and P. Baron eds., Van Nostrand Reinhold, New York, 876 p.

Lyon, J., J. McCarthy, J. Heinen, 1986, Video digitization of aerial photographs for measurement of wind erosion damage on converted rangeland, Photogrammetric Engineering and Remote Sensing, Vol. 52(3), pp. 373-377.

Malcolm, L.P. and M.R. Raupach, 1991, Measurements in an air settling tube of the terminal velocity distribution of soil material, Journal of Geophysical Research, Vol. 96, No. D8 pp. 15,275-15,286.

Marticorena, B., G. Bergametti, D. Gillette, and J. Belnap, 1997, Factors controlling threshold friction velocity in semiarid and arid areas of the United States, Journal of Geophysical Research, Vol. 102(D19), pp. 23277-23287.

McVay, K., 1998, Shape Warp 2.1, available free of charge at www.esri.com.

Micallef, A., C. Deuchar, and J. Colls, 1998, Kinetic Sequential Sampling (KSS) System: an automated sampling system for measuring vertical concentration profiles of airborne particles, Journal of Air and Waste Management Association, 48, pp. 757-762.

Mulligan, K., 1995, Field methods in a study of the process response system controlling dune morphology, Salton Sea, California, pp. 131-152, in Tchakerian, V. ed., Desert Aeolian Processes, Chapman and Hall, New York, 326 p.

Musick, H. and D. Gillette, 1990, Field evaluation of relationships between a vegetation structural parameter and sheltering against wind erosion, Land Degradation and Rehabilitation, Vol. 2, pp. 87-94.

Musick, H., S. Trujillo, and C. Truman, 1996, Wind-tunnel modelling of the influence of vegetation structure on saltation threshold, Earth Surface Processes and Landforms, Vol. 21, pp. 589-605.

Nickling, W. and J. Gillies, 1989, Emission of fine-grained particulates from desert soils, in: Paleoclimatology and Paleometeorology: Modern and Past Patterns of Global Atmospheric Transport, Kluwer Academic Publishers, Boston, pp. 133-165.

Okin, G., and D. Gillette, 2001, Distribution of vegetation in wind-dominated landscapes: implications for wind erosion modeling and landscape processes, Journal of Geophysical Research, Vol. 106, D9, pp. 9673-9683.

Peters, A. J., Eve, M. D., Holt, E. H. and Whitford, W. G.,1997, Analysis of desert plant community growth patterns with high temporal resolution satellite spectra, Journal of Applied Ecology, Vol. 34, pp. 418-432.

Pye, K., 1987, Aeolian Dust and Dust Deposits, Academic Press, London, 334 p.

Pye, K. and Haim Tsoar, 1990, Aeolian Sand and Sand Dunes, Unwin Hyman, London, 396 p.

Raupach, M., 1992, Drag and drag partition on rough surfaces, Boundary-Layer Meteorology, Vol. 60, pp. 375-395.

Raupach, M., D. Gillette, and J. Leys, 1993, The effect of roughness elements on wind erosion threshold, Journal of Geophysical Research, Vol. 98, D2, pp. 3023-3029.

Raupach, M. and J. Leys, 1999, The efficacy of vegetation in limiting spray drift and dust movement, CSIRO Land and Water, Technical Report 47/99, 42 p.

Roberson, J. and C. Crowe, 1993, Engineering Fluid Mechanics, Fifth Edition, Houghton Mifflin Company, Boston, 823 p.

SAS Institute Inc., 1990, SAS/STAT User's Guide (Version 6, 4th Ed.), Vol. 2, Cary, North Carolina, USA.

Schwartz, R., D. Fryrear, and A. Juo, 1997, Simulation of wind forces and erosion in a field with windbreaks, Soil Science, Vol. 162(5), pp. 372-381.

Sensit, Company, 2002, Data Processing and Calibrations, retrieved 5/3/2002 from http://www.sensit.com/dnLoad.htm

Shao, Y. and M. Raupach, 1992, The overshoot and equilibration of saltation, J. of Geophysical Research, v. 97, pp. 20559-20564.

Shao, Y., G. McTainsh, J. Leys, M. Raupach, 1993, Efficiencies of sediment samplers for wind erosion measurements, Australian Journal of Soil Research, 31, pp. 519-532.

Shao, Y, M. Raupach, and P. Findlater, 1993, The effect of saltation bombardment on the entrainment of dust by wind, J. Geophysical Research, pp. 12719-12726.

Shao, Y., 2000, Physics and Modelling of Wind Erosion, Kluwer Academic Publishers, Boston, 393 p.

Skidmore, E., 1986, Wind erosion control, Climatic Change, Vol. 9, pp. 209-218.

Stockton, P. and D. Gillette, 1990, Field measurement of the sheltering effect of vegetation on erodible land surfaces, Land Degradation and Rehabilitation, Vol. 2, pp. 77-85.

Stout, J.E., and Zobeck, T.M., September 1996, "The Wolfforth Field Experiment: A Wind Erosion Study," Soil Science, v. 161, No.9., pp. 616-632.

TSI, Inc., 2000, DUSTTRAK™ Aerosol Monitor Model 8520 Operation and Service Manual, TSI, Inc., St. Paul, MN.

U.S. Department of Agriculture, 2002, "About the Jornada Experimental Range," in Jornada Experimental Range, http://usda-ars.nmsu.edu/index.htm , 8 p.

U.S. Department of the Interior, 1996, Standards for Digital Orthophotos, Part 1 General, U.S. Geological Survey, National Mapping Division, 9 p.

U.S. Environmental Protection Agency, 1995, "13.2 Introduction to Fugitive Dust Sources" in Compilation of Air Pollutant Emission Factors, AP-42, Fifth Edition, Volume I: Stationary Point and Area Sources, AP-42, Washington, D.C.

U.S. Environmental Protection Agency, 2002, National Ambient Air Quality Standards, Code of Federal Regulations, Title 40 Part 50.

U.S. Environmental Protection Agency, 1998, National Air Quality and Emissions Trends Report, EPA-454/R-98-016, Research Triangle Park, N.C.,184 p.

Van Dijk, P., S. Arens, and J. Van Boxel, 1999, Aeolian processes across transverse dunes II: Modeling the sediment transport and profile development, Earth Surface Processes and Landforms, Vol. 24(5), pp. 319-333.

Wiggs, G., I. Livingstone, D. Thomas, and J. Bullard, 1996, Airflow and roughness characteristics over partially vegetated linear dunes in the southwest Kalahari Desert, Earth Surface Processes and Landforms, Vol. 21, pp. 19-34.

Willeke, K. and P. Baron, 1993, Aerosol Measurement Principles, Techniques, and Applications, Van Nostrand Reinhold, New York, 876 p.

Wolfe, S. and W. Nickling, 1996, Shear stress partitioning in sparsely vegetated desert canopies, Earth Surface Processes and Landforms, Vol. 21, pp. 607-619.

Yanosky, J., P. Williams, D. MacIntosh, 2002, A comparison of two direct-reading aerosol monitors with the federal reference method for $PM_{2.5}$ in indoor air, Atmospheric Environment, 36(1), pp. 107-113.

APPENDIX 1

Copyright permission letters for Figures 2-3 and 2-5 are attached.

kluwer

Van Godewijckstraat 30
P.O. Box 17
3300 AA Dordrecht
The Netherlands

+31 (0) 78 65 76 000
+31 (0) 78 65 76 254
www.wkap.nl
services@wkap.nl

Ms. A. Pitchford
U.S. EPA, NERL/ESD/LEB
P.O. Box 93478
Las Vegas, NV 89113-3478
USA

03/05/2002

Re: Shao: *Physics and Modeling of Wind Erosion* (2000), f. 5.7, p. 128, f.5.9, p. 131

Dear Ms. Pitchford,

With reference to your request (copy herewith) to reprint material on which Kluwer Academic Publishers control the copyright, our permission is granted, free of charge, and at the following conditions:

- it concerns original material which does not carry references to other sources (if material in question appears with credit to another source, authorization from that source is required as well);
- permission is granted for all languages;
- permission is also obtained from the author (address is given on the imprint page, or with the article);
- permission includes use in an electronic form, if password protected, on intranet, or CD-Rom/E-book;
- full credit (Kluwer Academic Publishers book/journal title, volume, year of publication, page, chapter/article title, name(s) of author(s), figure number(s), original copyright notice) is given to the publication in which the material was originally published, by adding: with kind permission of Kluwer Academic Publishers.

Sincerely yours,

Iris Jägers
Rights and Permissions
Tel: +31 (0)78 6576130
Fax: +31 (0)78 6576254
E-mail: iris.jager@wkap.nl
KLUWER ACADEMIC PUBLISHERS

PS.PLEASE BE CERTAIN TO INCLUDE OUR REFERENCE IN ALL CORRESPONDENCE

27 May 2002

Ann Pitchford
Environmental Scienes Division
United States Environmental Protection Agency
Landscape Ecology Branch
PO Box 93478
Las Vegas
Nevada 89193-3478
USA

Dear Ann Pitchford

Thank you for your letter requesting permission to use the above material from :

Figure 3.9, p49, Kenneth Pye: Aeolian Dust and Dust Deposits

We are happy to grant permission for this use of your material provided that (1) complete credit is given to the source, including the Academic Press copyright notice (2) the material to be used has appeared in our publication without credit or acknowledgment to another source and (3) if commercial publication should result, you must contact Academic Press again.

We realize that University Microfilms must have permission to sell copies of your thesis, and we agree to this. We would point out, however, that this does not apply to separate sale of your article.

Thank you for approaching us in this matter.

Yours sincerely

CATHERINE JOHN (Ms)
Rights and Permissions Manager

APPENDIX 2

Software Used to Process VSAT Data (adapted from Chen, pers. comm.)

```
DECLARE SUB Temperature (TR!, ABVIS!, RHOF!)
CLS : KEY OFF
    'PROGRAM GNSZVST5.BAS --THE LAST VERSION ON AUGUST 1, 1997.
LOCATE 6
COLOR 15, 4

PRINT "THIS PROGRAM  CALCULATES SETTLING TIME AND SIZE PARAMETERS
    "
PRINT "OF PARTICLES BY VERTICAL SETTLING AEROSOL TUBE--A SEDIMENTATION
METHOD."
PRINT "THE LAST VERSION BY CHEN---AUGUST 1, 1997"
PRINT "PROGRAM STEPS CHECKED, DOCUMENTATION AUGMENTED"
PRINT "EXCEL OUTPUT FILE ADDED; INTENDED FOR SINGLE INPUT FILE
     PROCESSING"
PRINT "REVISIONS BY PITCHFORD, 2001 "

    'SOME COMMENTS AND DEFINITIONS

    'ABVIS        --ABSOLUTE VISCOSITY (KG/M SEC)
    'AZ           --VERTICAL ACCELERATION (METERS/SEC^2)

    'BNDA         --BASE NUMBER FOR DATA FILES

    'D            --DIAMETER OF PARTICLE (METERS)
    'DT           --TIME INTERVAL FOR INTEGRATION (SEC) (DELTA T)

    'FD           --FINEST GRAIN SIZE, MICRONS
    'FT (ND)      --TIME IN COMPLIANCE WITH THE ASCENDING PARTICLE-SIZE
                   IN PHI UNIT
    'FTA (ND)     --FALLING TIME
    'FT1 (ND)     --FALLING TIME AFTER GROUPING

    'G            --ACCELERATION OF GRAVITY (9.81 M/SEC^2)

    'H            --LENGTH OF TUBE (6.2013 M)

    'K            --COUNTER FOR FALLING PARTICLE, ALSO FOR PHI SIZE ARRAY
    'KK           --NUMBER OF PARTICLE SIZES (ND-FD+1)
    'K1           --PREVIOUS K, ALSO COUNTER FOR TIMES

    'ND           --COARSEST GRAIN SIZE (MICRONS)
    'NR           --RADOLDS NUMBER

    'P1(7)        --PERCENTILE DIAMETERS
    'PHISD(ND)    --PARTICLE-SIZE IN phi UNITS IN DESCENDING ORDER
    'PHID (ND)    --PARTICLE-SIZE IN phi UNITS IN ASCENDING ORDER
    'PHID1(ND)    --PARTICLE-SIZE IN phi UNITS IN ASCENDING ORDER AFTER
                    COMPARISON WITH THE RECORDED SETTLING TIME
    'PHID2(ND)    --GROUPED PARTICLE-SIZE IN phi UNITS
    'PHIWtP(ND)   --WEIGHT PERCENT IN COMPLIANCE WITH PHID1(ND)
    'PRESSURE     --BAROMETRIC PRESSURE (INCHES HG)

    'Q            --COUNTER FOR NUMBER OF SAMPLES
    'Q1           --COUNTER FOR NAMING DATA FILES

    'RG           --ACCELERATION OF GRAVITY, G, CORRECTED FOR RELATIVE
                    DENSITIES OF AIR AND PARTICLES
    'RHOF         --DENSITY OF FLUID (AIR, KG/M^3)
    'RHOP         --DENSITY OF PARTICLE (KG/M^3)
```

```
    'RN           --REYNOLDS NUMBER
    'RST(850/0.3)--RECORDED SETTLING TIME BY VSAT TEST IN 300
                   MILLISECOND INTERVALS
    'RWtG(850/0.3)--RECORDED WEIGHT IN GRAMS BY VSAT TEST IN ASCENDING
                    ORDER
    'RWtG1 (ND)   --WEIGHT IN GRAMS IN COMPLIANCE WITH PARTICLE-SIZE
    '               WHICH HAS BEEN COMPARED WITH THE VSAT RECORD
    'RWtP (ND)    --WEIGHT PERCENT OF THE RECORDED CUMULATIVE FREQUENCY
    'RWtP1(ND)    --CUMULATIVE WEIGHT PERCENT IN COMPLIANCE WITH THE
                    GROUPING DIAMETER
    'RWtP2(GN)    --WEIGHT PERCENT IN EACH GROUP

    'S            --NUMBER OF SAMPLES TO BE PROCESSED
    'SAMWEIGHT(I) --SAMPLE WEIGHT FOR EACH EXPERIMENT BEING PROCESSED
    'SD (ND)      --J*10^3, FOR PARTICLE-SIZE IN mm STORED IN DESCENDING
                    ORDER
    'SD1 (ND)     --PARTICLE-SIZE AFTER COMPARISON WITH THE VSAT RECORD

    'TEMP(I)      --MEASURED TEMPERATURES FROM TOP, MIDDLE, AND BOTTOM
                   OF TUBE
    'TR           --TEMPERATURE IN RANKINE DEGREES
                       =(CENTIGRADE+273.15)*1.8
    'T            --TIME
    'T1           --PREVIOUS T

    'WREL         --RELATIVE VELOCITY, Vr (M/SEC)

    'Z            --VERTICAL DISTANCE ALONG TUBE (M)
    'Z1           --PREVIOUS Z

    'DATA INPUT

LOCATE 7
COLOR 15, 2

FD = 10         'FINEST GRAIN-SIZE (MICRONS)
ND = 500        'COARSEST GRAIN-SIZE (MICRONS)
G = 9.81        'ACCELERATION DUE TO GRAVITY (M/S^2)
RHOP = 2600     'PARTICLE DENSITY (KG/M^3)
                'RHOP = 2320 (OPTIONAL DENSITY)
H = 6.2013      'LENGTH OF THE TUBE (M)
DT = .001       'TIME INCREMENT OF INTEGRATION (SEC)


INPUT "BASE FILE NAME OF Sample--e.g.,V3120101 drop last digit, .dat
   assumed "; VSAMNAM$
    'Input the former part of the sample number
    'SAMSIT$ = "Washington State"
INPUT "HOW MANY FILES WILL BE PROCESSED? "; S
INPUT "ENTER A BASE NUMBER FOR THE DATA FILES"; BNDA
INPUT "ENTER THE FULL FILE NAME WITH EXTENSION"; VNAME$
INPUT "ENTER THE AIR PRESSURE IN INCH Hg "; PRESSURE

DIM TEMP(3), RST(ND / .3), RWtG(ND / .3), RWtP(ND / .3)
DIM SAMWEIGHT(S), FTA(ND), PHIDA(ND), RWtGA(ND), RSAMWT(S)
DIM PHID(ND), PHID1(ND), PHISD(ND), FT(ND), TT(ND), RWtG1(ND)
DIM PHID1A(ND), RWtG1A(ND), FT1(ND), FT2(ND), FT3(ND), PHID1$(ND)
DIM P1(7 * ND)

INPUT "ENTER SAMPLE ID"; SAMID$
```

```
INPUT "ENTER OTHER ID"; OTHID$
INPUT "ENTER REPLICATE NUMBER"; REPNUM$
INPUT "ENTER START DATE OF SAMPLING PERIOD"; SAMDATEI$
INPUT "ENTER END   DATE OF SAMPLING PERIOD"; SAMDATEF$
INPUT "ENTER ANALYSIS DATE"; ANDATE$
INPUT "ENTER ANALYSIS TIME"; ANTIME$
INPUT "ENTER TEST LENGTH (s)"; TESTLEN
INPUT "ENTER RECOVERED SAMPLE WEIGHT (g)"; RSAMWT(Q)

PRINT "TEMPERATURE AT THE TOP, MIDDLE, and BOTTOM IN DEG CENTIGRADE "
    FOR I = 1 TO 3
        PRINT "TEMP("; I; ")";
        INPUT TEMP(I)
    NEXT I

    'PRINT "INPUT SAMPLE I.D.(Q)"    'OPTIONAL INPUT
    'Note:  Current version 8 and higher don't support SAMID$(Q)
                'FOR Q = 0 TO S - 1
                    'PRINT "SAMID$("; Q + 1; ")";
                    'INPUT SAMID$(Q)
                'NEXT Q

INPUT "INPUT RELATIVE HUMIDITY:  TOP"; HUMTOP

INPUT "INPUT RELATIVE HUMIDITY:  BOT"; HUMBOT

PRINT "INPUT SAMPLE WEIGHT(Q) "
    FOR Q = 0 TO S - 1
        PRINT "SAMWEIGHT("; Q + 1; ")";
        INPUT SAMWEIGHT(Q)
    NEXT Q
              'LPRINT "    J         T         Z         WREL"

'***BEGIN WRITING HARD-COPY OUTPUT


LPRINT "File name: "; VNAME$; "          "; "Sample I.D.: "; SAMID$
LPRINT " "
LPRINT "          GRAIN-SIZE PARAMETERS FOR AIRBORNE PARTICLES"
LPRINT
LPRINT "  Md(phi)         Md(mm)         Wt(%)           Cum. Wt%"




'***COMPUTE TIME FOR EACH SIZE PARTICLE TO REACH BOTTOM OF VSAT TUBE
'***START WITH THE SMALLEST DIAMETER, FD, AND WORK TO LARGEST,
    ND(MICRONS)

FOR J = FD TO ND          'STEP 20
    COLOR 15, 3
    PRINT J;
        D = J * .000001   'CONVERT DIAMETER TO METERS
        WREL = 0          'INITIALIZE RELATIVE VELOCITY, Vr (M/SEC)
        T = 0             'INITIALIZE TIME
        Z = 0             'INITIALIZE DISTANCE ALONG TUBE

'***LINEAR INTERPOLATION TO FIND TEMPERATURE AND OTHER PARAMETERS ALONG
    TUBE
```

```
IF Z < (H / 2) THEN
    TEM = Z * (TEMP(2) - TEMP(1)) / (H / 2) + TEMP(1)
            'CALL Temperature(TR, ABVIS, RHOF)
            'GOSUB AIRPROPERTY
    TR = (TEM + 273.15) * 1.8
    ABVIS = ((.317 * TR ^ 1.5 * (734.7 / (TR + 216))) * 10 ^ -10) *
           (4.788 * 10 ^ 1)
    RHOF = .041206 * (PRESSURE / TR) * 5.155 * 10 ^ 2

ELSE
    TEM = (Z - H / 2) * (TEMP(3) - TEMP(2)) / (H - H / 2) + TEMP(2)
            'CALL Temperature(TR, ABVIS, RHOF)
            'GOSUB AIRPROPERTY
    TR = (TEM + 273.15) * 1.8
    ABVIS = ((.317 * TR ^ 1.5 * (734.7 / (TR + 216))) * 10 ^ -10) *
           (4.788 * 10 ^ 1)
    RHOF = .041206 * (PRESSURE / TR) * 5.155 * 10 ^ 2

END IF



FOR K = 1 TO 15000000

    RATIO = RHOF / RHOP
    RG = G * (1 - RATIO)
    RN = RHOF * WREL * D / ABVIS

    IF RN < 1 THEN
        AZ = RG - 18 * ABVIS * WREL / (RHOP * D ^ 2)
        '18 is 3/4 of 24 from CD = 24 / RN
    ELSE
        CD = 24 / RN + 3 / SQR(RN) + .3
            'should be 0.34 by Fair, 1963, for 0.5<=RN<=10^4
            'CD = .25 + 24 / RN + 6 / (1 + SQR(RN))
            '(White, 1974. 0.25 may be replaced by 0.4)

        AZ = RG - .75 * RATIO * CD * WREL ^ 2 / D

    END IF

    Z = Z + WREL * DT + .5 * AZ * DT ^ 2
        'UPDATE POSITION

    WREL = WREL + AZ * DT
        'UPDATE RELATIVE VELOCITY

    IF Z >= H THEN
        'CHECK IF PARTICLE HAS LANDED

        IF ABS(Z - H) > ABS(Z1 - H) THEN
             'ENSURE PARTICLE HAS PASSED END COMPLETELY

            Z = Z1
             'RESET Z TO PREVIOUS VALUE (Z1)

            T = T1
             'RESET T TO PREVIOUS VALUE (T1)

        END IF
```

```
        GOTO 50

        END IF

        IF Z >= (H - .2) THEN
            'USE A FINER TIME STEP IF PARTICLE IS NEAR BOTTOM OF TUBE

        DT = .0005

        END IF

        T = T + DT                          'INCREMENT TIME
        T1 = T                              'STORE NEW T
        Z1 = Z                              'STORE OLD Z AS "PREVIOUS Z"

    NEXT K

50 :

    'LPRINT USING "####.##   ##.####   #####.###   ###.####  ##.####";
     J; T; Z; WREL

    TT(J) = T
        'STORE TERMINAL TIME FOR EACH SIZE PARTICLE

    PHISD(J) = (-1.4427) * (LOG(J * .001))
        'THE PHI SCALE IS BASED ON MILLIMETERS

NEXT J  'REPEAT FOR NEXT LARGER PARTICLE SIZE


'***FILL PHI PARTICLE SIZE ARRAY AND TRAVEL TIME ARRAYS IN ASCENDING
 ORDER

K = 0

FOR J = ND TO FD STEP -1            'FOR PARTICLES LARGEST TO SMALLEST
    K = K + 1                       'COUNT FROM 1 TO TOTAL
    PHID(K) = PHISD(J)              'MATCH SIZE ARRAY ASCENDING TO DESCENDING
    FT(K) = TT(J)                   'MATCH TIME ARRAY ASCENDING TO DESCENDING

    'LPRINT USING "####.##   ##.####   #####.###   ###.####  ##.####";
     J; PHISD(J); TT(J); WREL; Z
NEXT J

KK = K                              'SAVE MAX VALUE OF K

'INPUT DATA FROM FILE WRITTEN BY VSAT DATA SYSTEM; OPEN OUTPUT FILES

FOR Q = 0 TO S - 1                  'INPUT DATA FOR EACH SAMPLE
    Q1 = BNDA + Q
    VSAMNAME$ = VSAMNAM$ + LTRIM$(STR$(Q1)) + ".DAT"
    DISTRINAME$ = VSAMNAM$ + LTRIM$(STR$(Q1)) + ".DIS"
    PARANAME$ = VSAMNAM$ + LTRIM$(STR$(Q1)) + ".PAR"
    HISTOGRAM$ = VSAMNAM$ + LTRIM$(STR$(Q1)) + ".HIS"
    Sample$ = VSAMNAM$ + LTRIM$(STR$(Q1)) + ".sam"

    OPEN "d:\qb45\" + VSAMNAME$ FOR INPUT AS #1
        'INPUT FROM HARD DRIVE
```

```
        'OPEN "A:\" + VSAMNAME$ FOR INPUT AS #1 'INPUT FROM DISKETTE

    OPEN "d:\qb45\" + DISTRINAME$ FOR OUTPUT AS #2
    OPEN "d:\qb45\" + PARANAME$ FOR OUTPUT AS #3
    OPEN "d:\qb45\" + HISTOGRAM$ FOR OUTPUT AS #4
    OPEN "d:\qb45\" + Sample$ FOR OUTPUT AS #5

    TARE = 0

DO UNTIL EOF(1)                 'EOF IS END OF FILE (DATA FROM VSAT)

    INPUT #1, RST, RWtG         'READ DATA FROM THE VSAT


'***COMPARE THE CALCULATED TIME AND THE RECORDED TIME
'***PUT PARTICLE DIAMETERS IN COMPLIANCE WITH THE RECORDED
'***CUMULATIVE WEIGHT IN GRAMS

    K1 = 0
    FOR K = 1 TO KK             'WORK IN ASCENDING ORDER

        IF RST <= 1 THEN        'AND RWtG > 0 THEN '1.3 SEC ~1200 MICRON;
                                '1.26 SEC ~1460 MICRON
            TARE = RWtG         'STORE THE TARE WEIGHT
        ELSE
        END IF

        IF RST > 1.3 THEN       '1.3 SEC ~1200 MICRON
            'FOR THIS CALCULATION, ONLY THE PARTICLES LARGER THAN 1500
            MICRON ARE CALCULATED.

            K1 = K1 + 1
            IF RST > FT(K - 1) AND RST <= FT(K) THEN
                FTA(K1) = FT(K)
                PHIDA(K1) = PHID(K)
                RWtGA(K1) = RWtG - TARE

            ELSE
            END IF

        ELSE
        END IF

    NEXT K

LOOP

CLOSE #1
KK1 = K1


K2 = 0
    FOR K1 = 1 TO KK1
      IF RWtGA(K1) > 0 AND RWtGA(K1) <= SAMWEIGHT(Q) THEN
                  K2 = K2 + 1
                  PHID1(K2) = PHIDA(K1)
                  RWtG1(K2) = RWtGA(K1)
                  FT2(K2) = FTA(K1)
                  KK2 = K2
                     'LPRINT FT2(K2); PHID1(K2); RWtG1(K2)
```

```
      ELSE
                  GOTO 100
      END IF
100 :

       FTA(K1) = 0: PHIDA(K1) = 0: RWtGA(K1) = 0
    NEXT K1

  FOR K2 = 1 TO KK2
     RWtP(K2) = ((RWtG1(K2) / RWtG1(KK2)) * 100)
     PHID1(K2) = PHID1(K2)                    ***problem area***
     FT2(K2) = FT2(K2)                        ***problem area***
     IF RWtP(K2) > 100 THEN
     GOTO 80
     END IF
  NEXT K2
80 :
L = 1
 FOR K2 = 1 TO KK2
   RWtP(L) = RWtP(K2)
    PHID1(L) = PHID1(K2)
     FT2(L) = FT2(K2)
       IF RWtP(L) <= RWtP(L - 1) THEN
          GOTO 82
       END IF
     L = L + 1
82 :
   NEXT K2

L = L - 1
KK3 = L

FOR I = 1 TO 7
  P(1) = 5: P(2) = 16: P(3) = 25: P(4) = 50: P(5) = 75: P(6) = 84: P(7)
= 95
     FOR K3 = 1 TO KK3
       TGA = ((RWtP(K3) - RWtP(K3 - 1)) / 10) / (PHID1(K3) - PHID1(K3 -
1))
           X = (PHID1(K3) - PHID1(K3 - 1)) / 20
           RWtPSPX = 0
              FOR PX = 1 TO 20
                  RWtPS = RWtP(K3 - 1) + TGA * PX * X * 10
                  PHID1S = PHID1(K3 - 1) + PX * X
                    IF P(I) > CINT(RWtPSPX) AND P(I) <= CINT(RWtPS) THEN
                      P1(I) = PHID1S
                     GOTO 911
                   ELSE
                   END IF
                   RWtPSPX = RWtPS
              NEXT PX
     NEXT K3
911 :
NEXT I

'***Calculating Grain Size Parameters

   Msphi = (P1(2) + P1(4) + P1(6)) / 3
   'Mean size in phi units    'Mean Diameter

   Msmm = (EXP(-.693 * Msphi))
```

```
   Mean size in millimeters

   Sorting = ((P1(6) - P1(2)) / 4) + ((P1(7) - P1(1)) / 6.6)
   'Standard Deviation

   SK = ((P1(6) + P1(2) - 2 * P1(4)) / (2 * (P1(6) - P1(2)))) +
        ((P1(7) + P1(1) - 2 * P1(4)) / (2 * (P1(7) - P1(1))))
   'Skewness

   KG = (P1(7) - P1(1)) / (2.44 * (P1(5) - P1(3)))
   'Kurtosis

   FLAG1 = 0: FLAG2 = 0: FLAG3 = 0: FLAG4 = 0: FLAG5 = 0: FLAG6 = 0:
       FLAG7 = 0: FLAG8 = 0
   VCS = 0: CS = 0: MS = 0: FS = 0: VFS = 0: CSILT = 0: PM20 = 0:
         PM10 =  0

FOR K3 = 1 TO KK3
IF PHID1(K3) < 0 THEN
   VCS = 100 - (100 - RWtP(K3))          'VERY COARSE SAND %
   FLAG1 = RWtP(K3)                     'FOR CALCULATION
   GOTO 495
     IF PHID1(K3) > 0 THEN
        FLAG2 = RWtP(K3)
        GOTO 595
     END IF
495 :
      ELSEIF PHID1(K3) > 0 AND PHID1(K3) <= 1 THEN
          CS = (100 - FLAG1) - (100 - RWtP(K3))
               FLAG3 = RWtP(K3)
                     'GOTO 695
595 :
      ELSEIF PHID1(K3) > 0 AND PHID1(K3) <= 1 THEN
          CS = (100 - FLAG2) - (100 - RWtP(K3))
               FLAG3 = RWtP(K3)
695 :
      ELSEIF PHID1(K3) > 1 AND PHID1(K3) <= 2 THEN
          MS = (100 - FLAG3) - (100 - RWtP(K3))
               FLAG4 = RWtP(K3)
      ELSEIF PHID1(K3) > 2 AND PHID1(K3) <= 3 THEN
          FS = (100 - FLAG4) - (100 - RWtP(K3))
               FLAG5 = RWtP(K3)
      ELSEIF PHID1(K3) > 3 AND PHID1(K3) <= 4 THEN
          VFS = (100 - FLAG5) - (100 - RWtP(K3))
               FLAG6 = RWtP(K3)
      ELSEIF PHID1(K3) > 4 AND PHID1(K3) <= 5.64 THEN
          CSILT = (100 - FLAG6) - (100 - RWtP(K3))
               FLAG7 = RWtP(K3)
      ELSEIF PHID1(K3) > 5.64 AND PHID1(K3) <= 6.64 THEN
               PM20 = (100 - FLAG7) - (100 - RWtP(K3))
                   FLAG8 = RWtP(K3)
      ELSEIF PHID1(K3) >= 6.64 AND PHID1(K3) < 7.64 THEN
                PM10 = (100 - FLAG8) - (100 - RWtP(K3))
      ELSE
      END IF
NEXT K3

'***DATA OUTPUT

PRINT #2, "    Time         Md(phi)         Md(mm)         Wt(%)
```

```
Cum. Wt%"
 FOR K3 = 1 TO KK3
  PRINT #2, USING "####.####       ##.####       ##.####       ###.####
            ####.####"; FT2(K3); PHID1(K3); EXP(-.693 * PHID1(K3)); (100
            - RWtP(K3 - 1)) - (100 - RWtP(K3)); RWtP(K3)
NEXT K3
CLOSE #2

'***CALCULATING FOR HISTOGRAMS
DIM SFNEW(1000)
   SFLAG = 0: PHID = 0
        FOR K3 = 1 TO KK3
          FOR J = -1 TO 32
                PHID = J * .25
                IF PHID >= PHID1(K3 - 1) AND PHID <= PHID1(K3) THEN
                             'IF PHID1(K3) > 3 AND PHID1(K3) < 3.25
                              THEN GOTO 666
                        SFNEW(K3) = (100 - SFLAG) - (100 - RWtP(K3))
                        IF SFNEW(K3) = 0 THEN GOTO 666
                        SFLAG = RWtP(K3)



PRINT #4, USING "###.####        ###.####       ###.####         ###.####";
          PHID1(K3); EXP(-.693 * PHID1(K3)); SFNEW(K3); RWtP(K3)
LPRINT USING "###.####        ###.####       ###.####         ###.####";
       PHID1(K3); EXP(-.693 * PHID1(K3)); SFNEW(K3); RWtP(K3)


                ELSE
                END IF
666 :
           NEXT J
        NEXT K3
CLOSE #4

PRINT #5, VSAMNAME$; " "; SAMID$; " "; OTHID$; " "; REPNUM$; " ";
SAMDATEI$; " "; SAMDATEF$; " "; ANDATE$; " "; ANTIME$; USING
     " #### ##.## ##.# ##.# ##.# ##.# ##.# ##.#### ##.#### ##.####
     ####.#### ##.#### ##.##### ##.##### ##.##### ##.##### ##.#####
     ##.##### ##.##### ##.##### ##.##### ##.#### ##.#### ##.#### ##.####
     ###.### ###.### ###.### ###.### ###.### ###.### ###.### ###.###
     ####.#### ####.#### ####.#### ####.#### ####.#### ####.####";
     TESTLEN; PRESSURE; TEMP(1); TEMP(2); TEMP(3); HUMTOP; HUMBOT;
     SAMWEIGHT(Q); RWtG1(KK2); SAMWEIGHT(Q) - RWtG1(KK2);
     ((SAMWEIGHT(Q) - RWtG1(KK2)) / SAMWEIGHT(Q)) * 100; RSAMWT(Q);
     TARE; EXP(P1(1) * -.693); EXP(P1(2) * -.693); EXP(P1(3) * -.693);
     EXP (P1(4) * -.693); EXP(P1(5) * -.693); EXP(P1(6) * -.693);
    EXP(P1(7) * -.693); Msphi; Msmm; Sorting; SK; KG; VCS; CS; MS; FS;
    VFS; CSILT; PM20; PM10; TT(10); TT(20); TT(50); TT(70); TT(100);
    TT(499)
CLOSE #5

   PRINT #3, "      GRAIN-SIZE PARAMETERS OF AIRBORNE PARTICLES  "
   PRINT #3, "  "
      'PRINT #3, "Sampling Site: "; SAMSIT$
   PRINT #3, "File name: "; VSAMNAME$  'TAB(30); "Sample I.D.: "; SAMID$
      'PRINT #3, "Sampling Date:"; SAMDAT$; TAB(30); "Sampling Height:";
       SAMHIT$; "cm"
```

```
   PRINT #3, "  "
   PRINT #3, "Proc. Sample Weight: "; SAMWEIGHT(Q); "g"; " Rec. Sample
     Wt.: "; RWtG1(KK2); "g"
   PRINT #3, "Wt. difference (g)"; USING " ##.####"; SAMWEIGHT(Q) -
  RWtG1(KK2)
   PRINT #3, "Sample loss (%)"; USING " ###.###"; ((SAMWEIGHT(Q) -
 RWtG1(KK2)) / SAMWEIGHT(Q)) * 100
   PRINT #3, "Tare weight (g)"; USING " ##.#####"; TARE
   PRINT #3, "  "

   PRINT #3, "    Percentages(%)   Diameter(phi)      Diameter(mm)"
FOR I = 1 TO 7
   PRINT #3, USING "    ##.##            ##.####             ##.####";
     P(I); P1(I); EXP(P1(I) * -.693)
NEXT I
PRINT #3, "  "
PRINT #3, "    MEAN(phi) MEAN(mm) Sorting  SKEWNESS KURTOSIS "
PRINT #3, USING "   ##.####   ##.####  ##.####  ##.####  ##.####";
  Msphi; Msmm; Sorting; SK; KG
PRINT #3, "  "
PRINT #3, "                      SIZE FRACTIONS"
PRINT #3, " VCS(%)  CS(%)  MS(%) FS(%)   VFS(%) CSILT(%)   PM20(%)
  PM10(%)"
PRINT #3, USING "##.###  ##.### ##.### ##.##   ##.### ##.###    ##.###
       ##.###"; VCS; CS; MS; FS; VFS; CSILT; PM20; PM10
PRINT #3,
CLOSE #3

'***CONTINUE HARD-COPY OUTPUT

    'LPRINT "Sampling Height: "; SAMHIT$; "cm"
LPRINT " "
LPRINT "Proc. Sample Weight: "; SAMWEIGHT(Q); "g"; " Rec. Sample Wt.: ";
RWtG1(KK2); "g"
LPRINT "Wt. difference (g)"; USING " ##.####"; SAMWEIGHT(Q) - RWtG1(KK2)
LPRINT "Sample loss (%)"; USING " ###.###"; ((SAMWEIGHT(Q) - RWtG1(KK2))
       / SAMWEIGHT(Q)) * 100
LPRINT "Tare weight (g)"; USING " ##.#####"; TARE
LPRINT
    'LPRINT "     SIZE DISTRIBUTION OF AIRBORNE PARTICLES "
    'LPRINT


    'LPRINT "                GRAIN-SIZE PARAMETERS OF AIRBORNE PARTICLES
           "
    'LPRINT
    'LPRINT "Sampling Site: "; SAMSIT$
    'LPRINT "File name: "; VSAMNAME$   'TAB(30); "Sample I.D.: "; SAMID$
    'LPRINT "Sampling Height: "; SAMHIT$; "cm"
    'LPRINT "Processed Sample Weight: "; SAMWEIGHT(Q); "g"; " VSAT
Sample Wt.: "; RWtG1(KK2); "g"
    'LPRINT "Wt. difference "; SAMWEIGHT(Q) - RWtG1(KK2); " Sample loss
    "; ((SAMWEIGHT(Q) - RWtG1(KK2)) / SAMWEIGHT(Q)) * 100; " %"
LPRINT
    'LPRINT " TIME, PARTICLE SIZE, AND WEIGHT DISTRIBUTION OF AIRBORNE
   PARTICLES "
    'LPRINT
    'LPRINT "  Time(s)       Md(phi)        Md(mm)        Wt(%)
          Cum. Wt%"
```

```
    'FOR K3 = 1 TO KK3
    'LPRINT USING "####.####      ##.####       ##.####      ###.####
     ####.####"; FT2(K3); PHID1(K3); EXP(-.693 * PHID1(K3)); (100 -
RWtP(K3 - 1)) - (100 - RWtP(K3)); RWtP(K3)
    'NEXT K3

LPRINT
LPRINT
LPRINT "             CHARACTERISTIC PERCENTAGE DIAMETERS           "
LPRINT "    "
LPRINT "    Percentage(%)    Diameter(phi)      Diameter(mm)"

FOR I = 1 TO 7
LPRINT USING "    ##.##            ##.####             ##.####"; P(I);
  P1(I); EXP(P1(I) * -.693)
NEXT I

LPRINT
LPRINT
LPRINT "                   GRAIN-SIZE PARAMETERS                "
LPRINT
LPRINT "    Mean(phi)  Mean(mm)  Sorting   Skewness  Kurtosis "
LPRINT USING "   ##.####    ##.####   ##.####   ##.####   ##.####";
Msphi; Msmm; Sorting; SK; KG
LPRINT
LPRINT
LPRINT "                     SIZE FRACTIONS"
LPRINT
LPRINT "   VCS(%)  CS(%)   MS(%)   FS(%)   VFS(%) CSILT(%) PM20(%)
PM10(%)"

LPRINT USING "  ##.###  ##.###  ##.###  ##.###  ##.###  ##.###  ##.###
    ##.###"; VCS; CS; MS; FS; VFS; CSILT; PM20; PM10
LPRINT
LPRINT : LPRINT : LPRINT : LPRINT : LPRINT
NEXT Q

'***AIR PROPERTIES:
       'TR = (TEM + 273.15) * 1.8
       'ABVIS = ((.317 * TR ^ 1.5 * (734.7 / (TR + 216))) * 10 ^ -10) *
(4.788 * 10 ^ 1)
       'RHOF = .041206 * (PRESSURE / TR) * 5.155 * 10 ^ 2
'RETURN

END

SUB Temperature (TR, ABVIS, RHOF)
       TR = (TEM + 273.15) * 1.8
       ABVIS = ((.317 * TR ^ 1.5 * (734.7 / (TR + 216))) * 10 ^ -10) *
(4.788 * 10 ^ 1)
       RHOF = .041206 * (PRESSURE / TR) * 5.155 * 10 ^ 2
END SUB
```

APPENDIX 3

Plots of Dust Collector Data by Site for Both Periods Combined

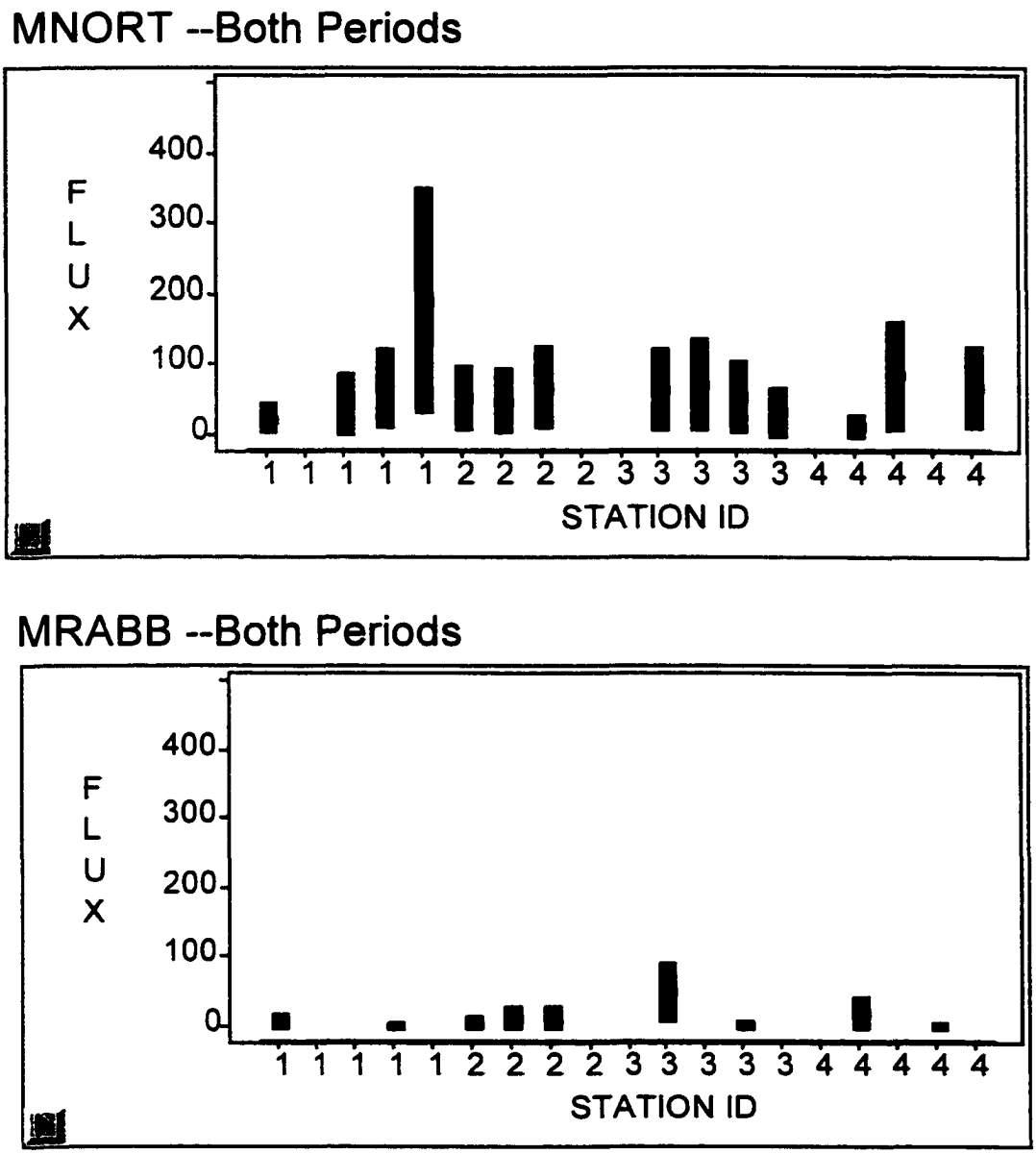

Figure Appendix 3-1. Variations among stations for total flux for Periods A and B combined for MNORT and MRABB sites. Units for total flux are g/cm.

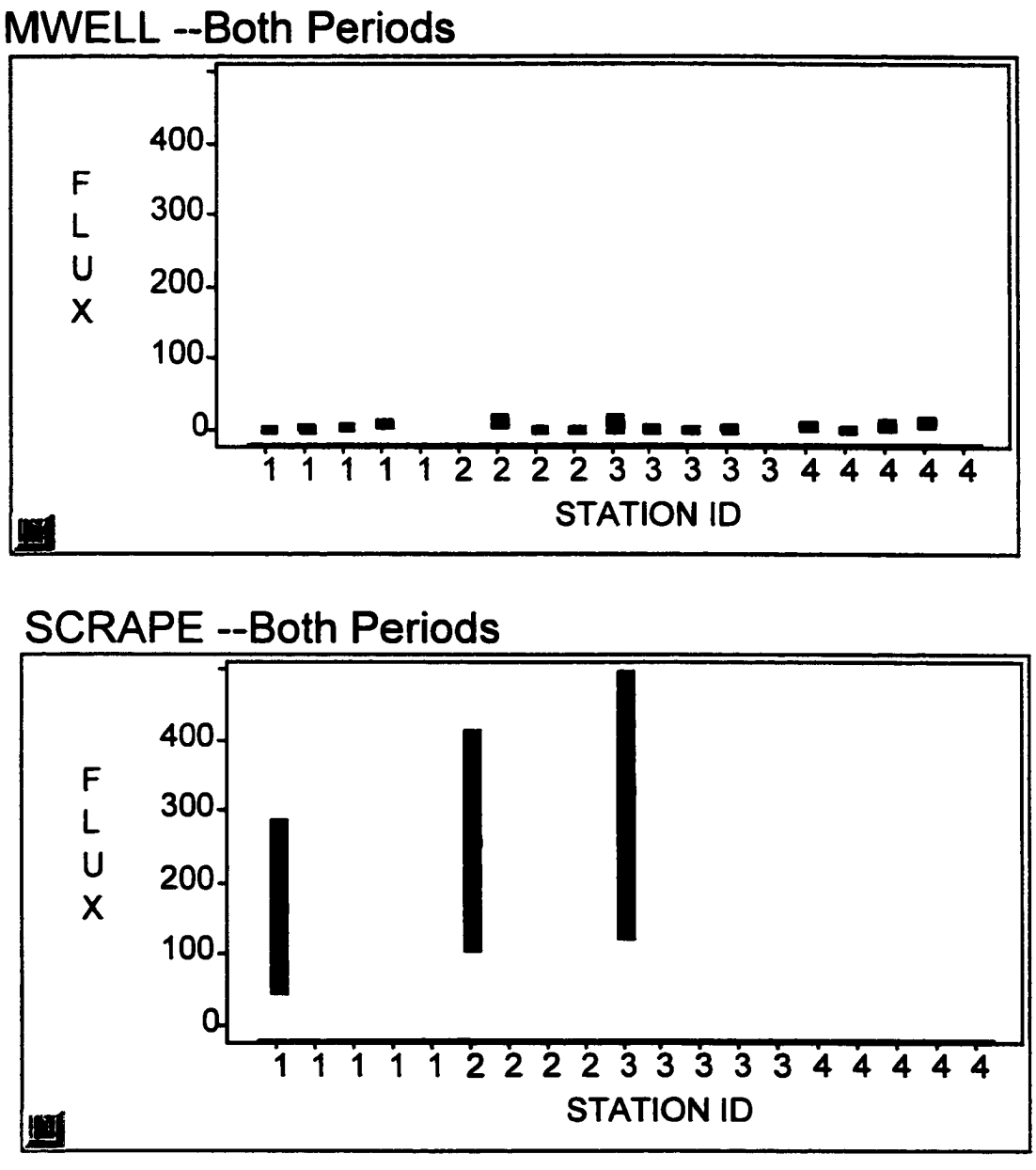

Figure Appendix 3-2. Variations among stations for total flux for Periods A and B combined for MWELL and Scrape sites. Units for total flux are g/cm.

APPENDIX 4

Minute-by Minute DustTrak™ Data

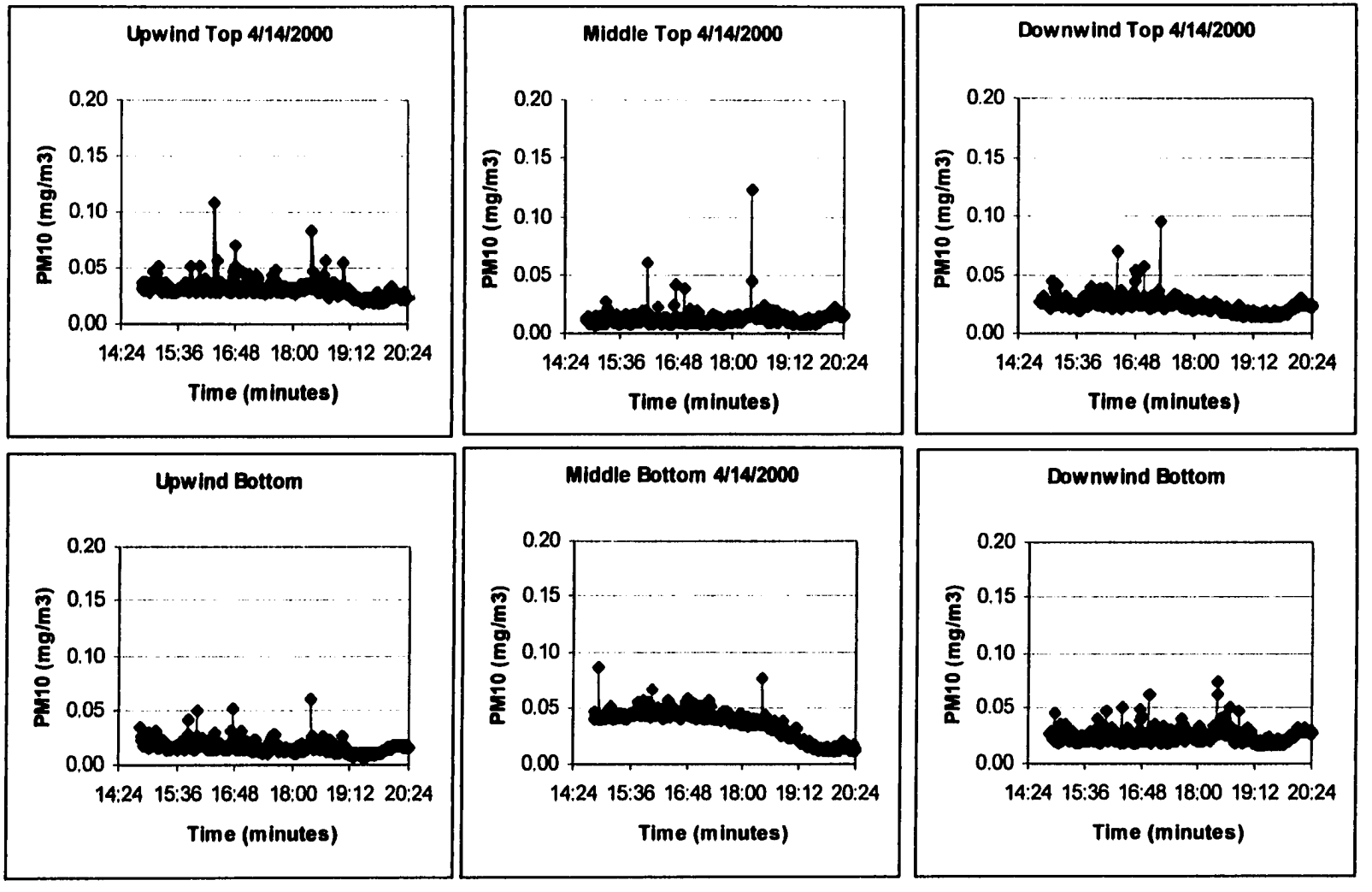

Figure Appendix 4-1. The individual DustTrak™ data for April 14, 2000 for each location at the dune site versus time, arranged on the page to suggest the spatial relationships of the instruments.

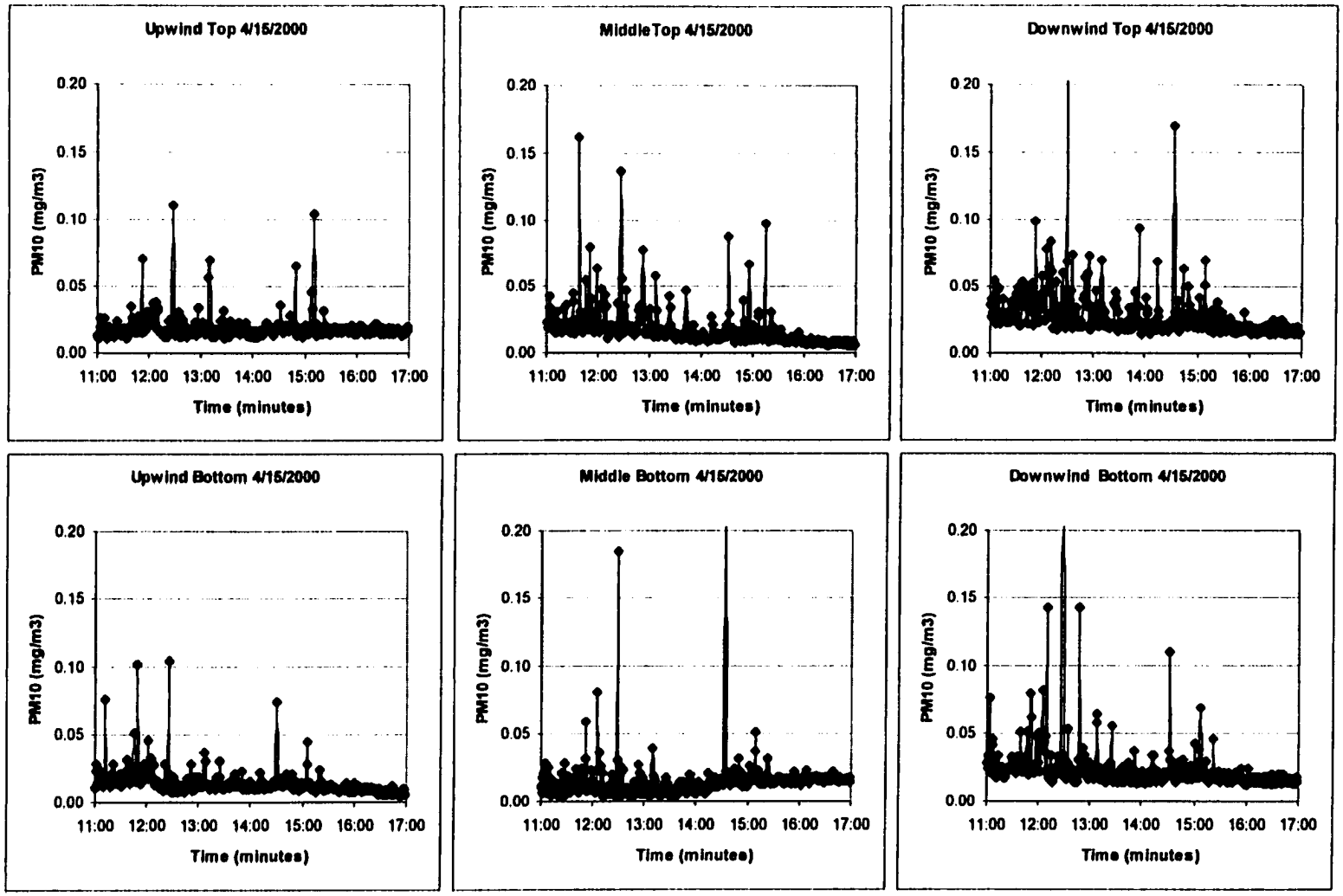

Figure Appendix 4-2. The individual DustTrak™ data for April 15, 2000 for each location at the dune site versus time, arranged on the page to suggest the spatial relationships of the instruments.

VITA

Graduate College
University of Nevada, Las Vegas

Ann Marleau Pitchford

Address:

Las Vegas, Nevada

Degrees:

Bachelor of Science in Physics, 1975
University of Nevada, Reno

Master of Science in Physics, 1978
University of Nevada, Las Vegas

Special Honors and Awards:

Sigma Pi Sigma (Physics National Honor Society) member
Sigma Gamma Epsilon (Earth Sciences National Honor Society) member

Publications:

Blumenthal, D., J. Trijonis, R. Kelso, M. Pitchford, M. McGown, T. Dodson, R. Flocchini, A. Pitchford, A. Waggoner, and J. Ouimette, 1987, Design and Initial Findings of the RESOLVE (Research on Operations-Limiting Visual Extinction) Desert Visibility Study, In: Visibility Protection: Research and Policy Aspects, a peer-reviewed transactions volume, P. S. Bhardwaja editor, Air Pollution Control Association, pp 87-98.

Jones, K., L. Williams, A. Pitchford, T. Slonecker, J. Wickham, R. O'Neill, D. Garofalo, K. Riitters, W. Kepner, and I. Goodman, 2000, A National Assessment of Landscape Change and Impacts to Aquatic Resources, a 10-year Research Strategy for the Landscape Sciences Program, *U.S. Environmental Protection Agency*, EPA/600/R-00/001.

Karakouzian, M., A. Pitchford, M. Leonard, and B. Johnson, 1996, Measurements of Soluble Mineral Content of Soil from Arid and Semiarid Regions. Geotechnical Testing Journal, Volume 19, No. 4, pp. 364-372.

Karakouzian, M., N. Hudyma, and A. Pitchford, 1996, Concurrent Measurements of Mechanical, Hydraulic, and Geophysical Properties of Geomaterial Under Triaxial Conditions. Geotechnical News, Volume 14, Number 3, pp. 18-21.

Malm, W., A. Pitchford, R. Tree, E. Walther, M. Pearson, and S. Archer, 1981, The Visual Air Quality Predicted by Conventional and Scanning Teleradiometers and an Integrating Nephelometer. Atmospheric Environment 15, (12), pp. 2547-2554.

Malm, W., M. Pitchford, and A. Pitchford, 1982, Site-Specific Factors Influencing the Visual Range Calculated from Teleradiometer Measurements, Atmospheric Environment, 16, (10), pp. 2323-2333.

Pitchford, A., J. Denver, A. Olsen, S. Ator, S. Cormier, M. Nash, and M. Mehaffey, 2000, Testing landscape indicators for stream vulnerability to pesticides and nutrients: Landscape Indicators for Pesticides Study for Mid-Atlantic Coastal Streams (LIPS-MACS), *U.S. Environmental Protection Agency*, EPA/600/R-00/087, 2000.

Pitchford, A., M. Pitchford, W. Malm, R. Flocchini, and T. Cahill, 1981, Regional Analysis of Factors Affecting Visual Air Quality. Atmospheric Environment, 15, (10/11), pp. 2043-2054.

Pitchford, A., M. Pitchford, D. Chaloud, and P. Feeney, 1984, Quality Assurance for RESOLVE–A Visibility Study in the California Desert. Proceedings of APCA/ASQC Conference on Quality Assurance in Air Pollution Measurements, Boulder, Colorado, 16 p.

Pitchford, A.M., A. Mazzella, K.R. Scarbrough, 1989, Soil-Gas and Geophysical Techniques for Detection of Subsurface Organic Contamination, ESL-TR-87-67, Air Force Engineering & Services Center, Tyndall Air Force Base, Florida

Pitchford, A., A. Mazzella and E. Heyse, 1987, Techniques for Delineating Subsurface Organic Contamination: A Case Study, in Detection, Control and Renovation of Contaminated Ground Water, American Society of Civil Engineers, New York, pp. 100-109.

Pitchford, M. and A. Pitchford, 1984, An Approach for Specifying the Influence of Upwind Areas using Back Trajectory Analysis, presented at the Air Pollution Control Association 77th Annual Meeting, June 24-29, 84-107.1, 15 p.

Pitchford, M. and A. Pitchford, 1985, Analysis of Regional Visibility in the Southwest Using Principal Component and Back Trajectory Techniques. Atmospheric Environment. 19, (8), pp. 1301-1316.